Graduate Theses & Non-Theses   Student Scholarship

Fall 2015

INVESTIGATING THE FEASIBILITY OF NITROGEN INJECTION IN TURNER VALLEY

Igor Koracin
Montana Tech of the University of Montana

Recommended Citation

INVESTIGATING THE FEASIBILITY OF NITROGEN INJECTION IN
TURNER VALLEY

by

Igor Koracin

A thesis paper submitted in partial fulfillment of the

requirements for the degree of

Master of Science in Petroleum Engineering

Montana Tech

2015

Abstract

The Turner Valley gas and oil field was discovered in 1913 and it was one of the main plays that sparked the growth of the petroleum industry in Canada. The Turner Valley formation is a Mississippian reservoir located at a mean depth of 7,546 feet. It is a heavily faulted field, 25 miles in length with an average width of 2 miles and is located 30 miles south-west of Calgary. It is an asymmetric anticlinal structure cut by the y axis with parallel thrust and normal faults.

Due to its early inception and the lack of resource development regulations, Turner Valley was produced without conservation. Most of the gas was flared as a result of the desire to produce naphtha as quickly as possible. At current conditions (2015), there are approximately 1.3 billion barrels of oil in place that are unable to be recovered through a primary drive due to the field's lack of energy.

A structural model of the field has been built and characterized with the purpose of evaluating if nitrogen injection as an enhanced oil recovery method is economically feasible. The model was history matched to field production from 50 wells and nitrogen injection as pressure maintenance was simulated. Three nitrogen cases have been run, varying in the number of injectors, and the results have been analyzed and compared on an economic basis with the "do nothing case".

In the first case a single well was converted from a gas producer to a nitrogen injection located at the crest of the gas cap with the remaining gas producers being shut in. The second case also assigned a single well to nitrogen injection at the top of the gas cap but left the remaining gas producers open to flow. The final case that was run converted six wells, located in the top half of the gas cap to nitrogen injection and shut in the remaining gas producers.

Economics were run at a discount rate of 10% and were evaluated at oil prices of 40$/bbl, 60$/bbl, and 80$/bbl. Nitrogen injection proved to be economically viable as an enhanced oil recovery mechanism at an oil price of 80$/bbl with the second case being the most attractive alternative. Although the NVP at 60$/bbl was positive, the value was too low to warrant a recommendation to apply a nitrogen injection method with the present project parameters. A price of 40$/bbl resulted in a negative NPV and therefore nitrogen injection in Turner Valley at such a low oil price should not be attempted.

Dedication

Lex.

Acknowledgments

I would like to acknowledge Susan Schrader's support, David Reichhardt's help, and Larry Smith's patience. I would also like to thank Devon Energy for supplying seismic sections, which made this project possible.

Table of Contents

List of Tables

List of Figures

List of Equations

1. Introduction

The discovery of the Turner Valley gas and oil field played an integral part in the establishment of the Canadian petroleum industry. After its discovery in 1913, the petroleum sector within Alberta exploded and made the oil-oriented city of Calgary what it is today. The Turner Valley field is located approximately 30 miles south-west of Calgary, stretching over a distance of 25 miles with a NNW-SSE strike and approximately 2-3 miles wide. The field is heavily faulted with substantial structural relief; the inclination of the Turner Valley formation reaches values as high as 60 degrees (Taylor, 1939) and is situated at a mean formation depth of 7,546 feet. Imperial units are used throughout most of the current work since much of the previous work was done prior to conversion to the metric system. Figure 1 is a map of Alberta, showing the location of the Turner Valley field outlined in red.
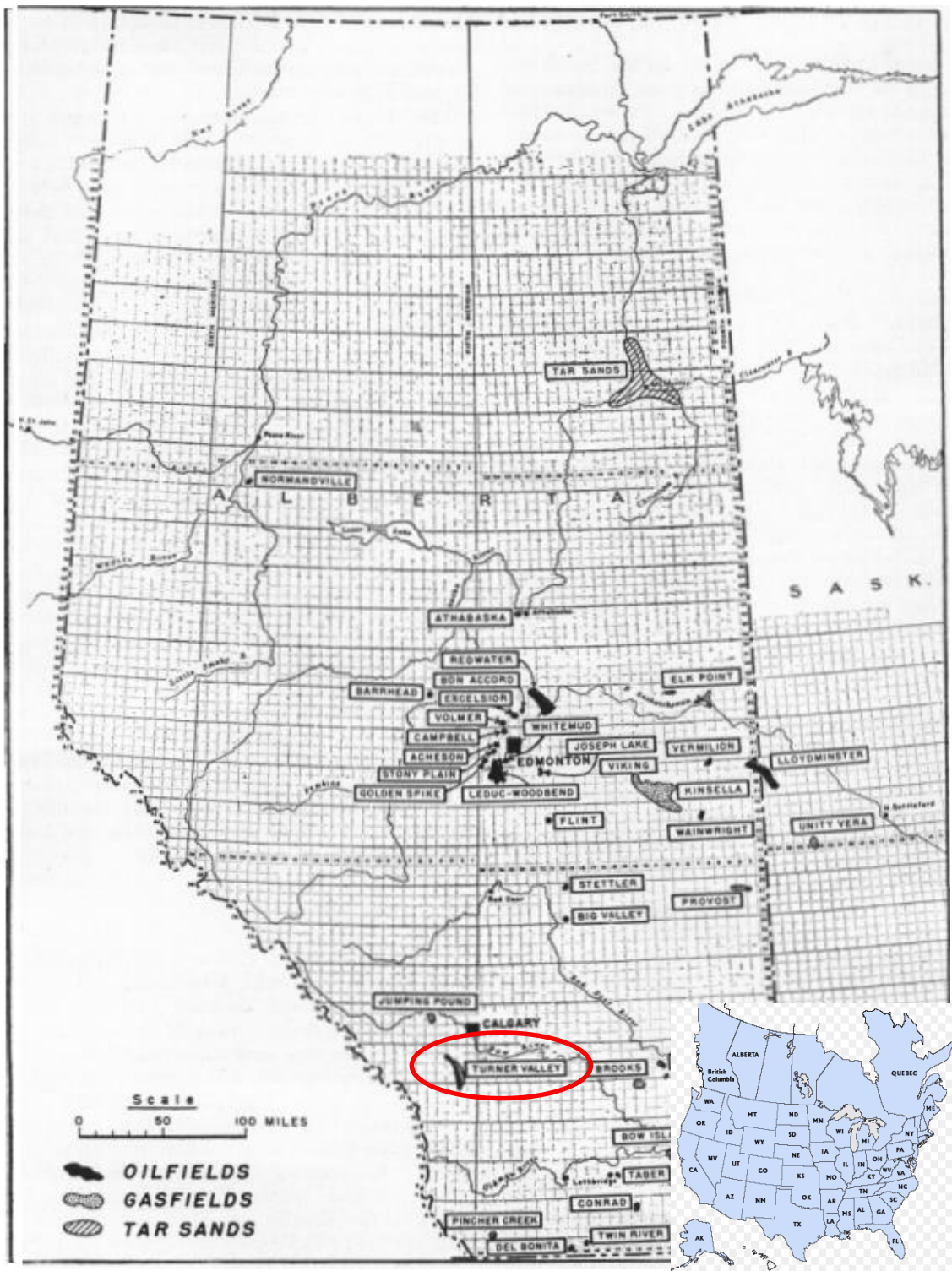
Figure 1: Map of Alberta.

Waterflooding in the field was initiated during the 1960's and is still being conducted. Even after waterflooding the field for over 50 years, it is estimated that over 1.3 billion barrels of oil remain in place and that an incremental 2% recovery can be achieved through solvent injection (Galas, et al., 2012).

Nitrogen has been selected as an injection medium due to its abundance. Nitrogen gas can be separated on site with portable separation units and supplied to injection sites with relatively low costs when compared to carbon dioxide. Due to the absence of carbon dioxide pipe lines in the area and because carbon dioxide cannot be separated from air in large quantities, carbon dioxide as an injection gas would result in substantially higher costs. Natural gas as an injection medium would also result in considerably higher operation costs due to its value. Nitrogen's inert properties were also considered when selecting solvent gas for injection. Natural gas is extremely hazardous and when combined with water, carbon dioxide can pose corrosion problems.

Nitrogen injection as an enhanced oil recovery mechanism can be used for both miscible and immiscible displacement. For miscibility between nitrogen and oil to be achieved at Turner Valley's depth, injection pressures as high as 6,000 psi (Mungan, 2000) need to be reached. This is unrealistic for the Turner Valley formation considering that its gas cap pressure is well below 1,000 psi and therefore nitrogen injection has been selected as a pressure maintenance system working immiscibly.

As described by Green & Willhite (1998), the screening criteria for nitrogen injection include: gravity of the oil, viscosity, formation type (conventional/non-conventional), net thickness, and depth (Green & Willhite, 1998). For a miscible displacement mechanism, a gravity of oil greater than 35 °API is ideal to achieve miscibility between nitrogen and oil. This

is also an important characteristic when pertaining to an immiscible system; higher gravity oils exhibit lower viscosities, consequently increasing the mobility of the oil. This is why viscosity is another important screening criteria when selecting nitrogen as an injection fluid; viscosities less than 0.4 cP are optimal.

Formation type is another consideration that must be taken into account. Nitrogen floods should only be performed in conventional reservoirs where the matrix would not be considered tight. The reasons for this are obvious, in extremely low permeability formations, the displacement of oil by nitrogen would prove to be impossible without fracturing the formation. The thickness of and dip of the reservoir are also important parameter. When attempting to re-pressurize the reservoir, if the formation is too thick and is not dipping, nitrogen would continue to expand horizontally above the surface of the oil until the bounds of the reservoir are reached. This would require substantially large volumes of nitrogen to achieve any kind of pressure increase. Finally, the depth of the formation is also critical when attempting to achieve miscibility. At standard conditions, nitrogen is not miscible with oil and therefore greater depths are required to encounter higher pressures, which in turn achieves miscibility between nitrogen and oil.

There are currently no carbon dioxide or nitrogen floods being conducted in Alberta. In 2002 a nitrogen injection pilot was conducted by Talismen Energy (New releases:PR Newswire, 2002) which was the first nitrogen injection project in Canada; the results have not been published. In 2004, a carbon dioxide flood was conducted by CNRL in the Enchant Arc A&B pools. By 2007, the pilot did not indicate if carbon dioxide injection was successful although CNRL did believe that increase oil recovery would be achieved if injection was continued (Tododo, 2008)

At initial conditions, Turner Valley was producing under a gas-cap drive mechanism. Presently, the primary recovery factor for Turner Valley is 12% (Galas, et al., 2012) which is relatively low when compared to average recovery factors of 25-30% for gas-cap drive reservoir. The low recovery factor is attributed to Turner Valley's initial wasteful development. By 1931, a total of 586 MMSCF of gas was flared from 46 wells (Taylor, 1939), which is a considerable volume when compared to the total of 34,537 MMSCF (Alberta Energy Regulator, 2012)which was flared in Alberta from all source in 2012. Unfortunately, due to the field's wasteful development, an enhanced oil recovery system is required to tap into the 1.3 billion barrels (Galas, et al., 2012) of oil that remain in the subsurface. The large target along with Turner Valley's structure and reservoir fluid properties make it a prime candidate for nitrogen injection when compared to enhanced oil recovery screening criteria (Green & Willhite, 1998).

The purpose of this project is to model a nitrogen injection within a portion of the energy depleted Turner Valley oil field and evaluate if the nitrogen injection is economically viable. Using seismic sections, a structural model of a six square mile section of the southern portion of the field has been built and characterized with available density porosity logs. The study area can be seen in Figure 2.
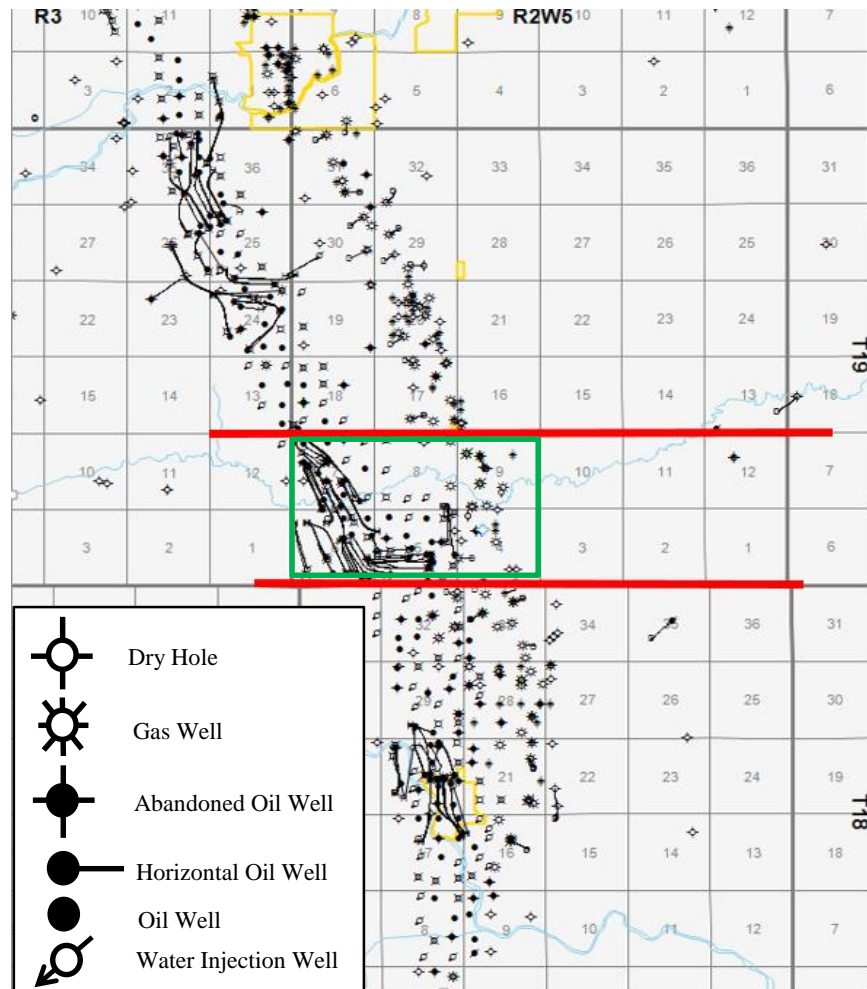
Figure 2: Study Area with a description of the well symbols; 1 square mile section lines and townships from the township map of Alberta; red lines denote seismic lines; figure generated using AccuMap.

The modeled area is outline in green while the red lines represent the locations of the

seismic sections used to construct the structural model. The model has been history matched to

verify the accuracy of the final hydrocarbon volumes and conditions currently present in the

reservoir. Nitrogen injection was simulated using a solvent model; a four component alteration of

the black-oil model. Three nitrogen injection cases have been run including injecting at a single

well located at the crest of the gas cap with all gas producers shut in, injecting at a single well

located at the crest of the gas cap with all gas producers open to production, and injecting at six

wells located in the upper portion of the gas cap with all gas producers shut in. The results from the simulation have been analyzed and compared on an economic basis with the "do nothing case."

1.1. History

The Turner Valley gas and oil field was officially discovered in 1913 when a well was drilled near a gas seepage. The well encountered light crude oil which was produced from Upper Cretaceous age beds. From 1913 until the early 1920's, sporadic drilling was performed, preceding limited oil production. In 1924, Royal Oil Company's No. 4 well was completed in the Cretaceous limestone at 3740 feet. It began producing 72° API gravity naphtha at a rate of 600 bbl/day accompanied by 20 MMSCF/day of gas (Taylor, 1939). Due to the high quality fluid produced from No. 4, Turner Valley began to gain attention not only from petroleum prospectors but from the public eye as well. It wasn't until 1928 that Turner Valley's true potential was realized, when a new well (Okalta No. 1) was drilled approximately 1.25 miles from Royal Oil Company's No. 4. Even at such a relatively short distance, Okalta No. 1 encountered the same structure approximately 1300 feet lower than Royal Oil Company's No. 4. With an initial production rate of 500 bbl/day of naphtha, Okalta No. 4 began the developmental boom of Turner valley (Taylor, 1939).

The majority of the wells drilled by the early 1930's were randomly placed along the eastern flank of the structure. Figure 3 shows a structure contour map of Turner Valley and the wells that have been drilled by 1939.
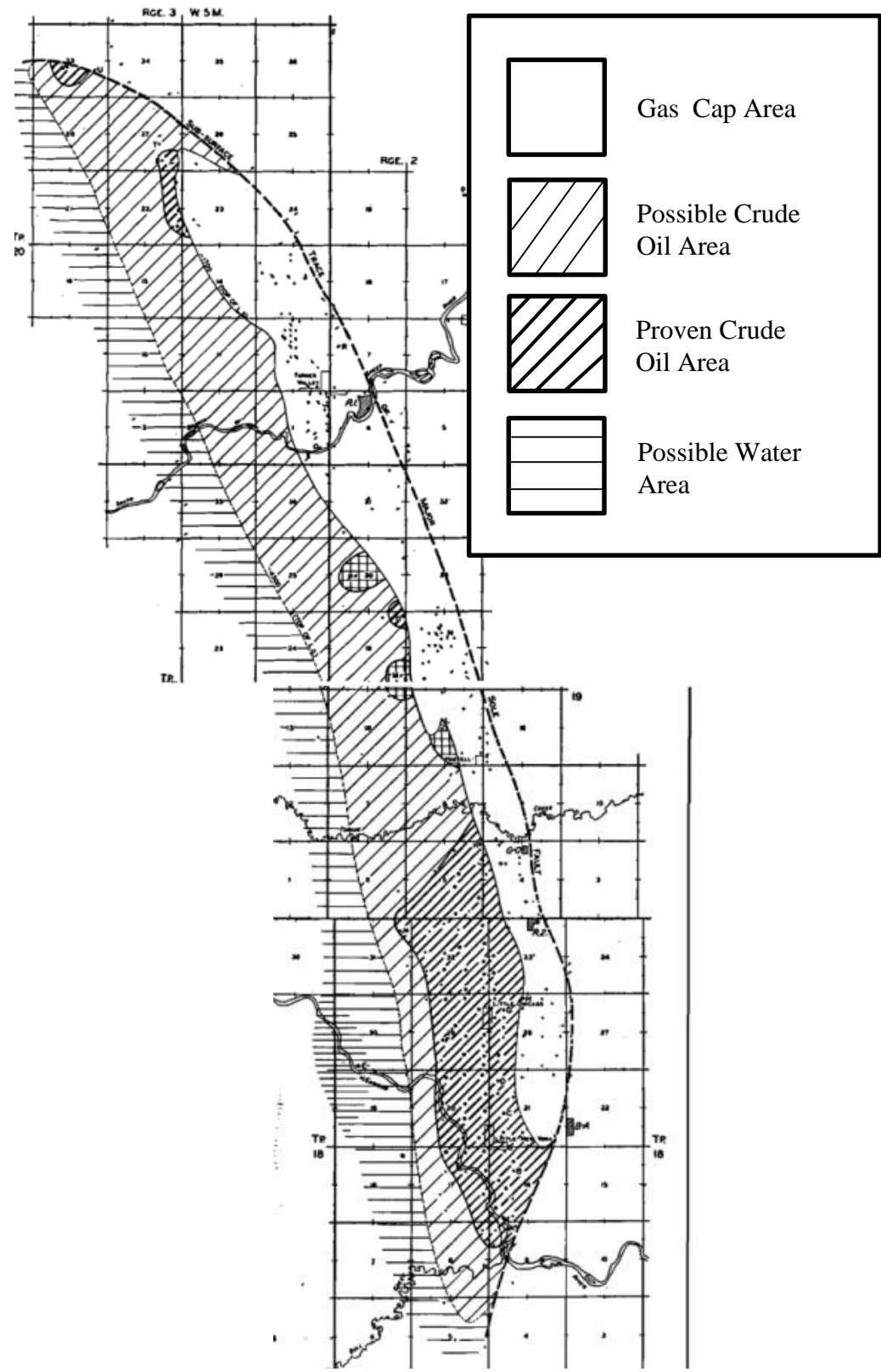
Figure 3: Turner Valley structure contour map (Taylor, 1939).

Most of the wells were completed as naphtha producers with a few wells being converted to crude-oil production (Naphtha within this document is referred to as a light end hydrocarbon consisting of five to six carbon chains). These converted wells reached the Cretaceous limestone at depths of 5800 feet. In 1936, a well was drilled which encountered the same limestone at an even greater depth of 6396 feet. Initially, it produced 850 bbl/day of 44 °API oil with 2 MMSCF/day of gas (Taylor, 1939). This development indicated the crude-oil potential of the western flank.

In June 1931, Turner Valley reached an oil production rate of 5300 bbl/day with 586 MMSCF of gas per day. At this point in time, a rapid decrease in the production of naphtha and a distinct increase in the gas-oil ratio was observed. In July 1931, an effort was made by the Provincial Department of Lands and Mines to conserve the field's gas. The department imposed a regulation in which all gas wells were to set production at 40 percent of open flow. Consequently, by the end of 1931 the production rate of naphtha had fallen to 2000 bbl/day and 380 MMSCF/day of gas. In 1932, the government appointed the Conservation Board (currently known as the Alberta Energy Regulator) which attempted to introduce an allowable acreage drilling spacing unit. Their proposal felt heavy opposition from the operators and the regulation returned to the original proration of 40 % of open flow (Taylor, 1939).

At the time only 35 MMSCF/day of gas was in demand and therefore, until the late 1930's, gasoline plants flared 75% of their residue gas. The surplus gas that was not flared was pumped into the Bow Island gas field (the previous gas source for the cities of Lethbridge and Calgary) at a rate of 5 MMSCF/day.

In 1938, the Conservation Board passed the acreage spacing unit regulation they attempted to introduce in 1931 in an effort to adequately and evenly drain the reservoir. The

Conservation Board agreed on 40 acre spacing units. Furthermore, in an attempt to conserve the gas cap, the Conservation Board passed a regulation in 1938 which used acreage, bottom hole pressures, and open flow to regulate the proration rating assigned to gas producing wells. This enabled the conservation board to assign a 50% rating to the gas cap wells with a 160 acre spacing unit and a 25 percent rating to wells governed by bottom hole pressures. The board also attempted to restrict gas cap wells to 40 MMSCF/day but was once again met with strong opposition. The limit of 108 MMSCF/day of gas was agreed upon and placed into effect. By the end of 1938, naphtha production had fallen to virtually nothing. In 1939, the board limited gas cap production to only fuel gas requirements (Taylor, 1939).

In the same year, the government appointed the Royal Commission to evaluate the direction the Canadian oil industry was heading. Several professional petroleum engineers were called upon to give their evaluation of the field. Pressurizing the field through gas injection was discussed but was later dismissed due to economic barriers.

Although signs of decreased production for naphtha started to show, the field was explored further for crude oil potential. After the initial crude-oil discovery on the western flank, shown in Figure 3, numerous exploratory wells were drilled to test the western portion of the field. All new wells were drilled in the southern end of the field near the initial crude-oil discovery. Most of these wells proved to be successful, and because of these results, an interest in the development of the north end of the field, shown in Figure 3, started to build. A well was drilled 6 miles north of the crude oil discovery but was relatively unsuccessful. Two more wells were drilled even further north, at a distance of 15 miles from the southern wells. One of the wells showed encouraging results with an initial oil production rate of 150 bbl/day. The well encountered the productive limestone at 6275 feet and after acidization was performed, the

well's production rate increased to 900 bbl/day. Another testing well was drilled one mile west of the southern producing wells; it was completed at a depth of 10209 feet and experienced the first sign of water influx (Taylor, 1939).

By 1938, 65 producing oil wells had been drilled; the highest rate of production coming from a single acidized well was 5,000 bbl/day. All wells within the area had been acidized, with successful results. The peak oil production within Turner Valley was reached in 1942, at this point 208 wells had been drilled, averaging an oil production rate of 26,478 bbl/day. Drilling continued, but unfortunately the field sustained an average decline rate of 9% per year. By 1961, the average daily production rate had fallen to 3,144 bbl/day (Paulson & Wahl, 1962).

After peak oil production had been reached in 1948 and a continuous decline was observed, Royalite Oil Company Limited conducted a water flooding pilot project in the upper porous limestone. This project included a total of 15 wells: one injection well and 14 producers on 40 acre spacing. By 1961, 4.9 million barrels of water had been injected with an incremental recovery of 513,805 barrels of oil (Paulson & Wahl, 1962).

In 1962, a new water flooding pilot was conducted in the northern portion of Turner Valley. The project included a total of 39 injection wells. These wells had an average injection rate of 38,000 bbl/day with a cumulative water injection volume of 21.73 million barrels within the first few months (Paulson & Wahl, 1962).

From 2002 to 2005, Talisman Energy performed a nitrogen injection pilot in the Turner Valley field. Unfortunately, their findings have not yet been published but have been reviewed by Sproule World Wide Petroleum consultants in an effort to identify and evaluate the potential for enhanced oil recovery projects within Alberta (Galas, et al., 2012). Sproule used the Alberta Energy Regulator database to apply their screening criteria to various fields. Turner Valley is

predicted to have a potential of reaching an incremental enhanced oil recovery factor of two percent. With an original oil in place of 1.3 billion barrels, the nitrogen injection project target could be as high as 26 million barrels (Galas, et al., 2012).

Currently there are over 950 wells drilled in the Turner Valley field. The primary recovery factor has been estimated to be only 14%, a relatively low number due to the wasteful development of the field during its early years (Galas, et al., 2012). Today there are 1.1 billion barrels of oil remaining in the reservoir, this number along with the field's structure and reservoir properties make it a prime candidate for nitrogen injection.

1.2. Structure, Geology, and Reservoir

The Turner Valley field is approximately 25 miles long and has an average width of 2 miles. It is a heavily faulted, elongated, anticlinal structure with as much as 2500 feet of structural relief. The eastern flank of the structure is bounded by a major thrust fault that underlies most of the field. The western flank of the field is also bounded by two similar thrust faults. Link and Moore (1934) developed a Turner Valley cross section (Figure 4) located in the northern section of the field. The cross section shows the bounding thrust faults on the eastern and western flanks of the field with the presence of reverse faulting in the middle of the formation.
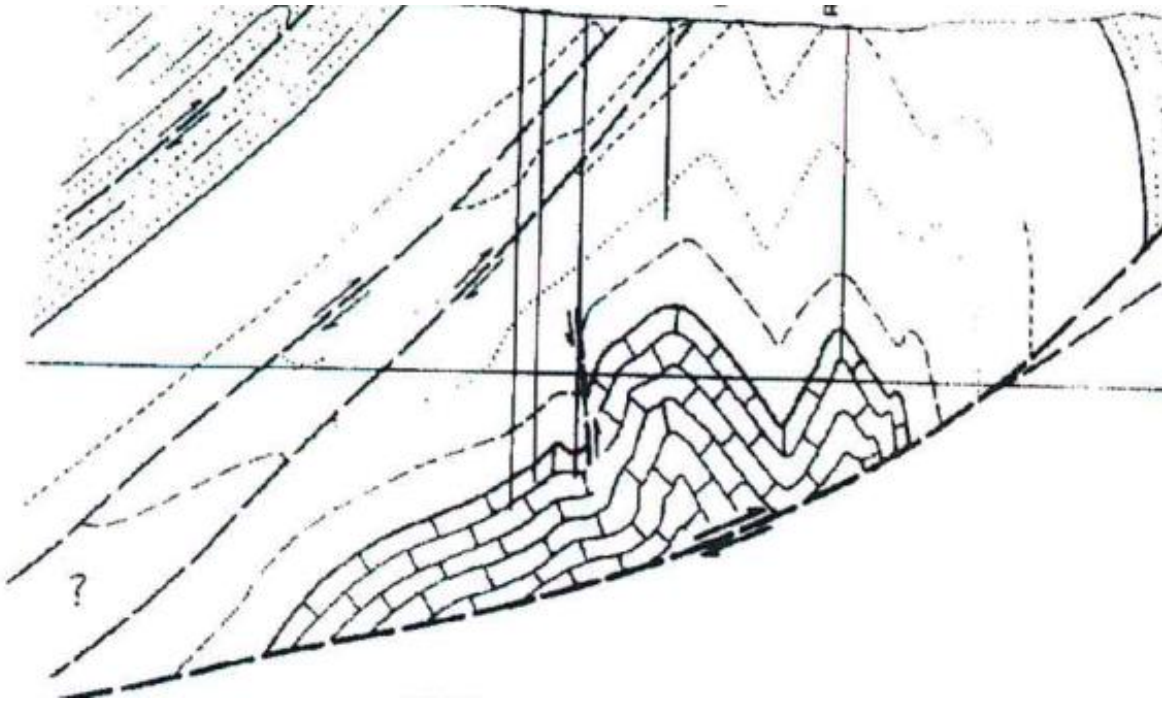
Figure 4: Cross section representing the northern portion of the field (Link & Moore, 1934).

Due to the presence of such high structural relief, dip angles can be as high as 60 degrees. Figure 5 shows a cross section developed by Paulson and Wahl (1962) of the northern portion of Turner Valley, exhibiting the high structural relief.
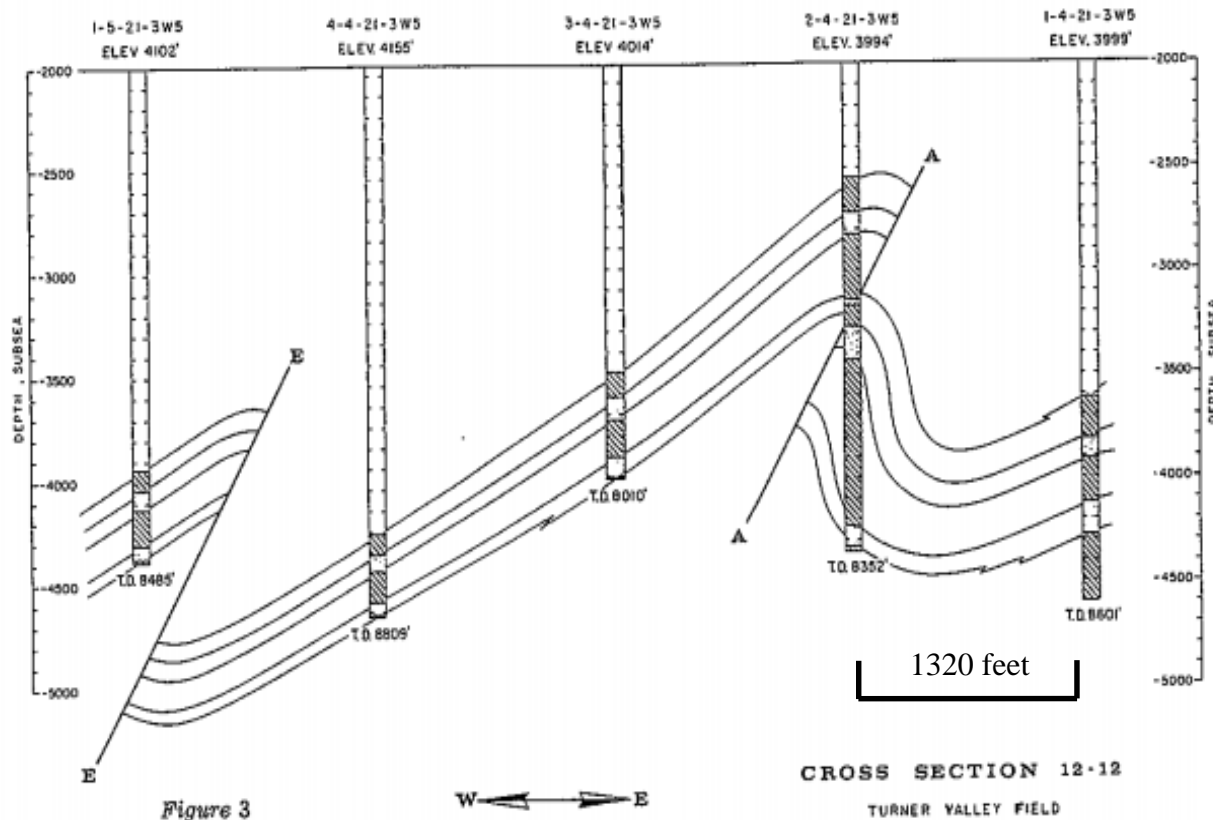
Figure 5: Northern Turner Valley cross section showing structural relief (Paulson & Wahl, 1962).

The productive zones in the subsurface of Turner Valley consist of the upper porous limestone and the lower dolomitic limestone, both Mississippian in age. The two porous beds are separated by a dense crystalline limestone interbedded with chert from which very limited production has been achieved. Due to the presence of faulting, these dolomitic limestones are segregated from their respective continuations on both the western and eastern sides of the field (Link & Moore, 1934). The upper porous zone has an average thickness of approximately 100 feet and the lower porous zone has an average thickness of 60 feet. The dense crystalline limestone that segregates the productive zones is about 75 feet thick. Figure 6 is a stratigraphic section of the south-central mountains and foothills in Alberta. The Turner Valley formation overlies the Shunda carbonate and belongs to the Rundle Group.
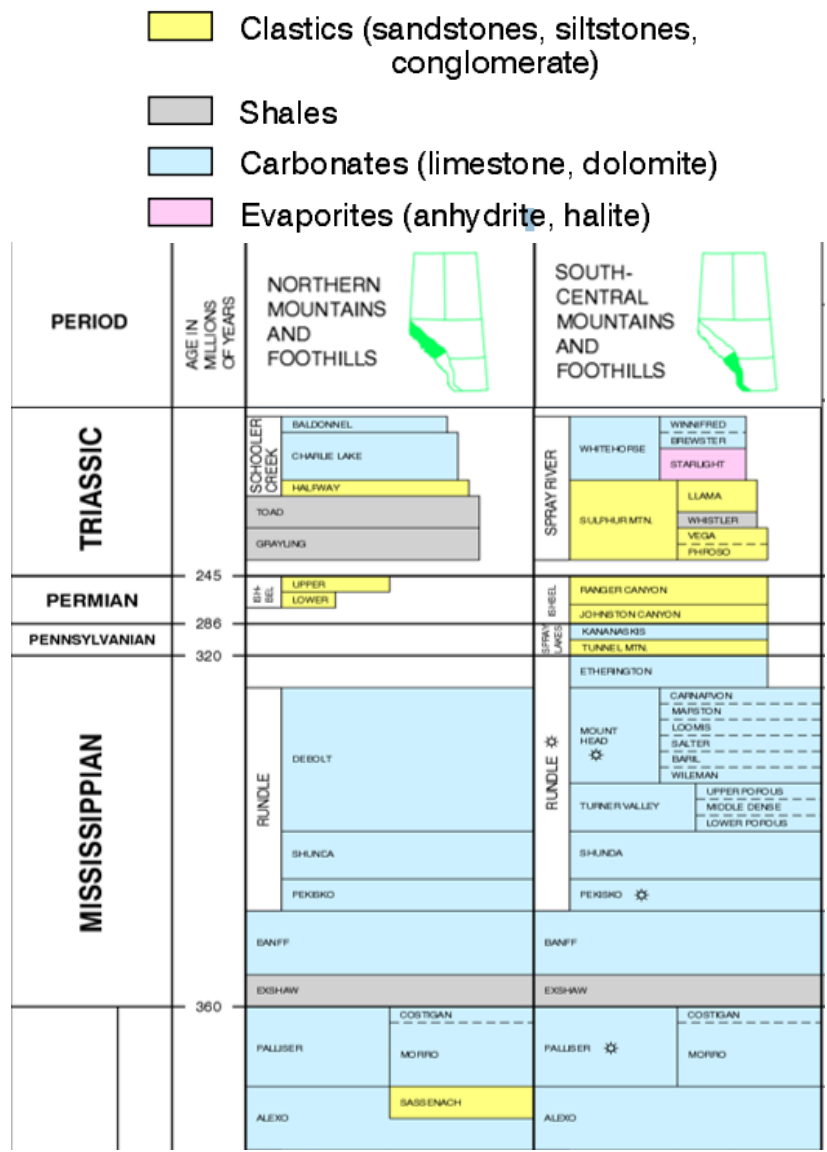
Figure 6: Stratigraphic section of the south-central mountains and foorhills in Alberta (Inc., 2015).

The porosity from the two porous zones ranges between 3-14 % with an average of 8%. Some core samples show porosity values as high as 20% (Paulson & Wahl, 1962). The porosity-permeability relationship, shown in Figure 7 was composed with data obtained from 160 core samples taken from 5 wells (Paulson & Wahl, 1962). Although in some locations the porosity

can be as high as 20%, reaching a permeability of 100 mD, the average porosity of 8%

corresponds to an average reservoir permeability of 3.1 mD.
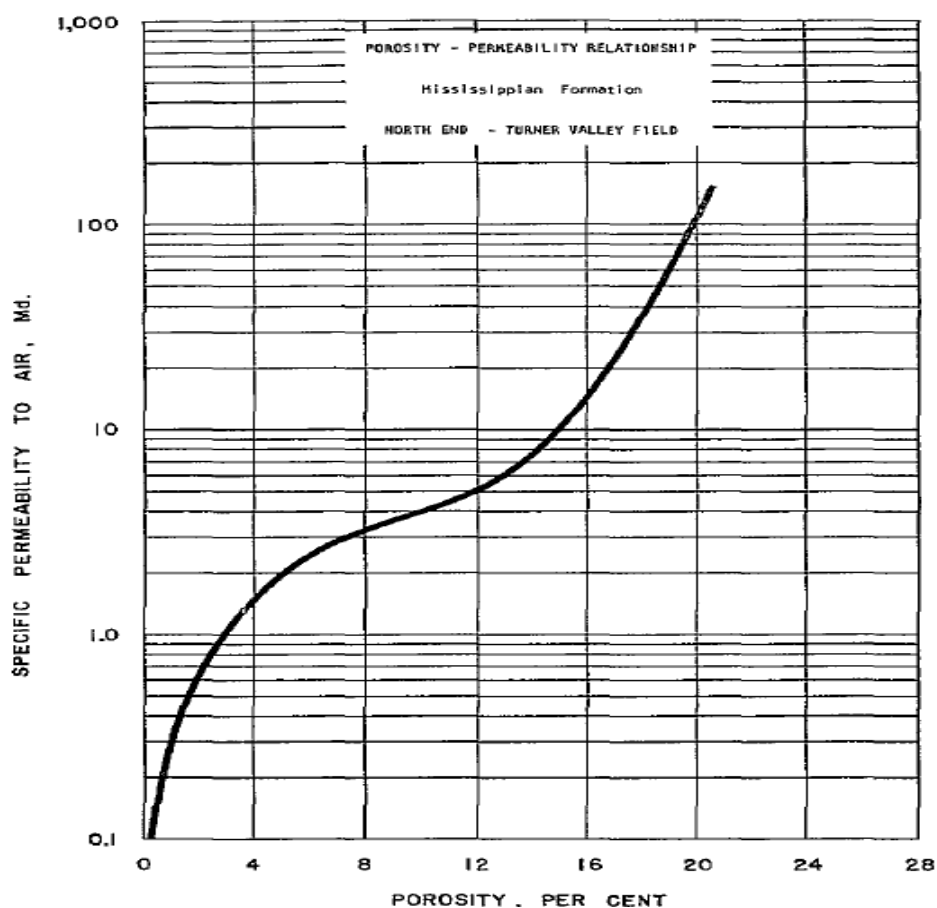
Figure 7: Porosity-Permeability Relationship of porous limestone zones (Paulson & Wahl, 1962)

The gas-oil contact was originally situated at a depth of 2,200 feet subsea and the original

oil-water contact was located at 4,600 feet subsea. At a depth of 3,550 feet subsea, the initial

reservoir pressure was 2,800 psig with a reservoir temperature of 140 °F. The saturation pressure

was estimated to be 2,400 psig, and at these conditions, the oil formation volume factor was

1.447 bbl/STB with an oil viscosity of 0.36 centipoise. The light oil in place has a gravity of 40

°API (Paulson & Wahl, 1962).

Figure 8 shows capillary pressure as a function of water saturation, created from capillary pressure data from both porous zones. As can be seen from the capillary pressure curve, the irreducible water saturation is 10% with a transition zone spanning 520 feet.
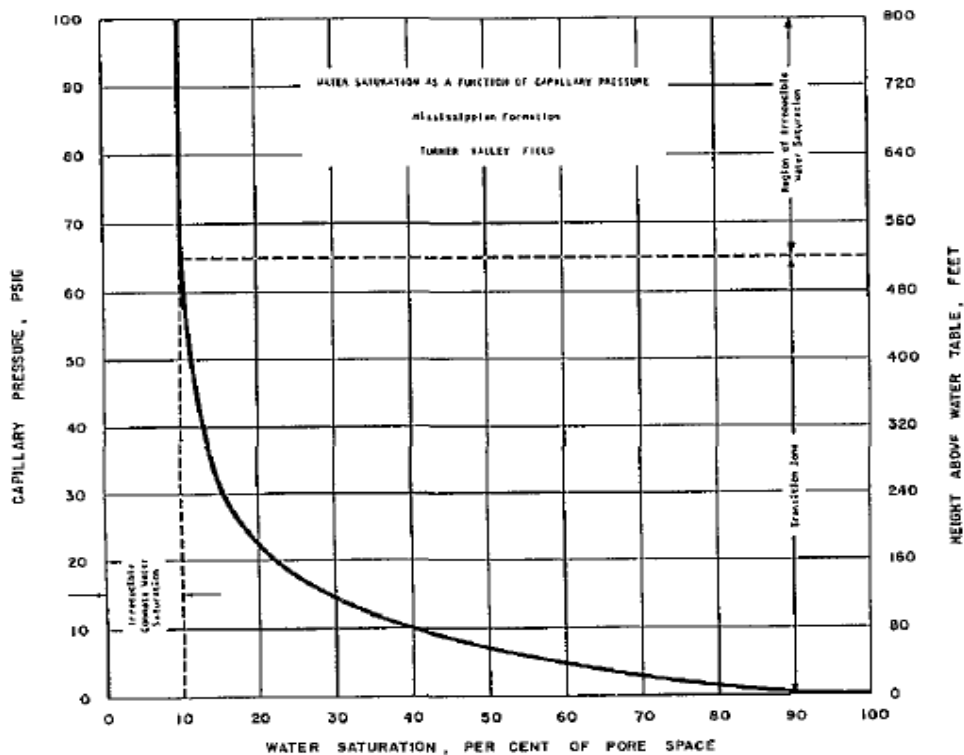
Figure 8: Capillary Pressure Curve for both porous zones (Paulson & Wahl, 1962).

According to Paulson and Wahl (1962), a core sample taken from Turner Valley was flooded with water in an attempt to improve the understanding of the relative permeability relationship for the dolomite formation. Figure 9 displays a relative permeability curve created with the data obtained from the flooded core.
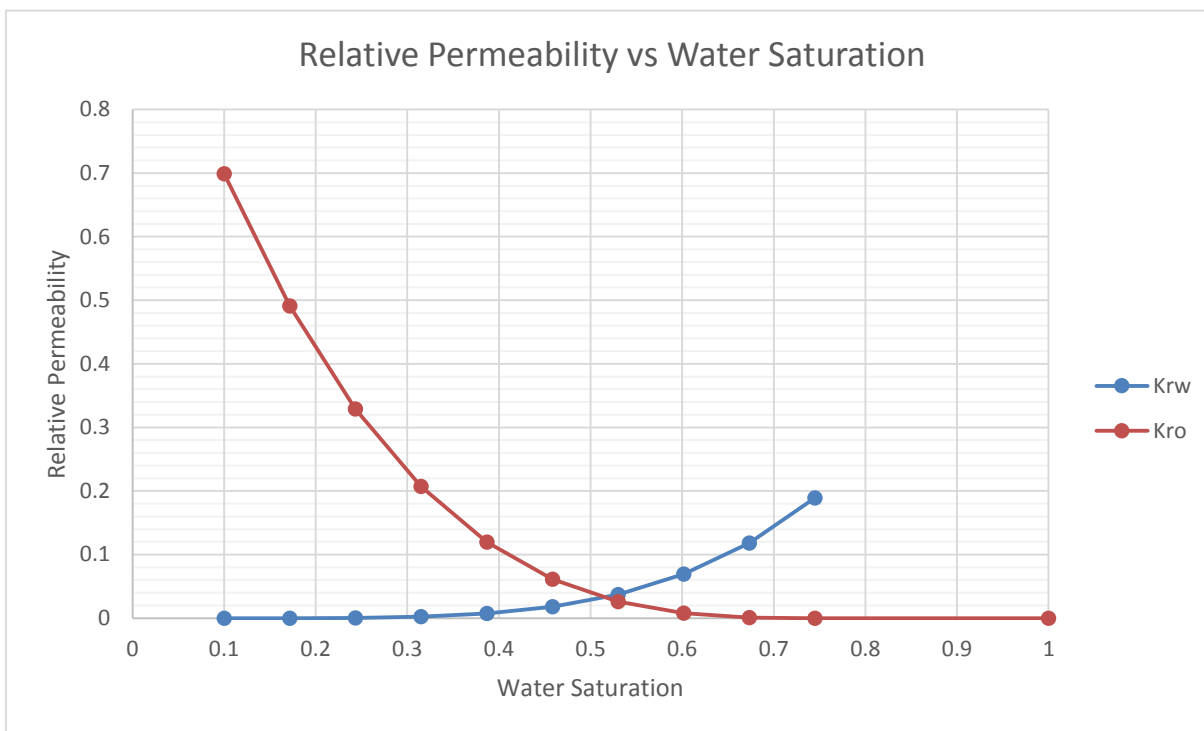
Figure 9: Oil-Water relative permeability curve.

The oil-water relative permeability curve in Figure 9 was generated with Petrel's Rock

Physics Function, using the end points specified by Paulson and Wahl (1962). At a residual oil

saturation of 25.5%, the formation's relative permeability to water is 0.175. At an irreducible

water saturation of 10%, Paulson specified an oil relative permeability 0.699 (Paulson & Wahl,

1962). This suggests that the oil phase is slightly more mobile in comparison to the water phase.

Corey exponents of three were used for both liquid phases. The same oil end points used to

produce the oil-water relative permeability relationship were also applied in the generation of the

gas-oil relative permeability.

Bennion et al. (2002) conducted a relative permeability study in an attempt to build a

database for various formations in the western Canadian sedimentary basin. Over 60 samples

from numerous reservoirs in western Canada were laboratory tested and the results were

recorded in an attempt to further the knowledge base of the relative permeability relationships of

oil-bearing formations. Samples were taken from both carbonate and sandstone reservoirs with

varying properties such as porosity, permeability and temperature. A carbonate formation, which

closely matched Turner Valley's characteristics, was selected from Bennion et al. (2002) for the

purpose of supplementing the gas-oil relative permeability relationship. The reservoir selected

had a mean temperature of 149 ^{0}F which is an exact match to Turner Valley's temperature. The

selected carbonate formation had a porosity of 9.8% and a permeability of 11.55 mD, which once

again closely matched Turner Valley's core porosity and permeability of 8% and 10 mD

respectively. Figure 10 shows the gas-oil relative permeability relationship generated using

values obtained from Bennion's et al. (2002).
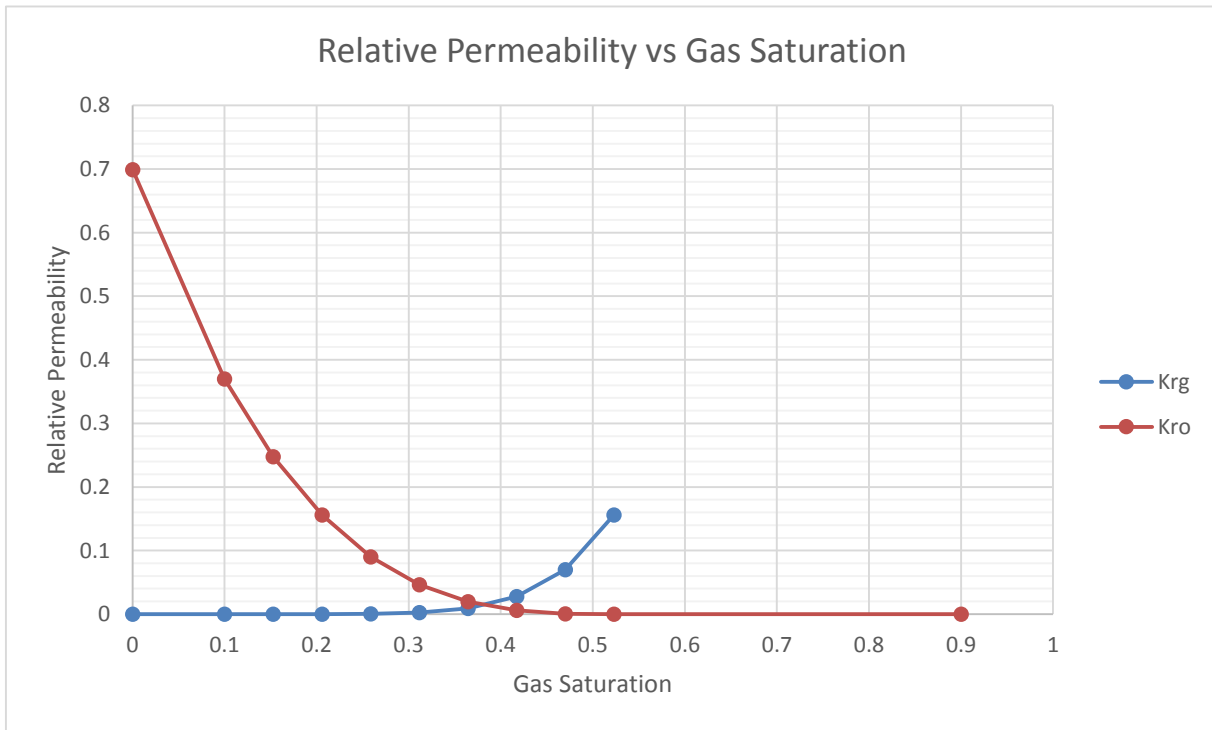
Figure 10: Gas-Oil relative permeability curve.

At a gas saturation of 52%, the database specified a gas relative permeability of 0.16. At residual gas saturation of 10%, the relative permeability for oil is 0.3 (Bennion et al. 2002). This relationship suggested that at gas saturations above approximately 53%, oil becomes completely immobile.

1.3. Case Studies

This section will discuss work that has been previously conducted on both artificial models and on real projects pertaining to nitrogen injection. A description of the physical characteristics for each reservoir will be given along with the fluid properties. The results, if available, will also be discussed.

1.3.1. Trinidad (Simulation)

A nitrogen injection project was simulated using a modeled offshore mature field in Trinidad. The sandstone reservoir is at depth of 3,340 feet with an initial pressure of 1,950 psi. The thickness of the reservoir ranged from 10 to 110 feet. The current reservoir pressure has fallen to 670 psi, much lower than the saturation pressure of 1,264 psi. The porosity and permeability ranges are 8-14% and 2-268 mD respectively (Sinanan & Budri, 2012).

The study was performed with four different scenarios: gas cap injection, oil zone injection, water zone injection, and simultaneous gas cap and water zone injection. Different parameter such as the number of injection wells and injection rates were also applied to the model. The study determined that injection into the gas cap would prove to most beneficial. The study also concluded that increasing the number of injection wells did not necessarily increase oil recovery. An increase in the number of wells and an increase in injection rates showed higher

production rates initially, but overall, these parameters shorten the lifetime of the project and lowered oil recovery due to faster nitrogen breakthrough times.

Observations were also made on the displacement mechanisms that developed throughout the course of the study. Immiscible displacement was only effective when gravitational segregation was exploited and the pressure provided by nitrogen injection was evenly distributed along the gas-oil contact. At high enough pressures, nitrogen also induced oil swelling and reduced the initially established residual oil saturation. Vaporization of the lighter hydrocarbons was another effect observed as a result of nitrogen contact. Although this increased the viscosity of the oil and consequently reduced its mobility, according to the study, this effect was "very small" (Sinanan & Budri, 2012).

A second artificial model was developed and simulations were run on several scenarios with changing porosity-permeability relationships. These relationships ranged from 15% and 20 mD up to 30% and 1000 mD. Varying degrees of dip and API gravity oils were studied with the goal of determining which of these parameters had the highest impact on nitrogen injection performance. Two producing wells were placed down dip in the 50 foot thick model with an injection well being placed up-dip. The model's pressure was set to 400 psi before the introduction of nitrogen. At a rate of 500 MSCF/day, the reservoir pressure was increased to and maintained at 700 psi (Sinanan & Budri, 2012). The result of this portion of the study concluded that the gravity of the oil and the dip of the reservoir have the greatest impact on nitrogen injection performance with very little effect attributed to the varying porosity-permeability relationships.

1.3.2. Ganhar Field – India (Simulation)

A simulation study was performed on the GS-4 reservoir of the Ganhar field located in India. The reservoir has a small inclination of approximately 1.5 degrees and is situated at a depth of 9,400 feet. The majority of the reservoir volume is populated by the gas cap; the gas-oil contacted is located at 9,700 feet and the water oil contact is at a depth of 9,875 feet. The sand has a relatively high porosity, ranging from 14% up to 22%. The permeability also has a wide range from 10 mD to-250 mD. The GS-4 reservoir has an estimated 48.8 million barrels of oil originally in place with a gravity of 42 °API. The gas cap is composed of a rich gas condensate with 307 billion standard cubic feet in place. Saturation pressures vary from 3,780 psi to 4,080 psi depending on depth. The reservoir pressure at discovery was 4,280 psi (Tiwari & Kumar, 2001).

The reservoir was first developed in 1986, and as of 2001, has had a cumulative oil production of 9.77 million barrels. In an effort to maintain reservoir pressure, currently at 4050 psi, a five-spot pattern water flood was initiated in 1991. Presently, the water is injected at an average rate of 8,050 bbl/day. A natural gas injection program began in 1997, also with the intention of successful pressure maintenance. Only five injectors were placed under operation and currently are injecting at a rate of 3.12 MMSCF/day. With no further development, the project is estimated to have a 40.2% recovery factor (Tiwari & Kumar, 2001).

A model representing 30% of the actual area covered by the GS-4 reservoir was built to perform the nitrogen injection study. The model was populated with one injector, two gas producers, two oil producers, and eight water injectors. The nitrogen injectors were placed 2.5 miles away from the gas producers to avoid contamination of the gas. The water-oil contact within the model was placed at a depth of 9,875 feet and the reservoir pressure was initially set at 4,280 psi with a temperature of 260 °F (Tiwari & Kumar, 2001).

Economics based on four different cases were examined in the study. Case one represented the current operating scheme while both case two and three included nitrogen injection. Case two and three had pessimistic and optimistic well deliverability respectively. Case four included only natural gas as the injection fluid. In addition, two scenarios were identified: scenario A was conducted under the assumption that nitrogen would be purchased from a third party while scenario B represented the capital investment of building a nitrogen production facility. Oil and gas recoveries along with the net present values of the project are summarized in Table I. Even with pessimistic deliverability, in both scenarios A and B, nitrogen injection (case 2 and 3) proved to have higher net present values and recoveries when compared to the other cases; that is the current operating scheme (case 1) and natural gas injection (case 4).

Table I: Project Evaluation for Simulation of Gandhar Oil Field (Tiwari & Kumar, 2001)

	Scenario A				Scenario B			
	Case 1	Case 2	Case 3	Case 4	Case 1	Case 2	Case 3	Case 4
NPV (MM$)	867	1158	1366	425	867	1591	1982	425
Recovery (%)	40.5	42.2	42.6	41.9	40.5	42.2	42.6	41.9

1.3.3. Carbonate Reservoir (Pilot Design)

Nitrogen injection performance in a faulted carbonate reservoir situated at a depth of 14,700 feet with an average permeability of 0.05 mD was subjected to a field study (Mungan, 2000). The porosity of the formation did not exceed 6%. The reservoir had a saturation pressure of 3,750 psi and the oil in place had a gravity of 39 °API. The oil formation volume factor was determined to be 1.75 bbl/STB with an initial solution gas-oil ratio of 1,500 SCF/bbl. The primary driving mechanism of the reservoir was fluid expansion with the presence of water influx from a small aquifer (Mungan, 2000).

Core samples from the carbonate reservoir showed the presence of micro fractures and vugs, occasionally these voids were cemented with calcite. The calcite cement accounts for as much as 15% of the pore volume. The majority of the vugs were small ranging from 1 mm to 4 mm; although, in the core samples a few larger vugs, ranging from 5 mm to 30 mm were also present. Along with calcite cement, some vugs showed the presence of asphaltenes. It is unclear whether the asphaltenes occurred naturally or if they formed during the drilling and core retrieval process. Due to the low permeability and the presence of calcite cement and asphaltenes, laboratory core tests showed that nitrogen injection pressures had to be as high as 800 psi to achieve oil displacement (Mungan, 2000).

The reservoir has an estimated 12 billion barrels of oil originally in place and after 15 years since its development, it has produced one billion barrels. Mungan et al. demonstrated that an estimated 10.5 million barrels of oil will become unrecoverable if no action was taken to preserve reservoir pressure above its saturation point.

The wells that were originally completed near the oil-water contact required recompletion at shallower depths due to severe water inflow. Water injection as a tertiary recovery method was declined for this very reason. Another concern was that water would channel through the fractures and therefore would inefficiently sweep the tight formation due to high capillary pressures, thus trapping much of the oil in place during the process.

Natural gas and carbon dioxide were fluids also considered for injection, but were soon rejected due to the high cost of natural gas and the tendency for carbon dioxide to facilitate corrosion. Air was another candidate for the pressure maintenance program but was soon declined because of its affinity to react with hydrogen sulfide. If air was injected into the formation, the reaction between oxygen and hydrogen sulfide could form a sulfur precipitate

which could reduce the permeability of the formation even further. Therefore, nitrogen injection was selected as the prime candidate (Mungan, 2000).

Tiwari and Kumar (2001) also discussed other physical properties of nitrogen that would have a positive impact on its effectiveness as an injection fluid. At the reservoir conditions specified for their study, the viscosity of nitrogen was 0.036 cp, higher than the viscosity of gas at reservoir conditions which had a viscosity of 0.03 cp. This viscosity difference produced a "reasonably" favorable mobility ratio of 0.8 between the nitrogen and reservoir gas. Equation 1 (Green & Willhite, 1998) defines mobility ratio.

$$M = \frac{\dfrac{k_{r\rho1}}{\mu_{\rho1}}}{\dfrac{k_{r\rho2}}{\mu_{\rho2}}}$$ **Equation 1**

Where,

$k_{r\rho1}$= Relative permeability of the less dense phase

$\mu_{r\rho1}$=Viscosity of the less dense phase

$k_{r\rho2}$= Relative permeability of the denser phase

$\mu_{r\rho2}$=Viscosity of the denser phase

Mobility ratios less than one are considered to be favorable. Displacement between fluids with a mobility ratio below one would exhibit a uniform displacement front. Mobility ratios greater than one result in viscous fingering. Viscous fingering generally occurs when a viscous phase is being displaced by a fluid with lower viscosity. Figure 11 shows the shape of the displacement front for a water flood and a polymer flood. Since polymer solution possesses a higher viscosity than oil, resulting in a mobility ratio less than one, a uniform displacement front develops.
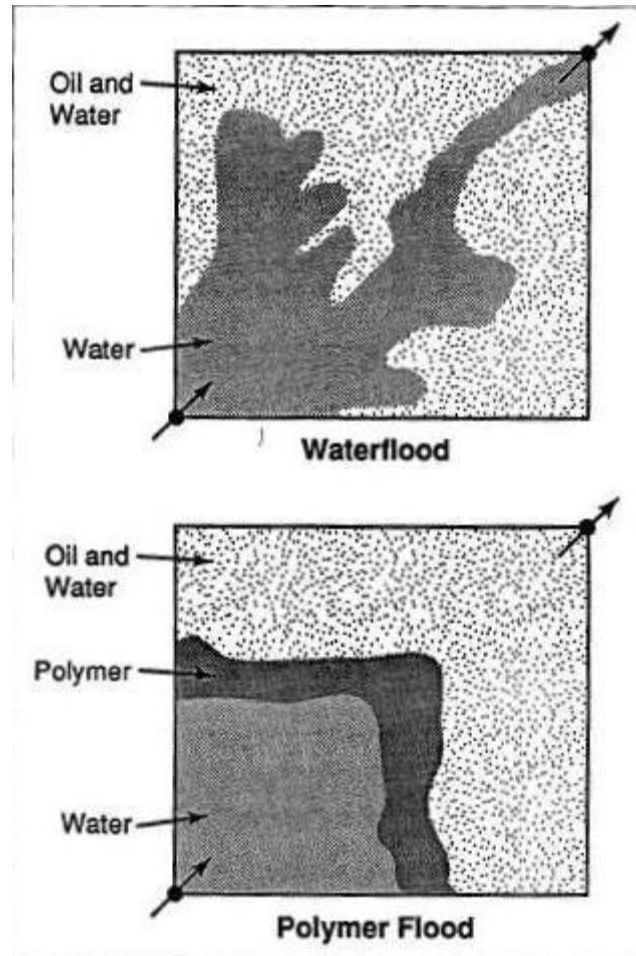
Figure 11: Shape of displacement fronts for water displacing oil and for polymer solution displacing oil (Green & Willhite, 1998).

Tiwari and Kumar (2001) also discussed how nitrogen exhibited a higher formation volume factor when compared to gas. They concluded that nitrogen would occupy 23% more volume than gas at reservoir conditions, reducing the energy required for pressure maintenance by 23% (Mungan, 2000).

Once the appropriate injection fluid was selected, the type of displacement performed by the nitrogen was defined. After reviewing capillary pressure data, it was determined that nitrogen would not succeed in displacing oil due to the presence of "ultra-high" capillary forces, therefore a miscible displacement mechanism was chosen (Mungan, 2000).

Laboratory tests were performed to determine the pressure required to achieve miscibility at reservoir conditions. Tests concluded that a minimum pressure of 6,000 psi must be realized to attain miscibility. At pressures this high, 2.89 MSCF of nitrogen would be required to replace the production of a single standard barrel of oil. Also, a four-stage compression system would be necessary to compress the nitrogen to the bottom-hole pressure of 6,000 psi. Due to these obstacles, natural gas was proposed as an intermediate injection fluid. Laboratory tests concluded that the minimum miscibility pressure would be reduce from 6,000 psi to 3,200 psi, therefore a natural gas was integrated into the program (Mungan, 2000).

The pilot project was designed as an inverted five-spot injection scheme with an injection rate of 60 MMSCF/day. With an economic limit of 500 bbl/day, the project was expected to run for three years. To monitor the project, tracers were introduced into the natural gas and nitrogen injected. Results are yet to be reported (Mungan, 2000).

1.3.4. Tensleep Reservoir (Field Case Study)

The Tensleep reservoir is located in the Elk Basin on the Wyoming-Montana border and is contained within an eroded anticlinal structure. The oil accumulation is located at approximately 4,900 feet below surface. The reservoir dips at an angle of 21 degrees on the western flank, gradually increasing to 45 degrees towards the eastern flank. It is a "well-cemented" Pennsylvanian aged sandstone (Lang, 1954) with laminations of dense dolomite scattered throughout the formation. The sand has a thickness of 200 feet and contains 35 °API oil which was initially under saturated with a saturation pressure of approximately 1,250 psi (Lang, 1954).

Early pressure-production performance showed that there was no active water drive and the primary recovery mechanism was solution-gas. The reservoir was initially non-unitized and

unrestricted gas flow was in practice. It was apparent that under these conditions, reservoir pressure would decline rapidly and recovery efficiency would be greatly reduced. Therefore unitization occurred at which point pressure maintenance of the reservoir was planned to maintain high production rates and desirable recovery factor (Lang, 1954).

Initially two pressure maintenance programs were proposed, the first being an artificial water drive through water injection below the oil-bearing zone. This option may have substantially increased recovery efficiency but unfortunately, developing a water source and the cost of drilling water injection wells would have been a sizeable financial drain. Most of the projects within the Tensleep reservoir performed gas re-injection, but the volume of gas re-injected into the gas cap was not enough to sustain reservoir pressure. Therefore, gas injection was the second pressure maintenance program considered. This option also proved to be unfeasible due to the fact that there was no source of "uncommitted" gas anywhere within 100 miles of the reservoir (Lang, 1954). As a result, inert gas (nitrogen) injection became the primary candidate for a pressure maintenance program.

Due to the high hydrogen sulfide presence within the reservoir (as high as 17%) a plant was designed to process the produced hydrocarbons and recover the sulfur from the hydrogen sulfide for commercial sale. The nitrogen required was obtained from the combustion of natural gas necessary for steam generation. The steam was used in steam turbines, generating the electricity required for plant operation. After the combustion process, the inert gas was composed of 90% nitrogen and 10% carbon dioxide with any oxygen being removed to reduce corrosion. The gas was compressed to 1,500 psig and was supplied to the field at a maximum rate of 15 MMSCF/day (Lang, 1954). The performance prior to and after the plant commenced operation can be seen in Figure 12.

After the first oil well discovery, production began to increase at an exponential rate with the introduction of more wells and reached a production rate of 16,000 bbl/day in 1948. Consequently, reservoir pressure was at a rapid decline as can be seen in Figure 12. After unitization in 1946, wells with high oil-ratios were shut in and therefore reservoir pressure began to decrease at a lower rate. Oil production began to stabilize and in 1949, production began to drop (down to 14,000 bbl/day) due to the continued decrease in reservoir pressure, eventually falling below saturation pressure (1,250 psi). After the injection of nitrogen commenced in September 1949, reservoir pressure began to increase at a steady rate. After 15 months of injection, oil production jumped up 19,000 bbl/day, clearly exhibiting the program's effectiveness. After two years of injection, reservoir pressure had climbed to almost 1,300 psi which was the targeted maintenance pressure. Monitoring of gas-oil ratios and pressure data from individual wells enabled the determination of the gas-oil contact location. Through these tests, it was observed that gas cap expansion was consistent in all areas examined (Lang, 1954).
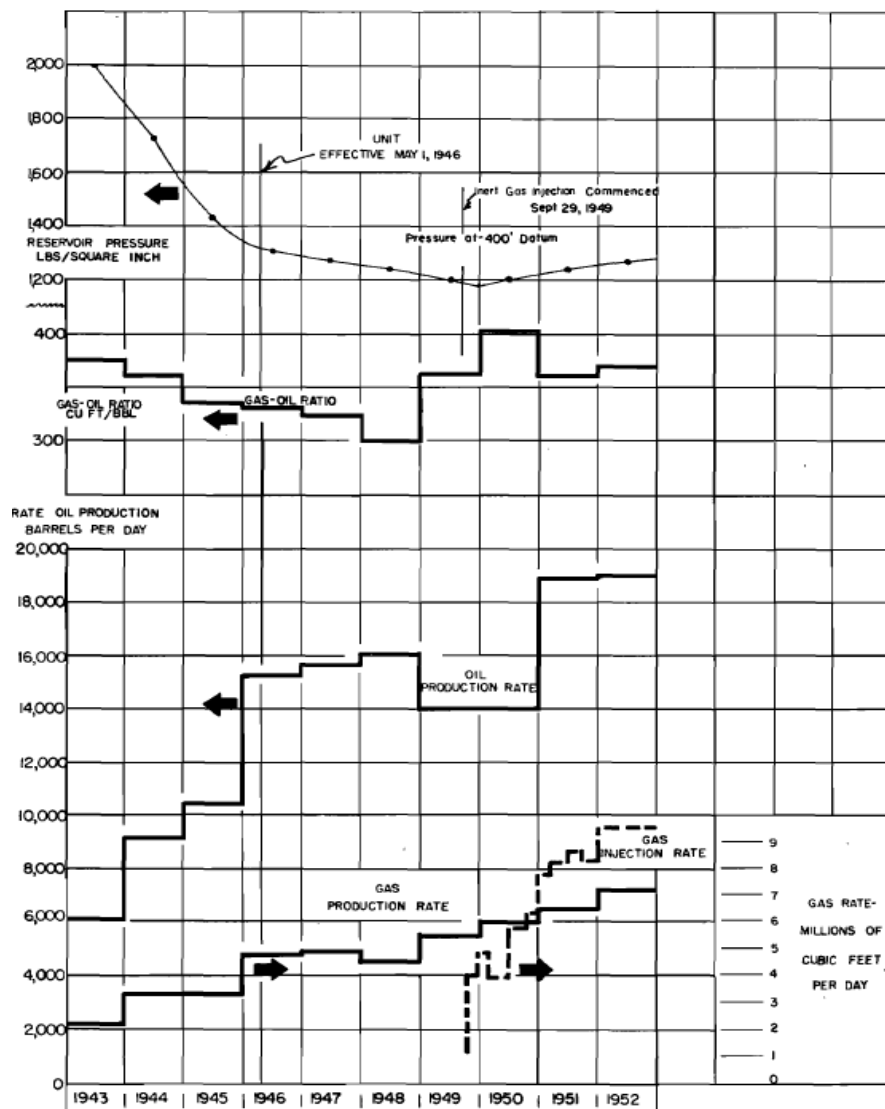
Figure 12: Tensleep Reservoir Performance (Lang, 1954)

1.3.5. Akal Field – Mexico (Field Case Study)

A nitrogen injection program was performed on the Akal field, located 49 miles offshore

from Campeche, Mexico. The field is approximately 7,550 feet below sea level. Its initial

reservoir pressure was approximately 3,800 psi with an oil gravity of 22 °API. The field was

under-saturated at discovery. It is composed of naturally fractured, vuggy carbonates. Porosities

within the field vary from 7% to as high as 25% with an average of 10%. The average

permeability is 0.3 mD with secondary porosity (fractures and vugs) attributing to permeably as high as 5,000 mD (Rodriguez et al.,2001).

The Akal field began production in 1979, with the first well having an initial production rate of 34,000 bbl/day. In 1981, the field reached a production rate of 1.16 MMbbl/day and through the use of 150 gas-lift assisted wells, the field reached a production rate of 1.6 MMbbl/day by 1997. Primary depletion caused the reservoir pressure to drop down to 1500 psi, forming a secondary gas cap, extending the initial gas cap down to 6,330 feet below sea level. Water influx from the present aquifer also migrated the oil water contact up to 8920 feet subsea, 1,575 feet above its original position (Rodriguez et al.,2001).

Reservoir forecasts of the Akal field showed that if tertiary recovery was not conducted, under natural depletion, by 2004 the reservoir pressure would decline to 1300 psi and the production rate would drop to 3,200 bbl/day. Under primary recovery, it would take 80 years to produce the reserves currently in place (Rodriguez et al.,2001). This would require the replacement of offshore equipment and facilities which would prove to be a heavy financial drain. Therefore, nitrogen injection was considered to accelerate depletion.

Simulations were run for the nitrogen injection program and the results showed that to achieve the desired 2 MMbbl/day production rate, an injection rate of 5,000 MMSCF/day of nitrogen would be required. Under these circumstances, after four years of injection the oil production rate would begin to decrease, lowering the nitrogen injection rate required. The project had an estimated recovery of 1324 million standard barrels of oil and 870 billion cubic feet of gas (Rodriguez et al.,2001). Reservoir performance of the Akal's field, since its first production, is shown in Figure 13. There is only one year of nitrogen injection performance available and therefore the project's effectiveness is open to interpretation. According to Figure

13, there was a steady pressure decline until nitrogen injection commenced, at which point the reservoir pressure seems to begin to stabilize. In the second half of the field's life, oil rate was dependent on and paralleled the number of wells producing. When nitrogen injection began in the year 2000, the oil production rate seems to spike even though there was no introduction of any new wells.
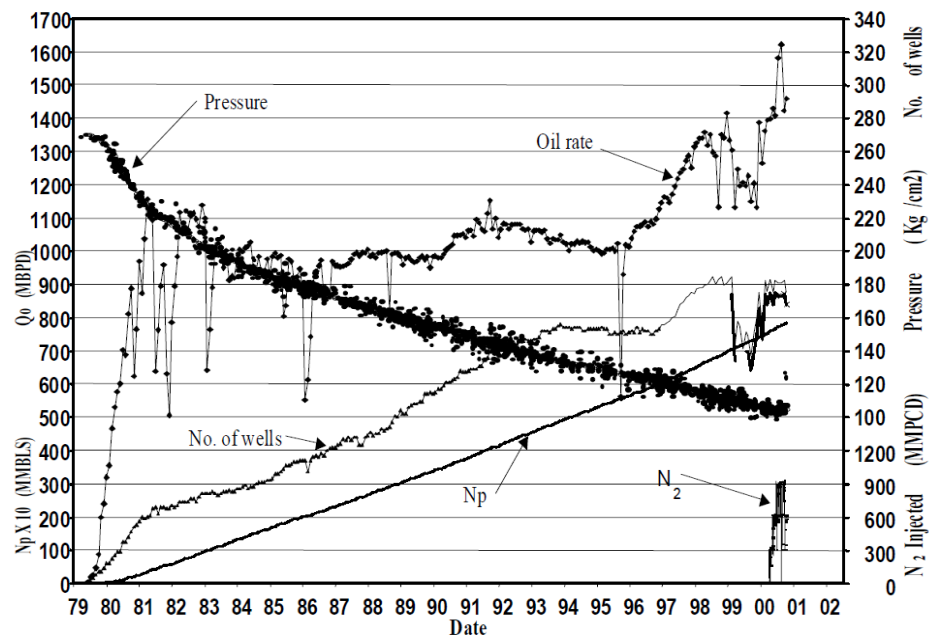
Figure 13: Akal Reservoir Performance (Rodriguez et al., 2001)

1.4. Literature Review Summary

Table II shows a summary of reservoir characteristics, fluid properties, and results of the case studies reviewed. Table II also makes a comparison between the case studies' reservoir properties to nitrogen injection screening criteria specified by Green and Willhite (1998).

Table II: Case Study Reservoir Characteristics and Results Summary

	°API	Viscosity (cP)	Formation	Net Thickness	Depth (ft)	Results
Willhite & Green Nitrogen Injection Criteria	>35	<0.4	Conventional (sandstone or carbonate)	Thin unless dipping	>6000	-
Artificial Reservoir (Trinidad Study)	Varied (25-30)	NA	Sandstone	50 ft with dip (from 10° to 30°)	NA	Study concluded that the porosity-perm relationship had very little impact when compared to dip and API gravity.
Ganhar Field (India)	42	NA	Sandstone	>200 ft	9400	Increased recovery by 2%.
Tensleep Reservoir (USA)	30	NA	Sandstone	200 ft with 21°-45° dip	4900	Increased reservoir pressure and production.
Akal Field (Mexico)	22	NA	Carbonate	NA	7550	Stabilized declining reservoir pressure and increased production.
Turner Valley (Canada)	>40	0.36	Limestone	100 ft with >60° dip	>6500	-

The simulation study performed on the Ganhar field (Tiwari & Kumar, 2001)and the

actual implementation of nitrogen injection in the Tensleep reservoir (Lang, 1954)and the Akal

Field (Rodriguez et al.,2001) showed promising results. Based on net present values and

recoveries, the Ganhar field simulation concluded that when compared to the operating scheme

currently in place, nitrogen injection proves to be a favorable alternative. The Tensleep reservoir

and the Akal field both showed signs of reservoir re-pressurization and increased oil rates after

the implementation of nitrogen, showing the effectiveness of the nitrogen injection program.

The Trinidad study showed that dip of the formation and the gravity of the oil have the most impact on the effectiveness of the nitrogen injection. Sinanan and Budri (2012) observed that crestal gas cap injection for immiscible displacement with nitrogen produced the best results, exploiting the gravitational segregation between the nitrogen and the oil.

Upon comparison to the fields mentioned above, Turner Valley shows potential for nitrogen injection. The field's oil gravity ranges in values all greater than 40 °API, depending on the location of the structure. Also, due to its high structural relief over relatively short distances, the inclination of Turner Valley reaches values as high as 60°. The Turner Valley oil field not meets all screening criteria and compares favorably to the characteristics of the fields that have already shown varying degrees of success after the implementation of nitrogen injection.

Taking into account Turner Valley's characteristics and the favorable properties exhibited by nitrogen, nitrogen seems to be a promising injection fluid. Although natural gas is more miscible with reservoir fluids, it is an expensive alternative due to its high heating value. Carbon dioxide is another option for injection, but supply is more difficult to attain due to the absence of carbon dioxide pipe lines. There is virtually a unlimited supply of nitrogen seeing how air is composed of 78% nitrogen. Also, nitrogen is an inert gas while carbon dioxide poses corrosion problems and natural gas is an explosive hazard.

2. Method

2.1. Structure Development

The first task of the project was to build an accurate representation of the Turner Valley

structure. An attempt was made to recreate the structure using formations top picks obtained

from AccuMap, which were present along the trajectory paths of most of the wells. It should be

noted that the Turner Valley and Rundle formation top picks obtained from AccuMap were

occasionally used interchangeably, leading to in accuracies in the generated surfaces. Due to the

faulting of the Turner Valley field, the surface generated using this method for the southern

portion of the field (Figure 2) could have potentially been inaccurate. Figure 14 illustrates the

resulting surface generated from the formation top picks.
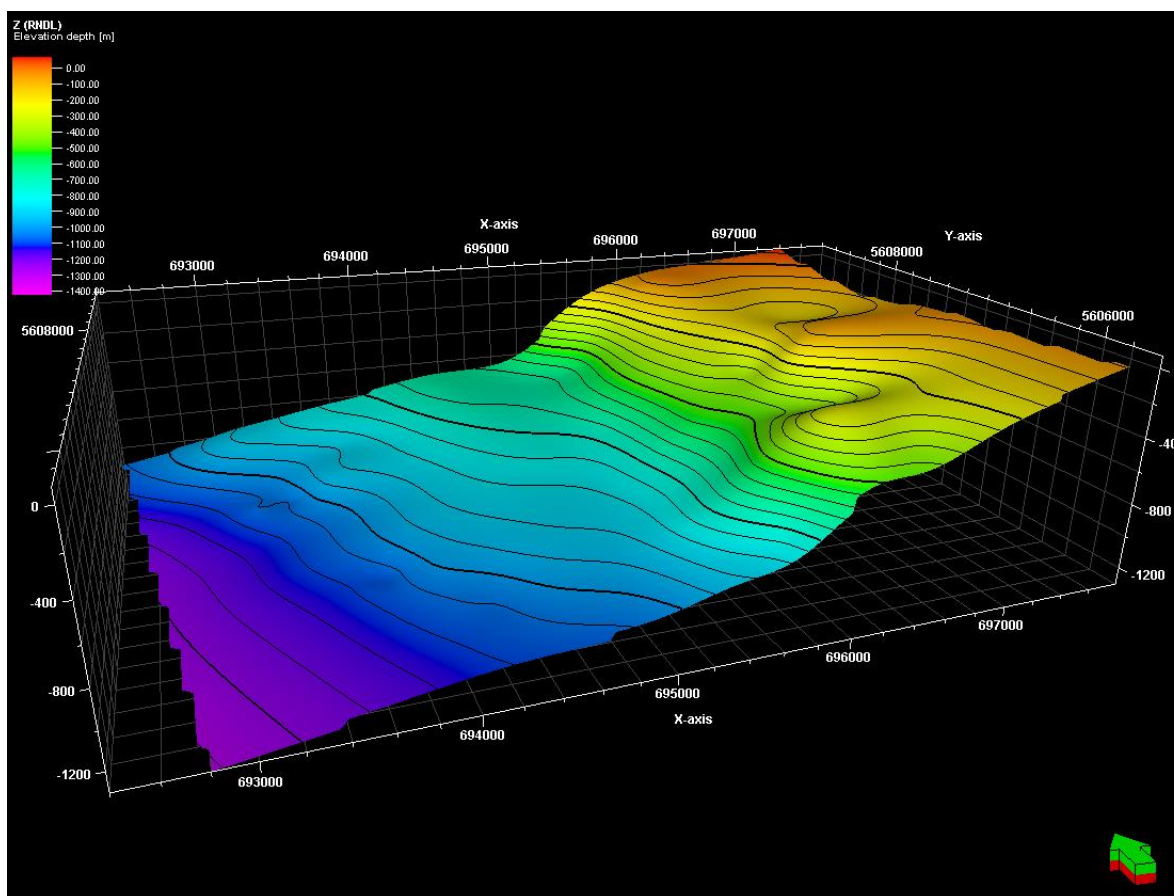
Figure 14: Turner Valley surface generated using formation top picks.

To verify the accuracy of the surface shown in Figure 14, seismic interpretation was used
as an alternative method of surface generation. Devon Energy agreed to work with Montana
Tech and donated two 2D seismic lines located in the southern portion of the Turner Valley field.
Figure 15 is a map of southern Turner Valley which displays the location of the obtained seismic
sections, outlined in red. The field is outlined by existing completed wells, represented by the
black dots.
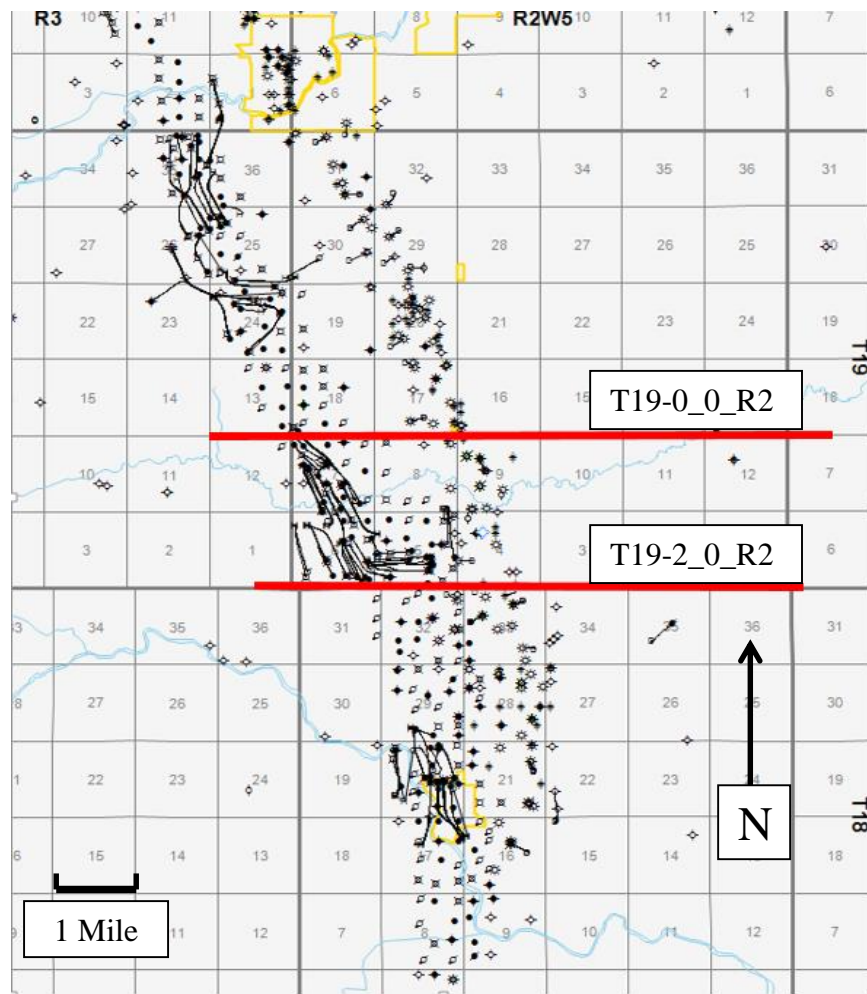
Figure 15: Township map (Generated in AccuMap)of the location of the two 2D sesmic lines.

The seismic lines are parallel and separated by two sections; approximately two miles apart. Although the lines enclose an area of roughly 12 square miles (7680 acres), the area of study was constrained to six square miles (3840 acres). As can be seen from Figure 15, the Turner Valley field occupies only half the area enclosed by the two parallel seismic sections. The area of study was selected primarily as a result of the available seismic and log data. Figure 16 and Figure 17 show sections of seismic lines T19-2_0_R2 and T19-0_0_R2 respectively. A comparison was made between Figure 16 and Figure 17, and it was concluded there was no substantial variation in the structural subsurface between the two lines.
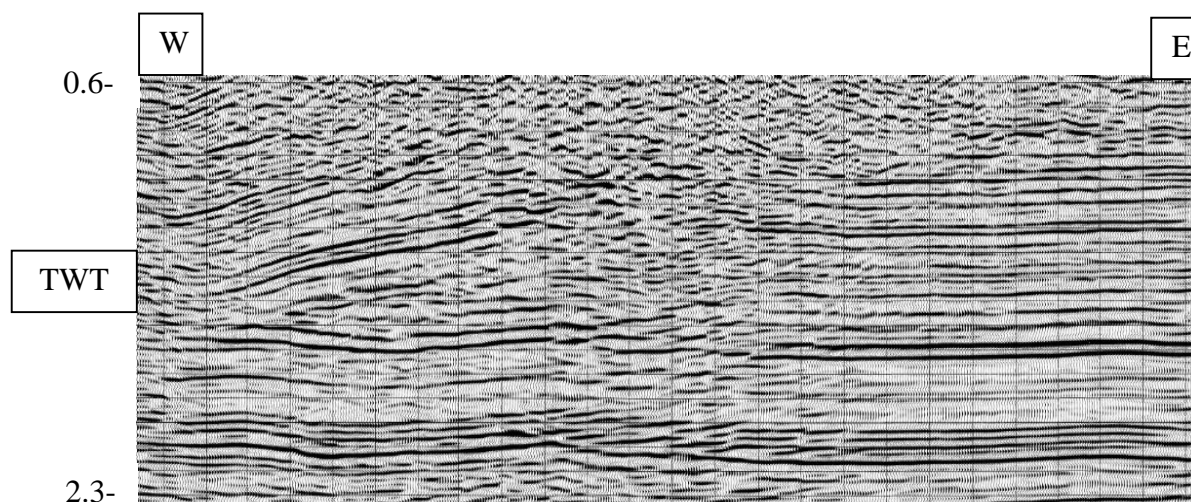
Figure 16: Northern (T19-0_0_R2) 2D sesmic section.
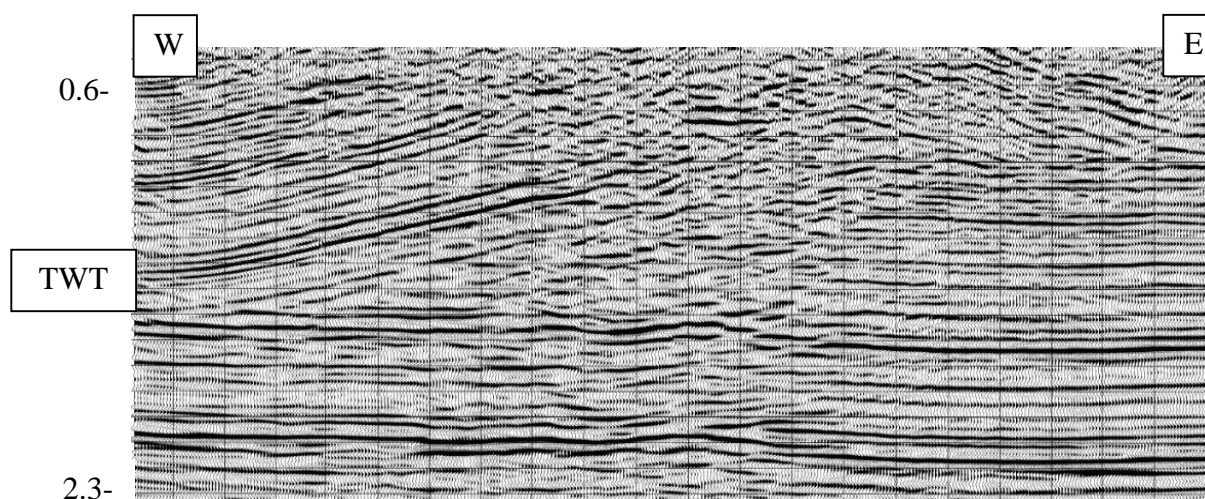
Figure 17: Southern (T19-2_0_R2) 2D sesmic section.

The northern line, T19-0_0_R2, has a total of 408 common depth points (CDP) which are spaced 82 feet apart, with a total length of 6.3 miles. The southern line, T19-2_0_R2, has a total of 336 CDPs, also spaced 82 feet apart, with a total length of approximately 5.2 miles. Both lines were shot by Anderson Exploration LTD in 1980 and were processes by Kelman Technologies in 2000. The seismic sections shown in Figure 16 and Figure 17 are oriented from west to east.

The seismic data was received in SEG-Y format, but had no coordinates allocated to the CDPs. The coordinates were required to position the seismic profiles in the model space. A map of the location of the lines and the station numbers was provided by Devon; this map is shown in Figure 18.
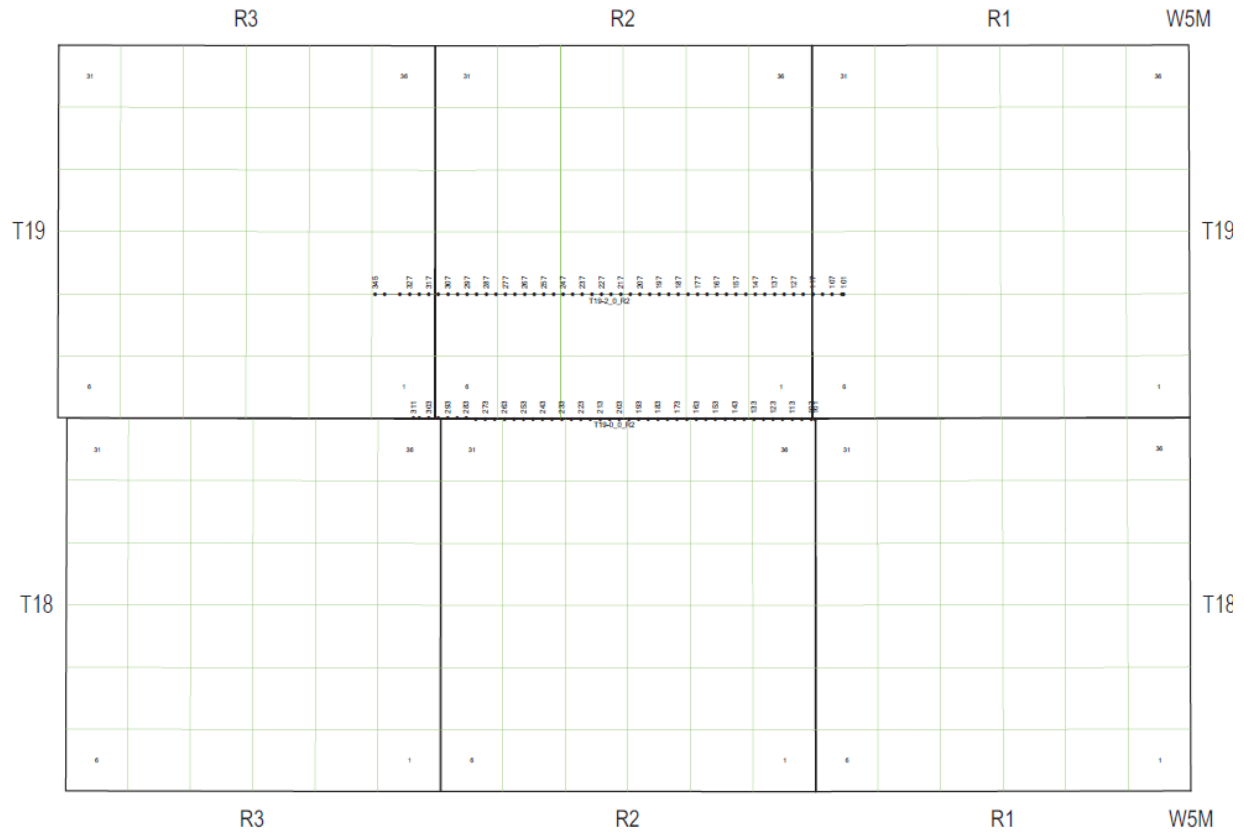
Figure 18: Township map used to determine CDP coordinates.ref

To define the coordinates of the CDPS, the exact coordinates of the south-eastern corner of section 1, the south-western corner of section 6, the north-eastern corner of section 7, and the north-western corner of section 12 were obtained. These values, along with Figure 18, were entered into ArcMap and the coordinates of the continuous seismic line and therefore the coordinates of the corresponding CPDs were found.

Using Petrel's seismic interpretation tools, the faults and the surface of the Turner Valley field were traced on both lines. The interpretations of both lines are shown in Figure 19 and Figure 20; the white line represents the Turner Valley surface pick while the colored lines represent the interpreted faults. The blue line represents the major thrust fault overlain by the Turner Valley Formation, bounding the reservoir on the eastern flank. To determine the location of the Turner Valley horizon on the seismic section, the formation depth (obtained from available formation top picks) was used in conjunction with the velocity picks provided by Devon. Line T19-2_0_R2 was of relatively high quality, thus the faults and surfaces were easily picked. The northern seismic line was of slightly lower quality after importation into Petrel, and it was difficult to determine if and at which location the faults connected between the two seismic lines. To successfully generate a fault, two planes must be present in the model space to attach the initial traces, forming a faulting plane between the two seismic planes. Therefore only faults that were continuous from the southern seismic line to the northern seismic line could be realized. 3D seismic would have alleviated this problem, but no such data was available at the time.
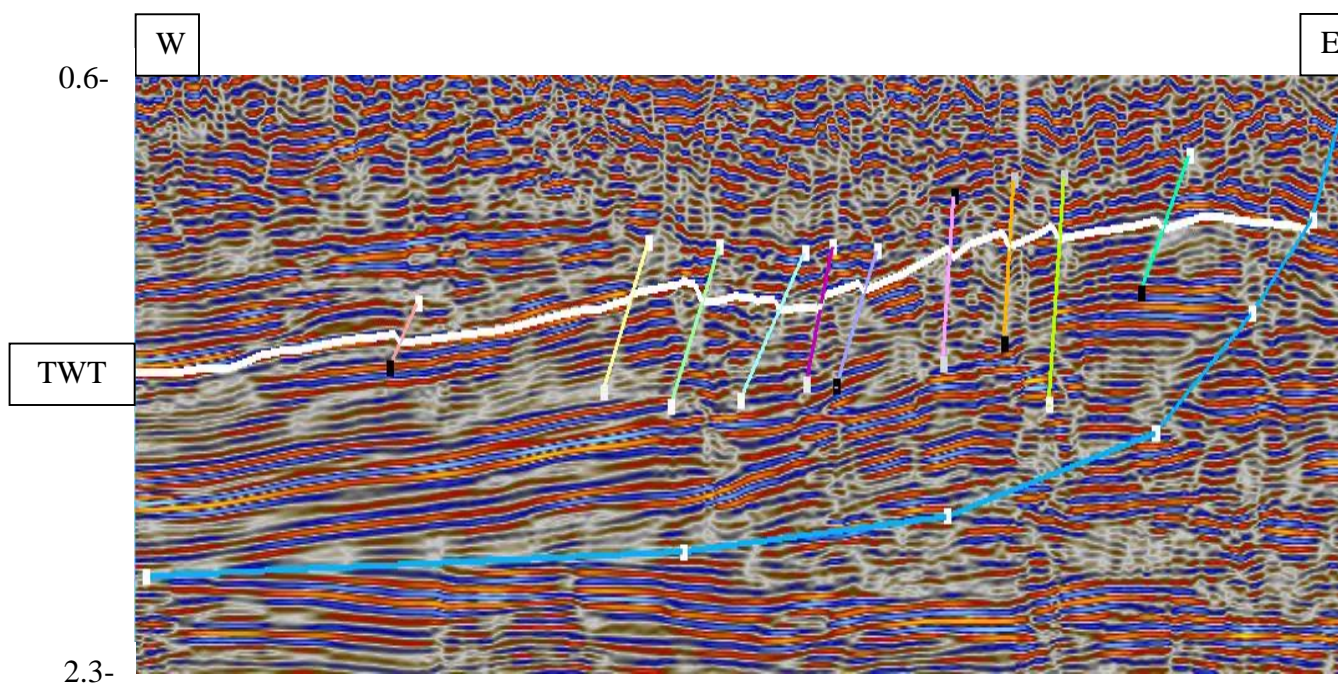
Figure 19: Interpreted southern (T19-2_0_R2) 2D sesmic section.
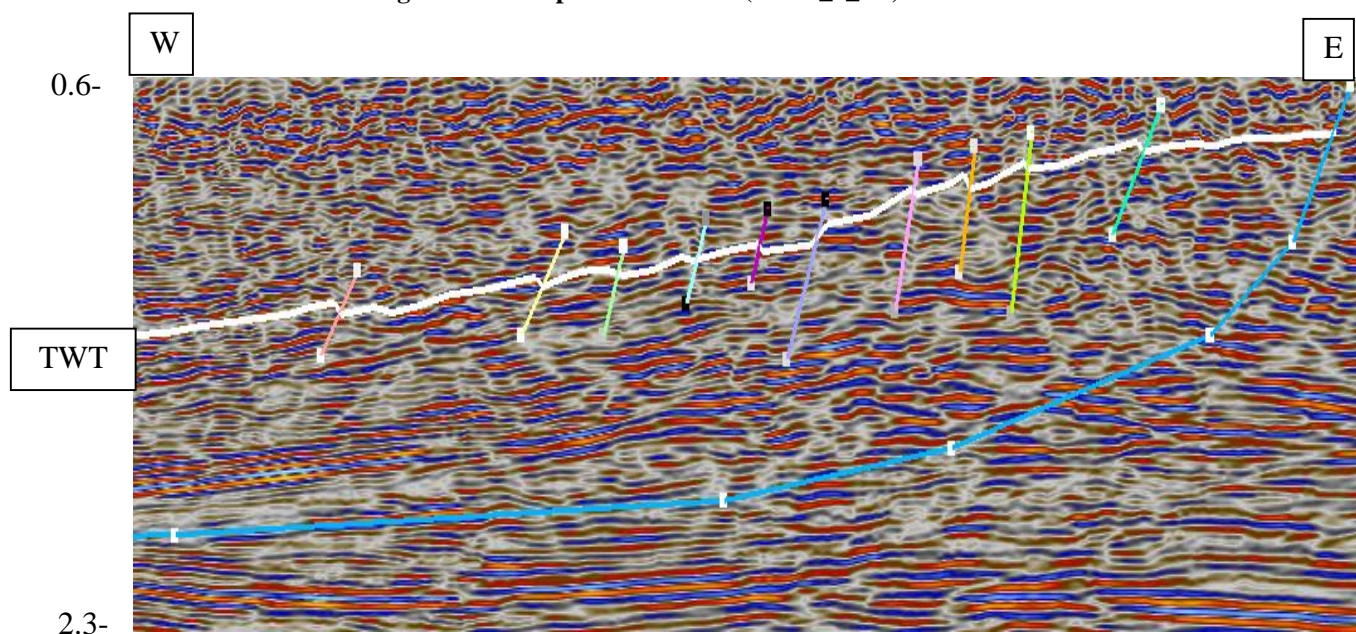
Figure 20: Interpreted northern (T19-0_0_R2) 2D sesmic section.

Once interpretation of the seismic lines was complete, the fault and surface
interpretations had to be converted from the time domain to the depth domain. As stated
previously, Devon Energy provided velocity picks that corresponded to several CDPs scattered
along the length of the seismic line; each velocity pick was accompanied by a two way travel

(TWT) time. Figure 21 shows a plot of TWT time vs Velocity. The plotted points have a relatively close cluster and the best-fit line applied to the data had minimal error. The total variance of data about the line of best fit (R^2), had a value of 0.9589, implying a close to ideal fit.
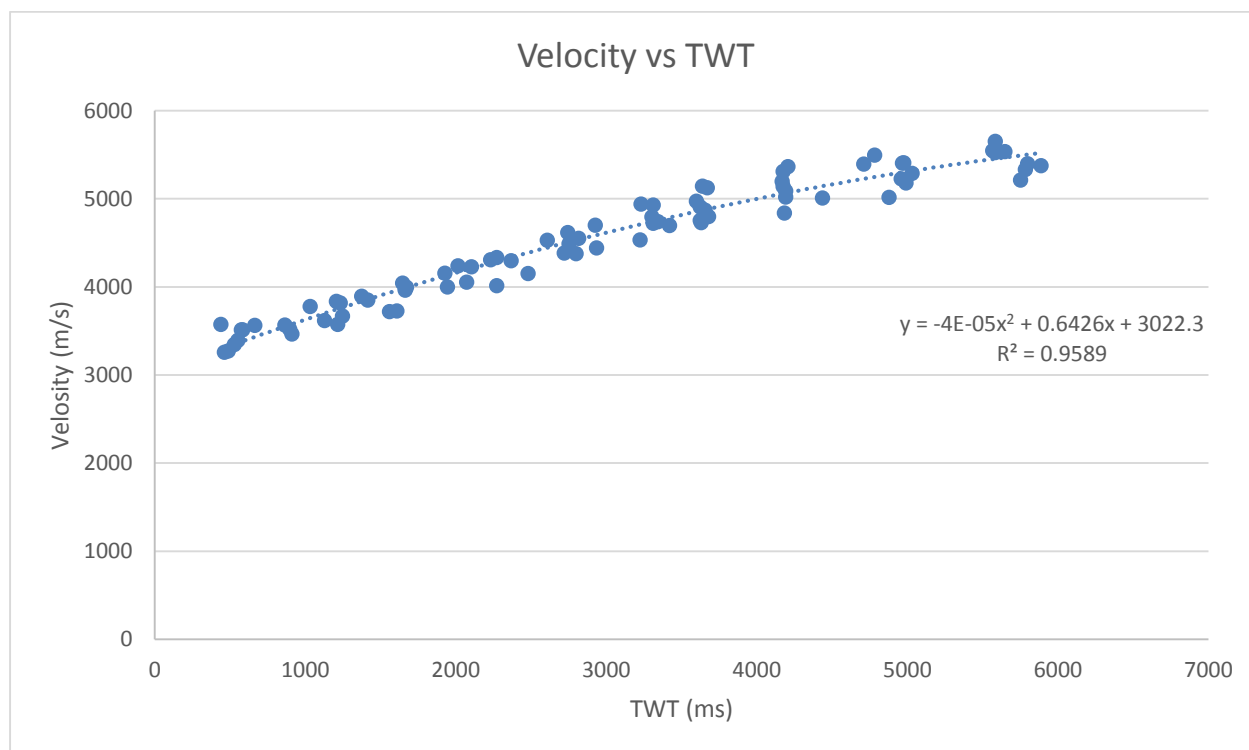
Figure 21: Velocity model used to develop a velocity-TWT relationship.

To build an adequate velocity model for conversion from the time domain to the depth domain, an average velocity property was required. For the purpose of property population, a grid with dimensions of 13,287 feet by 20,636 feet was created which was of sufficient size to envelope the entire area of study. The function obtained from Figure 21 was then imported into Petrel and used for creating the average velocity property, which populated the newly created grid. The average velocity property was then used to create the velocity model and subsequently convert the fault and surface picks to the depth domain. Figure 22 illustrates the average velocity

property that was used in the creation of the velocity model. Figure 22 shows a uniform average velocity property which is verified by the tight scatter seen in Figure 21.
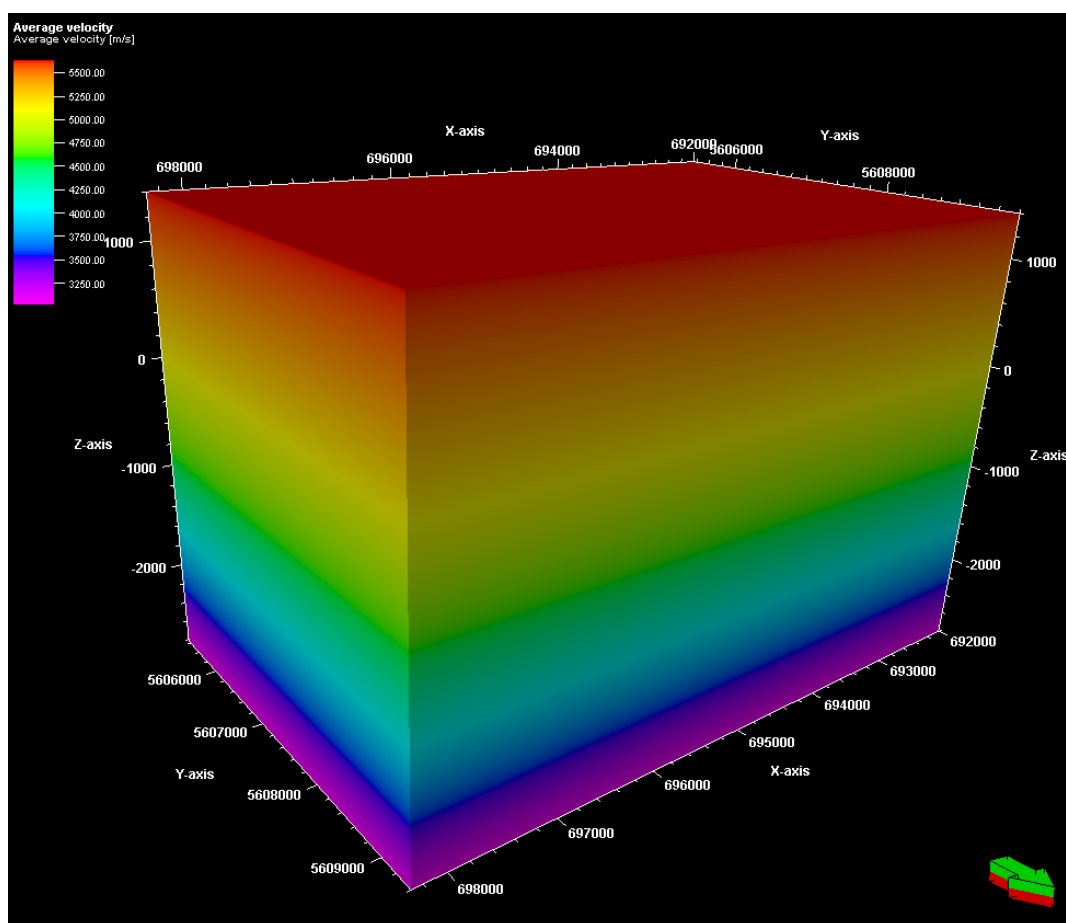
Figure 22: Generated spacial average velocity property.

A total of 10 faults were interpreted from the obtained seismic lines. There are two thrust faults which are located down dip, or the western portion of the structure. The remaining eight are reverse faults and are located further up-dip, or on the eastern portion of the formation.

Once the seismic interpretations had been generated and converted to the depth domain, steps were taken to conclude if the faults present were sealed. An initial attempt was made to determine the sealing nature of the faults by examining the observed water injection and production history of injectors and producers that were located across a fault from each other.

Figure 23 shows the placement of the producers and injectors, along with the location of each fault.
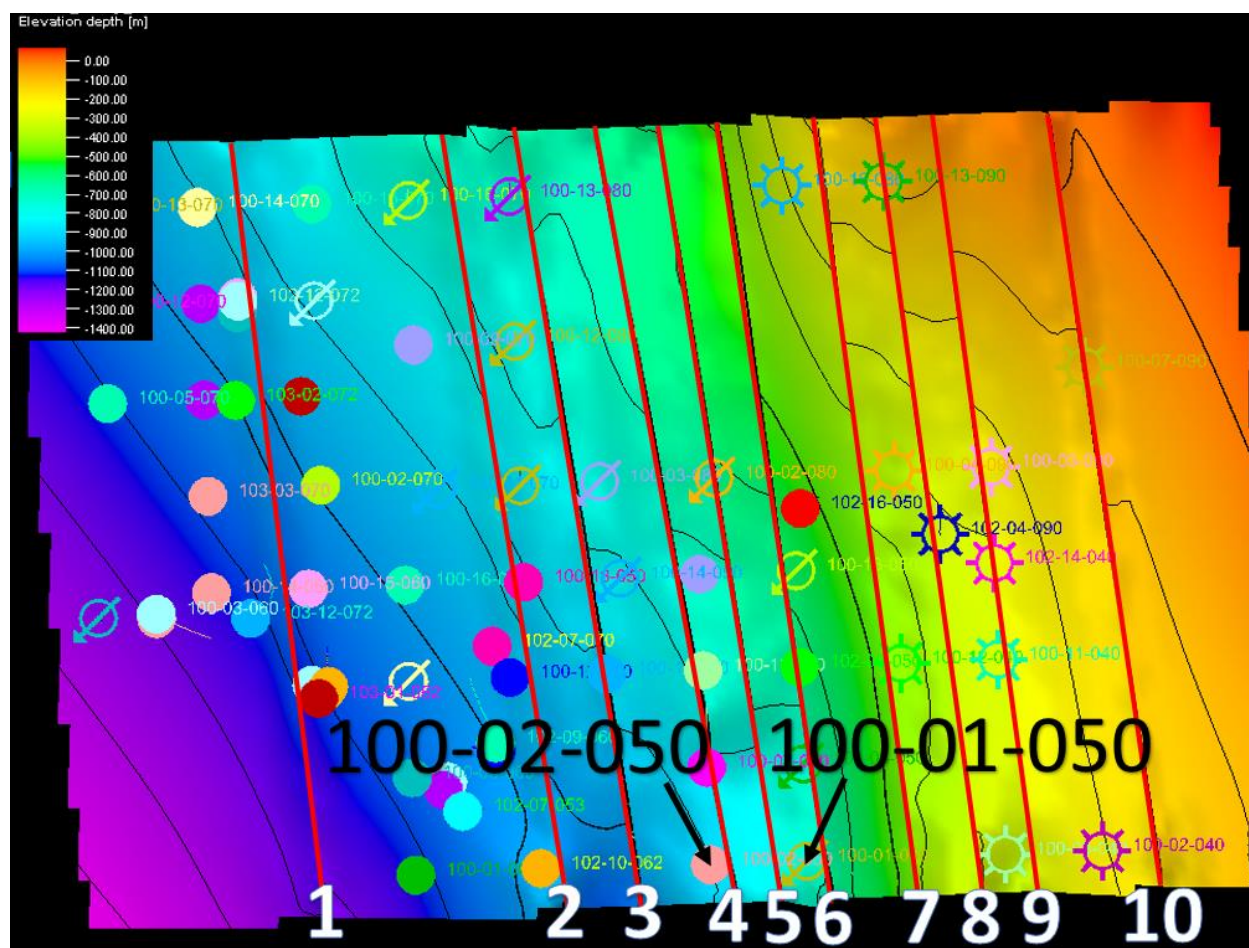
Figure 23: Turner Valley surface and faulting placement.

The faults have been numbered for convenience and are represented by the red lines. Wells 100-02-050 (producer) and 100-01-050 (injector) were initially chosen for inspection due to their location and separation by faults 4 and 5. After examining the observed production from well 100-02-050, it was determined that water production occurred in the oil well before water injection began at well 100-01-050. After further examination, this method proved to be unreliable due to the long water transition zone present above the water/oil contact. This is because the water production that occurred at 100-01-050 could be attributed to the migration of

the oil water contact. Figure 24 is a plot of water saturation and capillary pressure, which illustrates a substantial transition zone.
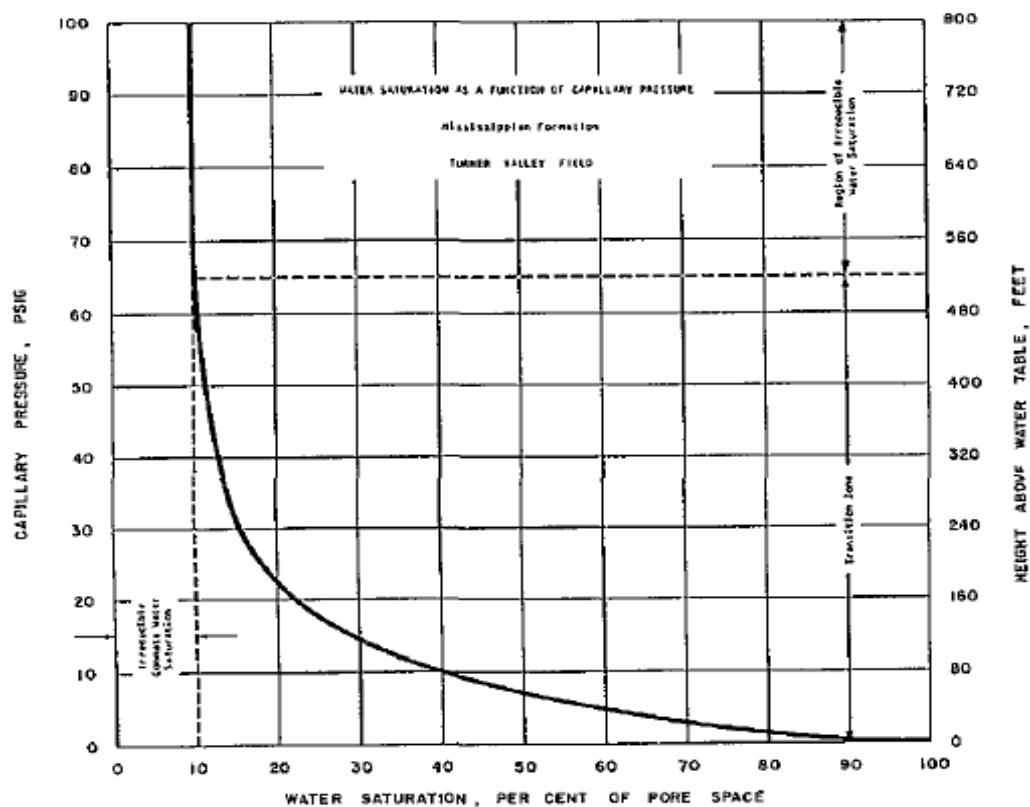
Figure 24: Turner Valley Capillary Pressure Curve (Paulson & Wahl, 1962).

The capillary pressure curve in Figure 24 shows that the irreducible water saturation is at 10%, extending the water transition zone 520 feet above the water/oil contact. Since the water-oil contact is located at 4,500 feet subsea and all wells have been completed at depths no greater than 4,101 feet subsea, it was determined that the water production experienced before water flooding commenced was due to the migration of the transition zone and the oil water contact. This implies that the faults present in Turner Valley do not segment the reservoir.

The thickness used in the model was determined through the examination of the formation top picks. The differences in depths throughout the model space between the Turner Valley and the Shunda were averaged and applied as constant thickness of 722 feet, creating the base surface of Turner Valley. Turner Valley and Rundle formation top picks obtained from the AccuMap database were interchangeably; attributing to the greater thickness of the Turner Valley formation than what was described in the literature review. Thus, the thickness of the reservoir was used as a history matching parameter.

Both surfaces (Turner Valley top and base) and the accompanying faults were used in producing a fault framework. The framework was then used to generate the final model grid for simulation. The dimensions of the grid are 110x69x60 with 160 feet increments in both the x and y direction.

2.2. Reservoir Characterization

A total of 12 logs from 12 wells within the study area were taken from the petroleum database AccuMap. Figure 25 shows the wells with accompanying logs and the purple polygon representing the modeled boundary. As can be seen from Figure 25, all the logs obtained from AccuMap are located in the western section of the field.
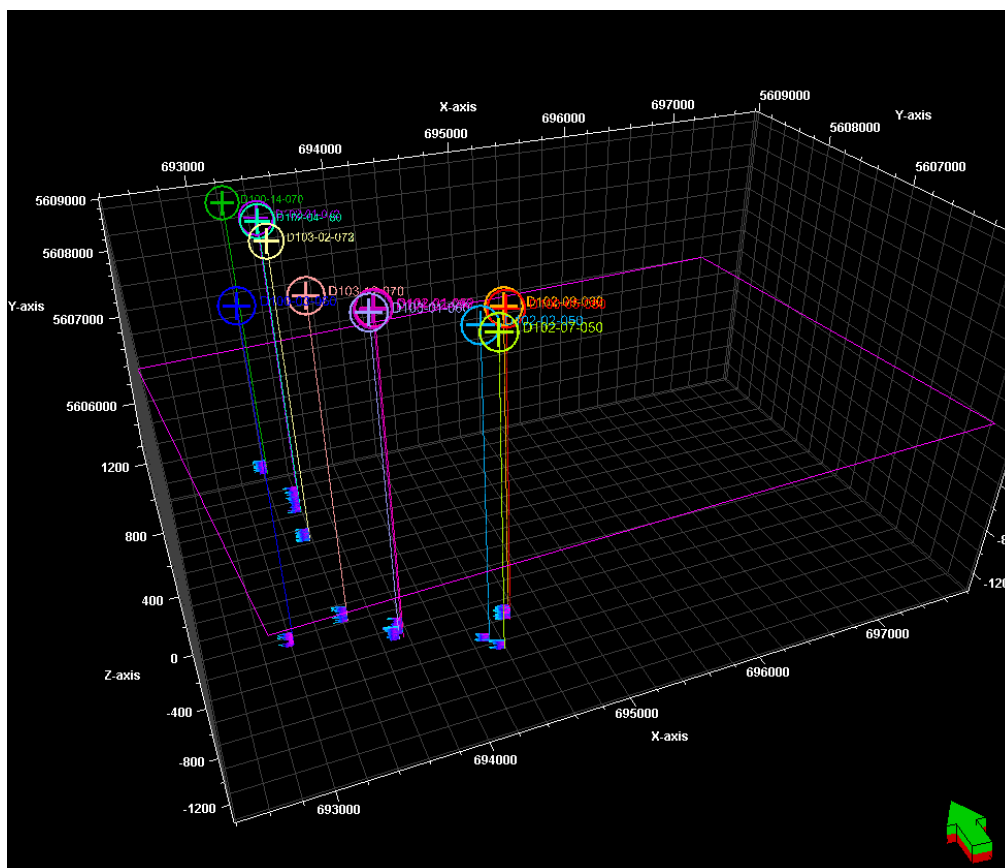
Figure 25: Locations of the wells possessing logs in the model space.

The logs shown in Figure 25 were all recorded on a true vertical depth scale. This was true even for wells that were deviated or had a horizontal leg. Most of the well paths were deviated which posed a problem with placing the wells logs accurately along the well path, subsequently causing inaccurate depth placement. To solve this problem, dummy vertical wells were created for the purpose of matching the correct true vertical depth values with those recorded in the well logs. The well log placement along the original measured depth deviated path of well 102-02-050 is shown on the right hand side of Figure 26. To the left of the original well path is the dummy vertical well accompanied by the corrected true vertical depth log. Figure 26 also shows a side by side comparison of the depth values assigned to the porosity log for both

the original and dummy vertical well. Assigning true vertical depth logs along a measured path

results in high placement when compared to the dummy wells.
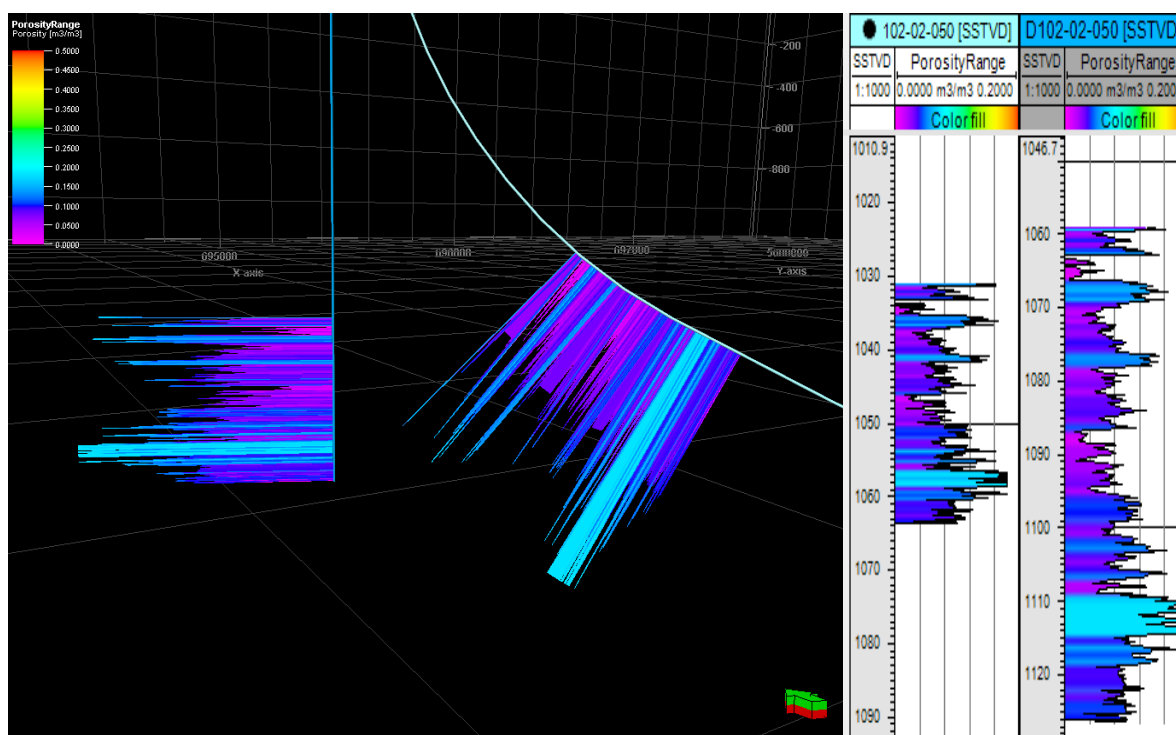
Figure 26: Comparison between the logs on a true vertical track and a measured depth track.

The greatest distance between the log on the vertical dummy path and the log on the

original deviated path is 656 feet. This is a separation when taking into account the entire scope

of the modeled area. To confirm if re-locating the logs a short horizontal distance from the

original well path was acceptable, the values and locations of the porosity logs were examined.

This was done to determine if there was an obvious relationship between positioning and

porosity values.

Evaluation of the porosity logs suggested major changes in porosity are experienced only

when traveling from the western flank to the eastern flank of the formation (along the x-axis of

the model). In the longitudinal direction, or in the north-south direction (along the y-axis of the

model), the porosity logs suggest that the reservoir is relatively homogenous, meaning that there are no great changes with respect to porosity. Figure 27 shows two logs corresponding to wells separated by 728 feet along the y-axis and 5623 feet along the x-axis. Figure 27 also compares well logs that are separated by 4646 feet along the x -axis and 1877 feet along the y-axis.
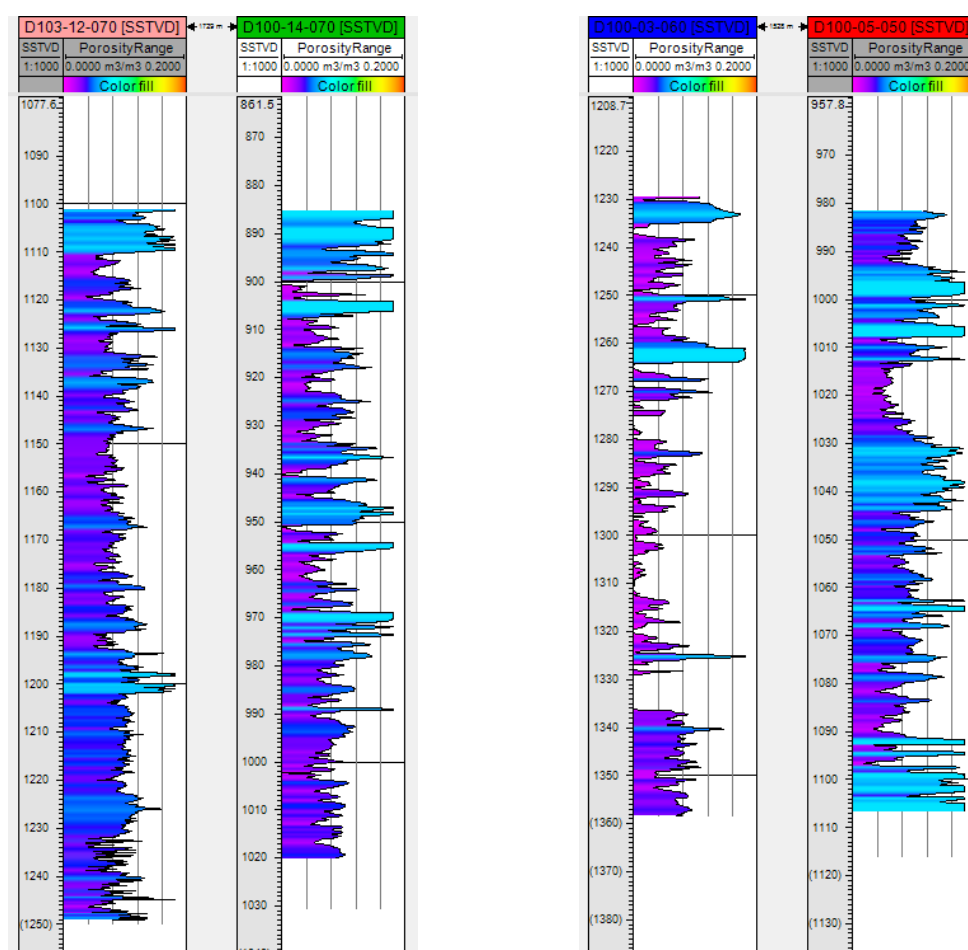
Separation x-axis: 728 ft Separation y-axis: 5623 ft   Separation x-axis: 4646 ft Separation y-axis: 1877 ft

Figure 27: Log comparison based on seperation in the x and y direction.

The logs in Figure 27 show that there is no substantial variation in porosity values in the y direction at similar depths. Since the vertical dummy wells are in close proximity to the original deviated path, and are not located a considerable distance up-dip or down-dip of the

original well, the assumption can be made that relocation of the logs a short distance away acceptable.

All imported well logs were density porosity logs; the porosity values were determined using three different matrixes including sandstone, limestone, or dolomite. Considering that the Turner Valley formation is primarily dolomite, all logs using sandstone or limestone matrix had to be converted to the dolomite. Equation 2 was initially applied to convert all porosities to bulk density values. Using Equation 2, a sandstone density of 2.65 g/cc was applied to the sandstone matrix logs and a limestone density of 2.71 g/cc was applied to the limestone matrix logs. Equation 1 was then rearranged to solve for porosity using dolomite bulk density of 2.87 g/cc to create a converted matrix porosity log. The logs used specified a fluid density of 1.00 g/cc.

$$\rho_b = \rho_{ma}(1 - \emptyset) + \rho_{fl}\emptyset$$

Equation 2

Where,

$\emptyset = porosity$

$\rho_{ma} = matrix\ density$

$\rho_b = bulk\ density$

$\rho_{fl} = fluid\ density$

The layering of the model was determined considering how well the up-scaled log data fit the actual recorded porosity values. All well sections containing logs were examined and initially 30 layers seemed to be a sufficient number of layers for a representative up-scaled porosity. Figure 28 shows wells sections for three wells; the top of each section is labeled with the well identification number. Each well section is split into two tracks, the left hand side represents the actual record porosity values after matrix conversion and the blocks on the right hand side represent the layers generated in the model. Most logs do not extend through the entire modeled reservoir. Figure 28 shows the portion of the wells sections that have log data with 30 layer spacing.
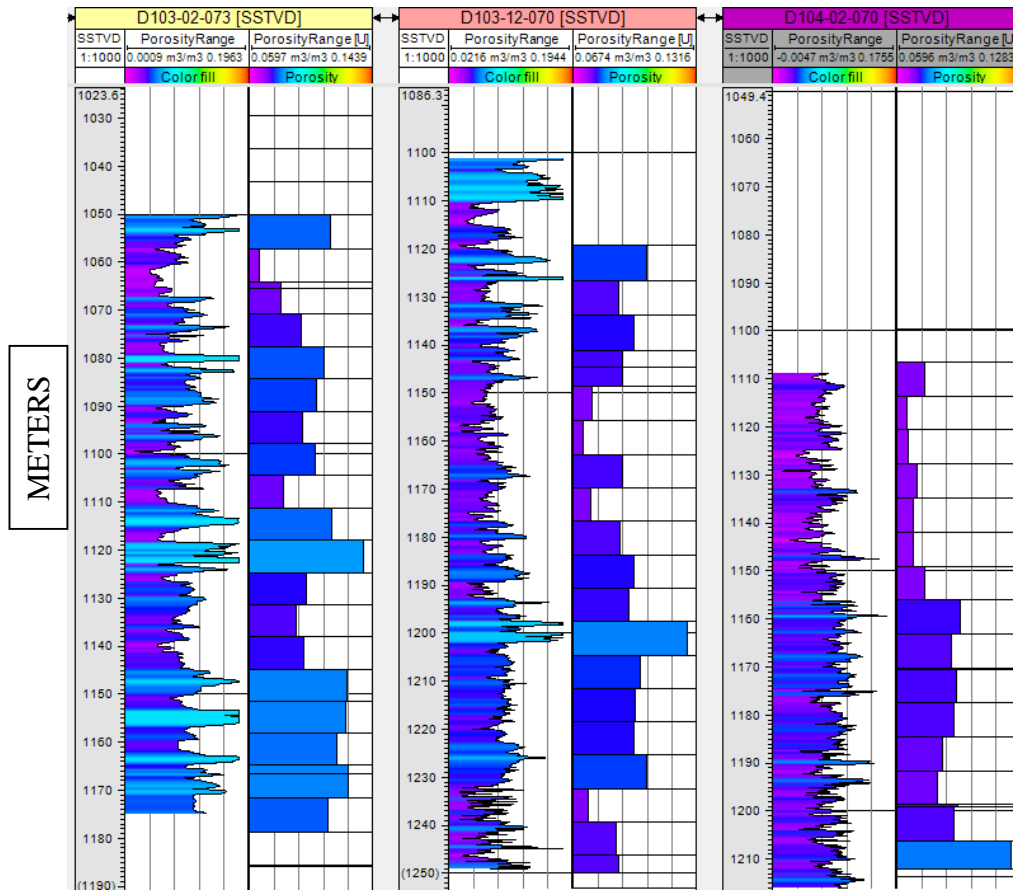
Figure 28: Comparison between actual log data and upscale data at 30 layers spacing.

An arithmetic averaging process was applied to up-scale porosity values for each layer. For the up-scaled data to be representative of the actual recorded values, the up-scaled porosity in the blocks must be a close match to the values in the porosity log track. The legend at the top of the porosity track in Figure 28 shows color and porosity value allocation. After examining Figure 28, it was concluded that most of the high and low values have been captured in the up-scaling process.

Once the up-scaled porosity was representative of the actual porosity logs, the process of conditioning the data began. The up-scaled porosity was transformed so that any directional

trends in the x, y, and z directions would be removed. This was done so that during the data analysis procedure, the variability of the porosity property could be determined without influence of any obvious directional trends. After conditioning the data, a spatial analysis of the porosity property was conducted. A variogram, which is a plot measuring the variability of a property based on spatial separation, was used to model the spatial variability of porosity in the vertical and horizontal planes. There is a much higher frequency of porosity data in the z direction on account of logs being run vertically. Therefore, the main priority was for the variogram to be representative of the spatial variability in the vertical direction, with the horizontal direction being a second priority.

Using the results of the spatial analysis, a porosity model was generated through kriging, which is a method of determining unknown property values in space through interpolation based on the weighted averages of known neighboring values. Figure 29 shows the porosity model created using the kriging method.
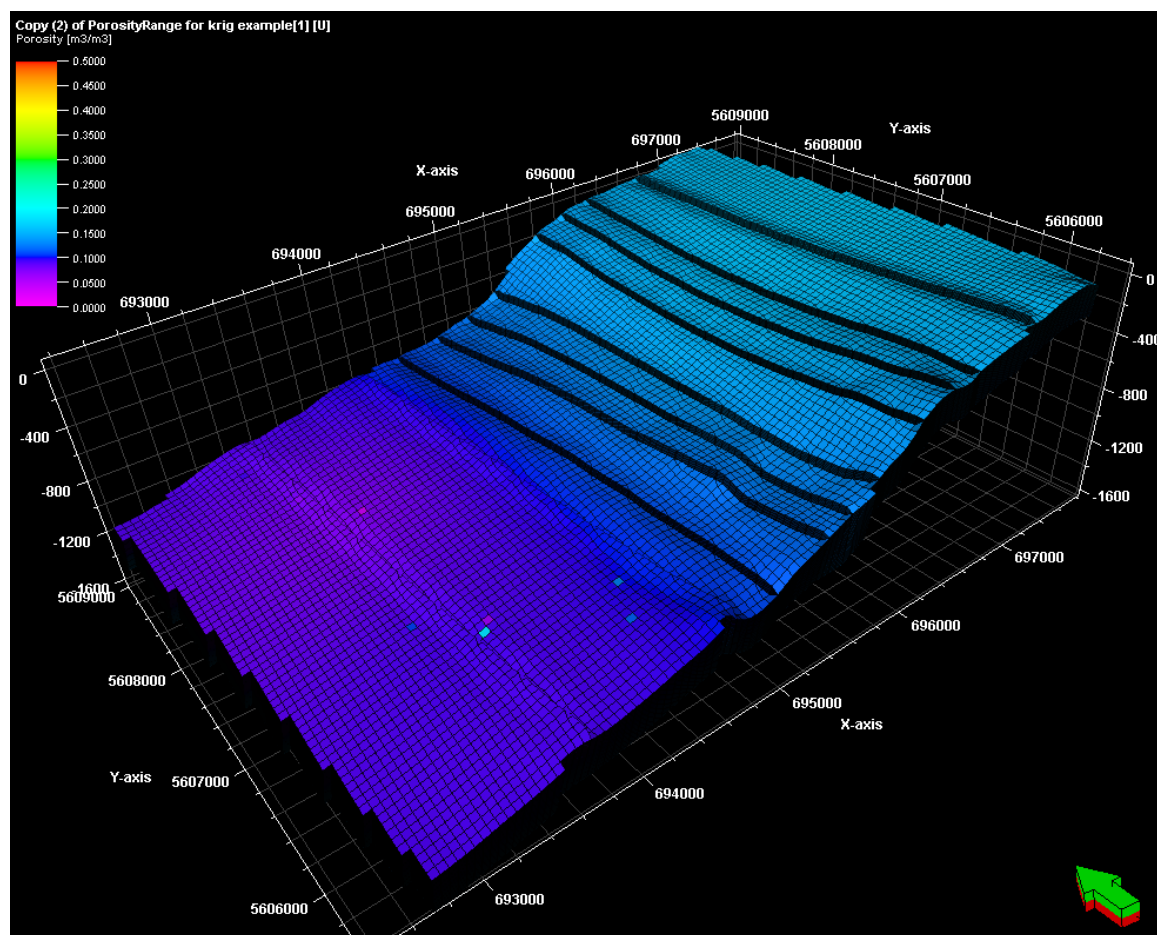
Figure 29: Porosity model generated using the kriging method.

As indicated by Figure 29, the kriging method results in smooth gradual changes of porosity, eliminating extreme values. It is for this reason that kriging may not be an ideal method for representing a carbonate reservoirs. The porosity in carbonate reservoirs is mostly vugular in nature and the changes in the property could be potentially more variable when compared to sandstone reservoirs. The kriging method does not capture abrupt property variations which could potentially be experienced in carbonate reservoirs. It should be noted that abrupt changes in porosity do not necessarily mean that there is more variability in the modeled property overall.

Figure 30 shows an example of five cell blocks in real reservoir space and demonstrates how values can suddenly change but still remain in the range of small variability. Figure 30 also displays an example of how kriging estimates unknown values for a carbonate reservoir.

5%	10%	6%	11%	15%
Actual reservoir porosity				
5%	7.5%	10%	12.5%	15%
Porosity generated using a weighted average				

Figure 30: Example: estimated porosity values using a weighted average.

The upper five cell blocks represent the porosity values that exist in the actual reservoir space, while the lower five cell blocks represent two known values at each end and three cells in between with unknown values that were estimated using the kriging method. The gradual smoothing of the property based on weighted averages, seen in Figure 30, could possibly assign porosity values to the unknown cells without representing the full variability present in the data. To avoid this, a second attempt was made to model the porosity property using Sequential Gaussian Simulation in Petrel. The Gaussian method picks values randomly from a set of probable values based on the known range (i.e. 5% to 15% from Figure 30) and assigns those values to the empty cells. In this case five different realizations were generated and compared to the log porosity data. The realization that exhibited the best match to the log data was selected as the porosity property to be used.

Figure 31 makes a comparison between the porosity model from the kriging method and the Sequential Gaussian Simulation porosity realization. It is apparent that the porosity property generated using the kriging method is much smoother when compared to realization that was created using the Gaussian method. As previously stated, due to the vugular nature of carbonate

formations, applying the sequential Gaussian simulation method resulted in what is most likely a statistically more accurate representation of the Turner Valley formation.

Kriging Method   **Gaussian Sequential Simulation Method**
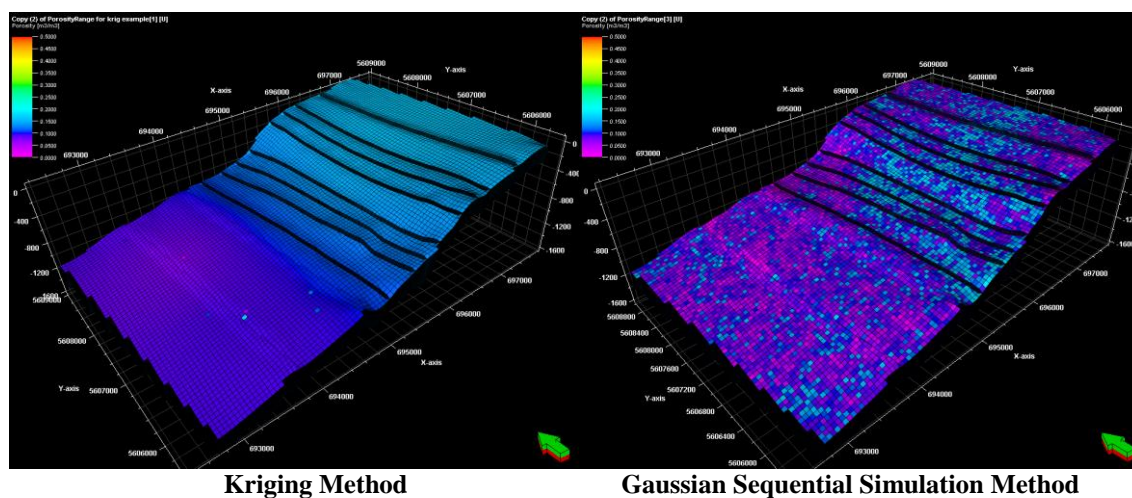
Figure 31: Comparison of the porosity property generated using different methods.

To ensure that the simulated porosity was representative of the actual reservoir, a relative frequency histogram of the log data and the porosity realization was generated, Figure 32. The x-axis is represented by porosity and the y-axis is denoted by the frequency of the data in percentage. The dark blue bars represent the simulated porosity values while the light blue bars signify the actual log data. The main objective of the histogram is for the simulated property and the actual observed data to match as closely as possible. The relative frequency histogram in Figure 32 shows that the modeled porosity is not an acceptable representation of the actual log data.
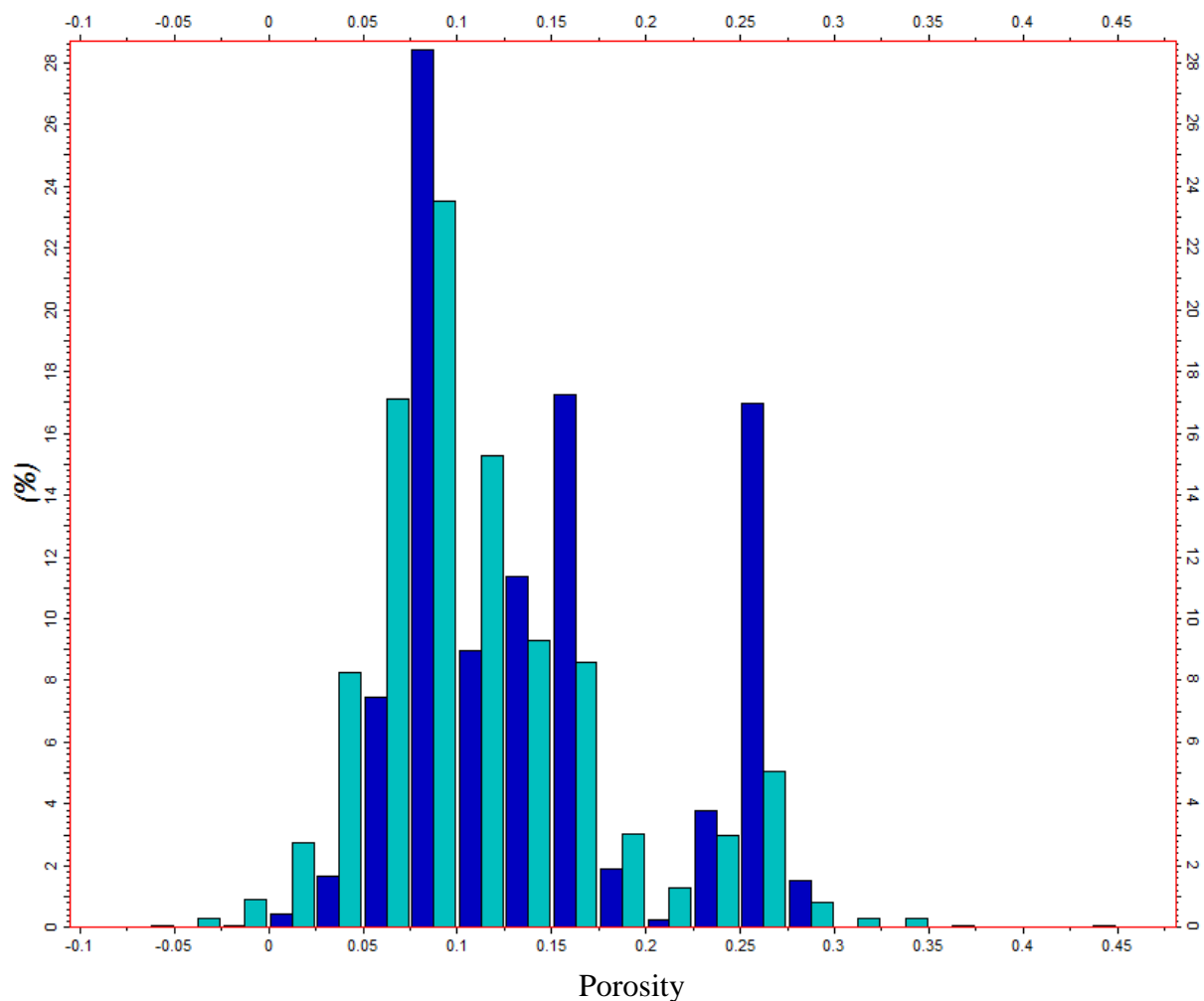
Figure 32: Histogram showing relative frequency of actual log data (light blue) and the generated porosity property (dark blue) for a 30 layer model.

Although the values near 10% are a close match, the low and high porosity values are not captured by the simulated porosity. In an attempt to generate a closer match, different cases were run varying in the number of layers applied to the model. Higher number of layers would result in a closer fit to the observed data, but computing power also had to be taken into consideration. Figure 33 shows a relative frequency histogram generated using a 60 layer model. Most of the high as well as the low porosity values are captured by the generated model. The general shape

of both histograms is also a close match. Considering both accuracy of the model and computing resource, the porosity model generated using 60 layers was determined to be an adequate match to the observed log data.
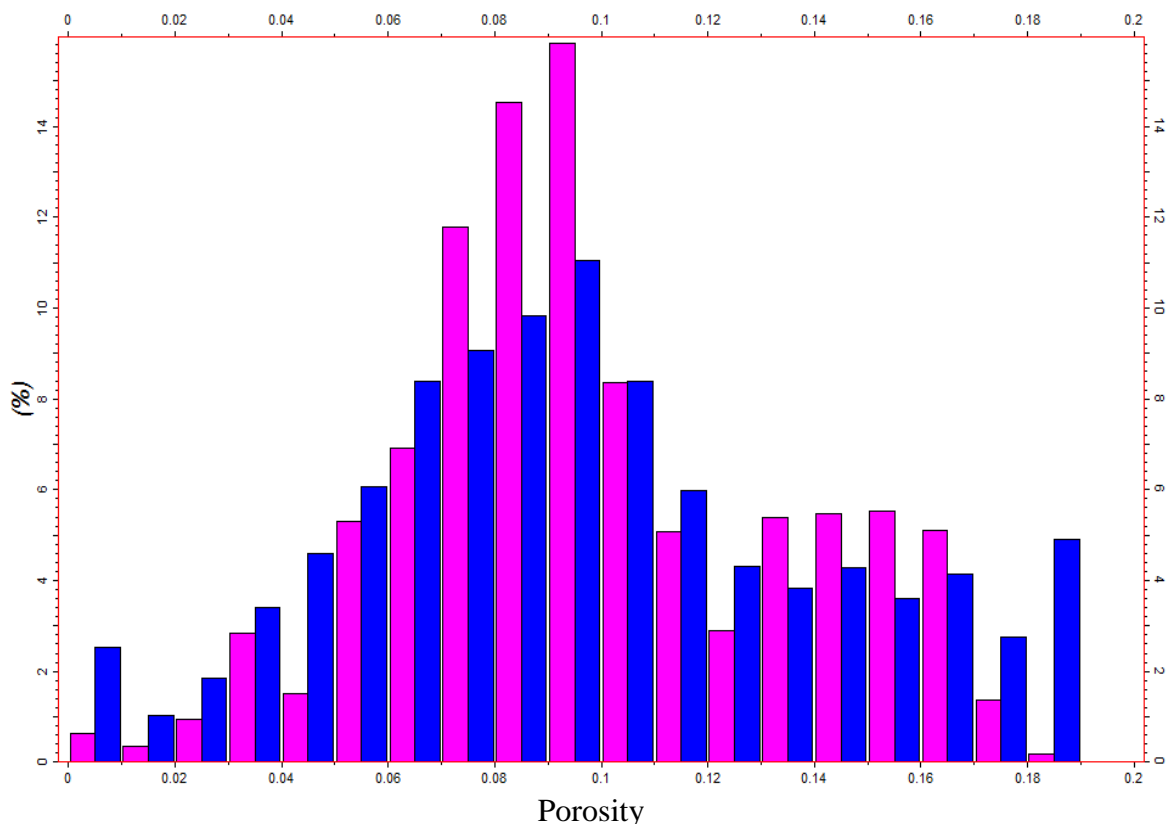
Figure 33: Histogram showing relative frequency of actual log data (blue) and the generated porosity property (pink) for a 60 layer model.

Core data from three wells was obtained from AccuMap for the purpose of building a porosity-permeability relationship. Figure 34 shows the locations of available core data. The area of study is outlined in pink and the wells with available core data are circled in red. The wells which core data was used from are labeled in the black boxes. There is only one cored well in the modeled area, thus cores from two wells neighboring the area of study were used.
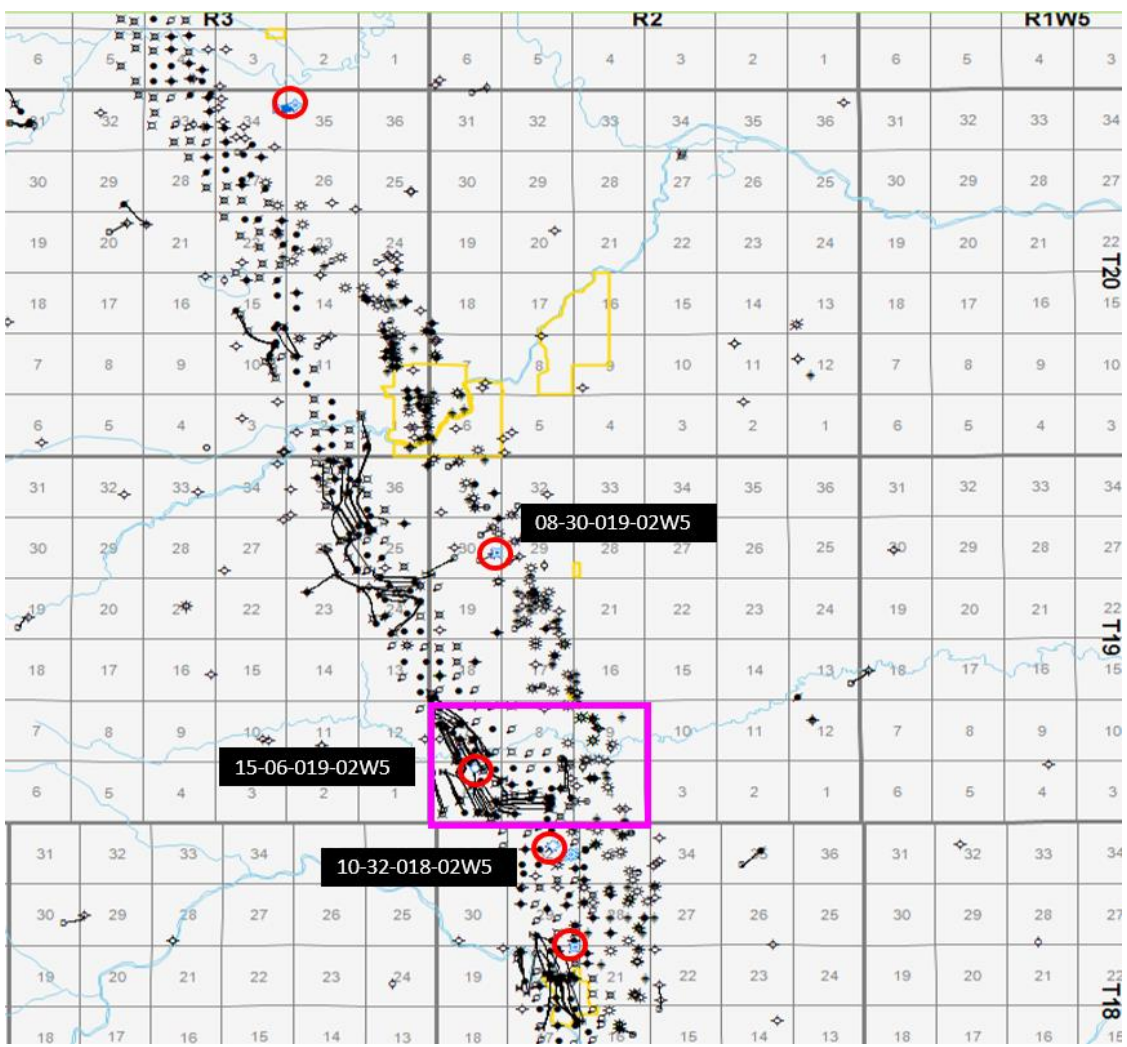
Figure 34: Map of available core data.

Examination of the core data from the surrounding wells showed that there is very little variation in porosity and permeability when compared to the well inside the modeled area. Therefore, it was determined that the nearby available cores could be used in conjunction with the core inside the study area to produce a porosity-permeability relationship. Table III compares the average horizontal permeability, vertical permeability, and porosity for the three wells. It

should be noted that well 8-30-019-02W5 is on the western flank of the structure (up-dip) and as stated previously, the most considerable amount of heterogeneity is experienced in the eastern direction.

Table III: Average core properties comparison.

Well	Average Horizontal Permeability (mD)	Average Vertical Permeability (mD)	Average Porosity (Fraction)
8-30-019-02W5	6.29	11.26	0.08
15-06-019-02W5	9.25	4.87	0.08
10-32-018-02W5	11.20	5.00	0.08

Both horizontal permeability and vertical permeability were plotted against porosity and an exponential best fit line was applied to the data. Equation 3 shows the generated correlation for the horizontal permeability-porosity relationship and Equation 4 represents the vertical permeability-porosity relationship. The core data used to generate these relationships is referenced in the Appendix A.

$$k_{hor} = 0.187e^{33.3\emptyset}$$ **Equation 3**

$$k_{vert} = 0.065e^{37.0\emptyset}$$ **Equation 4**

To further verify the accuracy of the modeled porosity property, an average of the modeled property was compared to the average of the porosity from the core data. The modeled porosity had a similar mean of 9% when compared to the core porosity average of 8%. Equations 3 and 4 were then applied to the porosity property to generate horizontal and vertical permeability properties, respectively. The horizontal permeability property model had an average of 10 mD, which was a close match to the horizontal permeability average of 9 mD obtained

from the core data. The vertical permeability property model was also a close match with an average of 6 mD, compared to the cored vertical permeability average of 7 mD.

The formation compaction was generated through Petrel using Newman's limestone correlation, shown in Equation 5 (Craft et al., 1990). Newman's correlation is valid for porosities ranging between 2% and 33%; the mean modeled porosity falls into that range at 9%. The porosity property was used in in modeling the formation compaction.

This ensured that no single compaction factor was applied to the reservoir, but instead the compaction varied depending on the location of the cell and the porosity value assigned to it.

$$c_f = \frac{0.853531}{(1 + 2.47664(10)^6 \emptyset)^{0.92990}}$$ **Equation 5**

2.3.   Fluid Properties

The PVT properties were generated using correlations specified below, along with known reservoir and fluid characteristics obtained through the literature review. The gravity of oil used in the PVT calculations was 43 ^{O}API, which was obtained from the AccuMap database. The temperature and bubble point pressure of 149 ^{O}F and 2,400 psi, respectively, were taken from Paulson and Wahl (1962). All fluid properties were calculated for pressures ranging from 14.7 psi to 8,000 psi.

Equation 6 (Craft et al., 1990) shows Standing's correlation which was used to calculate the solution gas-oil ratio below the bubble point pressure. Standing's correlation is valid for bubble point pressures ranging from 130 psi to 7,000 psi, a temperature range of 100 ^{O}F to 258 ^{O}F, and an oil gravity of 16.5 ^{O}API to 63.8 ^{O}API.

$$R_{so} = \gamma_g \left(\frac{P}{18(10)^{\gamma_g}} \right)^{1.204}$$ **Equation 6**

Where, $T = temperarute\ in\ {}^0F$

$\gamma_g = gas\ specific\ gravity$ $\rho_O = oil\ density, {}^0API$

$Y_g = 0.00091T - 0.0125\rho_O$ $P = pressure, psia$

The oil formation volume factor, for pressures at or below bubble point, was calculated

using Standing's correlation shown in Equation 7 (Craft et al., 1990).

$$B_o = 0.972 + 0.000147F^{1.175}$$

Equation 7

Where, $\gamma_o = oil\ specific\ gravity$

$$F = R_{so}\left(\frac{\gamma_g}{\gamma_o}\right)^{0.5} + 1.25T$$ $T = temperarute\ in\ {}^0F$

For pressures above bubble point pressure, the oil formation volume factor was generated

using Standing's correlation shown in Equation 8 (Craft et al., 1990).

$$B_o = B_{ob}\exp[c_o(p_b\text{-}p)]$$

Equation 8

Where,

$B_{ob} = oil\ formation\ volume\ factor\ at\ bubble\ point\ pressure$

$c_o = oil\ compressibility$, psi^{-1}

$p_b = bubble\ point\ pressure$, psia

$p = pressure, psia$

Oil compressibility was calculated using the Villena-Lanzi correlation shown in Equation

9 (Craft et al., 1990). Villena-Lanzi developed the correlation to be used for black oils. The

database used to develop the correlation included pressures between 500 psig and 5,300 psig, a

temperature range of 78 ^{0}F to 330 ^{0}F, and an oil gravity ranging from 6 ^{0}API to 52 ^{0}API.

$$c_o = -0.664 - 1.430 \ln(p) - 0.395 \ln(p_b) + 0.390 \ln(T) + 0.455\ln(R_{sob})$$
$$+ 0.262\ln(\rho_O)$$

<div align="right">**Equation 9**</div>

Where,

$R_{sob} = solution\ gas - oil\ ration\ at\ bubble\ point\ pressure$

To accurately calculate oil viscosity below and at bubble point pressure, Beggs and Egbogah's correlations were used in conjunction. Egbogah developed a correlation, Equation 10 (Craft et al., 1990), to calculate dead oil viscosities at pressure below and equal to the bubble point pressure. The correlation is known to be accurate for a temperature range of 59 $^{\circ}$F to 176 $^{\circ}$F and for an oil gravity range of 5 $^{\circ}$API to 58 $^{\circ}$API.

$$log[log(\mu_{od} + 1)] = 1.8653 - 0.025086\rho_O - 0.5644\log(T)$$

<div align="right">**Equation 10**</div>

Where,

$\mu_{od} = dead\ oil\ viscosity, cp$

After the dead oil viscosity was determined for pressures equal to and below bubble point pressure, Beggs' correlation, Equation 11 (Craft et al., 1990), was used to generate live oil viscosities at the same specified pressures. Beggs' correlation is valid for a pressures up to 5,250 psi, for temperatures between 70 $^{\circ}$F and 295 $^{\circ}$F, and for an oil gravity range of 16 $^{\circ}$API to 58 $^{\circ}$API.

$$\mu_o = A\mu_{od}{}^B$$

<div align="right">**Equation 11**</div>

Where,

$A = 10.715(R_{so} + 100)^{-0.515}$

$B = 5.44(R_{so} + 150)^{-0.338}$

The oil viscosity above bubble point pressure was calculated using Vasquez's correlation shown in Equation 12 (Craft et al., 1990). Vasquez's correlation is known to be accurate for pressures between 126 psi and 9,500 psi and for an oil gravity range of 15.3 ^{O}API to 59.5 ^{O}API.

$$\mu_o = \mu_{od} \left(\frac{p}{p_b}\right)^m$$

Equation 12

Where,

$m = 2.6p^{1.187} \exp[-11.513 - 8.98(10)^{-5}p]$

$\mu_{ob} = oil\ viscosity\ at\ bubble\ point, cp$

Gas compressibility factors were generated using Standing and Katz correlation. Once the compressibility factors had been determined for varying pressures, the gas formation volume factors were calculated using the correlation presented by Craft and Hawkins, shown in Equation 12 (Craft et al., 1990).

$$B_g = 0.02829 \frac{zT}{p}$$

Equation 12

Where,

B_g = Gas formation volume factor, ft^3/SCF

The correlation used to calculate gas viscosity, shown in Equation 13 (Craft et al., 1990), was developed by Lee, Gonzalez, and Eakin. The correlation was produced for a pressure range of 100 psi to 8,000 psi, a temperature range of 100 ^{O}F to 340 ^{O}F, and a carbon dioxide mole fraction range of 0.9% to 3.2%. The gas in Turner Valley has a carbon dioxide mole fraction of 2.85%.

$$\mu_g = (10^{-4})Kexp(X\rho_g{}^Y)$$

Equation 13

Where,

$$X = 3.5 + \frac{986}{T} + 0.01 M_w$$

$\rho_g = gas\ density, g/cc$

$$Y = 2.4 - 0.2X$$

$$K = \frac{(9.4 + 0.02 M_w) T^{1.5}}{209 + 19 M_w + T}$$

$T = temperature, ^oR$

$M_w = gas\ molecular\ weight$

2.4. Development Strategy

The final step before initiating simulation was to develop a production strategy for the field. There are a total of 101 wells, including 87 producers and 14 water injectors. The water injection rates varied monthly and therefore an average monthly injection rate was applied to each year. The producing wells are controlled by a bottom hole pressure restriction which is set to 60% of the static oil column pressure. This was done in accordance to the Alberta Energy Regulator's proration of 40%, set in 1931. Frictional pressure loss was initially calculated to determine circulating bottom hole pressures, but due to the high grade of the oil and consequently low viscosity, frictional losses were negligible. Flow velocities were also low, playing a factor in the low frictional pressure loss.

2.5. History Matching

Figure 35 shows the initial simulated gas and oil production before any of the model parameters had been modified for the history matching process. The circles represent the actual observed production while the thin line shows the simulated results. The brown set of lines represents gas production and the green set of lines represent oil production. The initial simulation that was run resulted in substantially higher cumulative production than that of the observed data for both oil and gas. It should be noted that not all wells possessed observed production and therefore the simulation was run only including wells for which the observed

production data existed. The history matching processes was based on cumulative production. Prior to 1962, records of observed production could not be located. For this reason, simulated results begin 30 years before the first observed production point.
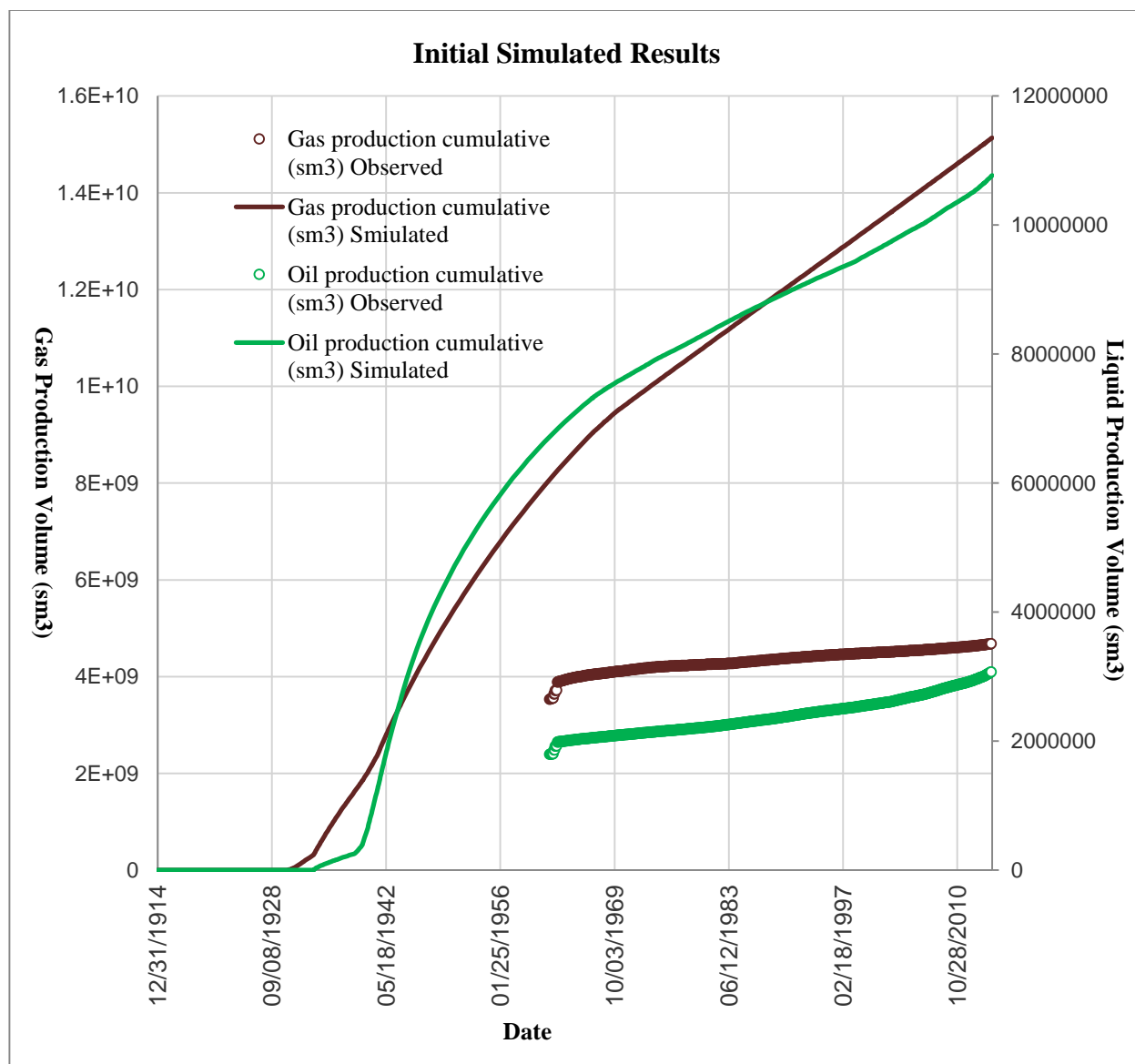
Figure 35: Initial simulation results with out history matching.

To understand where the extra hydrocarbon volumes originated from, all the parameters used to construct the model were considered to determine which properties were generated with

the highest degree of confidence. The generated porosity model is relatively accurate, considering that the distribution of the modeled property captures the general shape of the histogram representing the log data (seen Figure 30). The average modeled porosity was also a close match to the calculated core porosity average. The horizontal and vertical permeability-porosity relationships generated permeability properties which were close matches to the core data and the relative permeability curve end points were obtained from Paulson and Wahl (1962) which reported core flooding results. The calculated PVT properties, such as solution gas-oil ratios and oil formation volume factors, were also a near perfect match to the value reported by Paulson and Wahl (1962). All these parameters have been incorporated into the model with a high degree of certainty.

The highest degree of uncertainty in the model is attributed to the thickness of the Turner Valley formation. The formation top picks are not always constant, even for the same wells that have been logged multiple times. The formation top names are also inconsistent, with the Rundle Group and the Turner Valley formation being used interchangeably. Formation top picks for the Shunda carbonate, which is the formation immediately below Turner Valley, are scarce making it difficult to identify the thickness of the reservoir. The depth of the water-oil contact is also uncertain; Paulson and Wahl (1962) provided a range for the water-oil contact with a difference of 200 feet in depth, depending on the location in the field. Boundary placement within the model space is also inexact. Although it is known that a major fault on the western flank of the reservoir underlays the Turner Valley formation, the exact location of the faulting boundary is uncertain given the available information. Therefore, the thickness of the formation, the water-oil contact, and the reservoir boundaries were selected as history matching parameter.

The major discrepancy between the simulated results and the observed data is the volume of hydrocarbons being produced. The simulated gas production is substantially higher than that of the actual observed gas production. Due to the fact that the reservoir dips toward the east and the gas cap occupies the western flank of the formation, the western boundary was selected for modification. Figure 36 shows the modeled structure of the reservoir and the wells within the model space. Well 100-07-090 (circled in green) is the most western well that was drilled within the study area and is located adjacent to fault 10. Fault 10 is the final fault on the eastern flank and thus was selected as the new boundary limit.

Figure 36: Well and fault placement within the model space.

To reduce the amount of gas volume within the model, a zero porosity value was applied to the entire portion of the porosity property which was located to the east the fault 10. This accomplished a reduction in the total pore volume of the model consequently decreasing the volume of gas. The western boundary modification successfully decreased the simulated gas production, but the total gas produced was still considerably higher than the actual observed production.

A closer examination of the available formation top picks revealed that the reservoir could potentially be thinning towards the western boundary. Figure 37 shows the location of well 102-16-052, which is the only well that possesses formation top picks for both Turner Valley and Shunda in the western portion of the reservoir. The formation top picks from this well show that the Turner Valley formation is 167 feet thick in the western portion of the reservoir while well 100-04-050, also shown in Figure 37, located 4,068 feet down dip of well 102-16-052, shows that the average Turner Valley thickness in that area is approximately 249 feet. This proves that there is a change in thickness of 82 feet over a distance of approximately 4,068 feet.
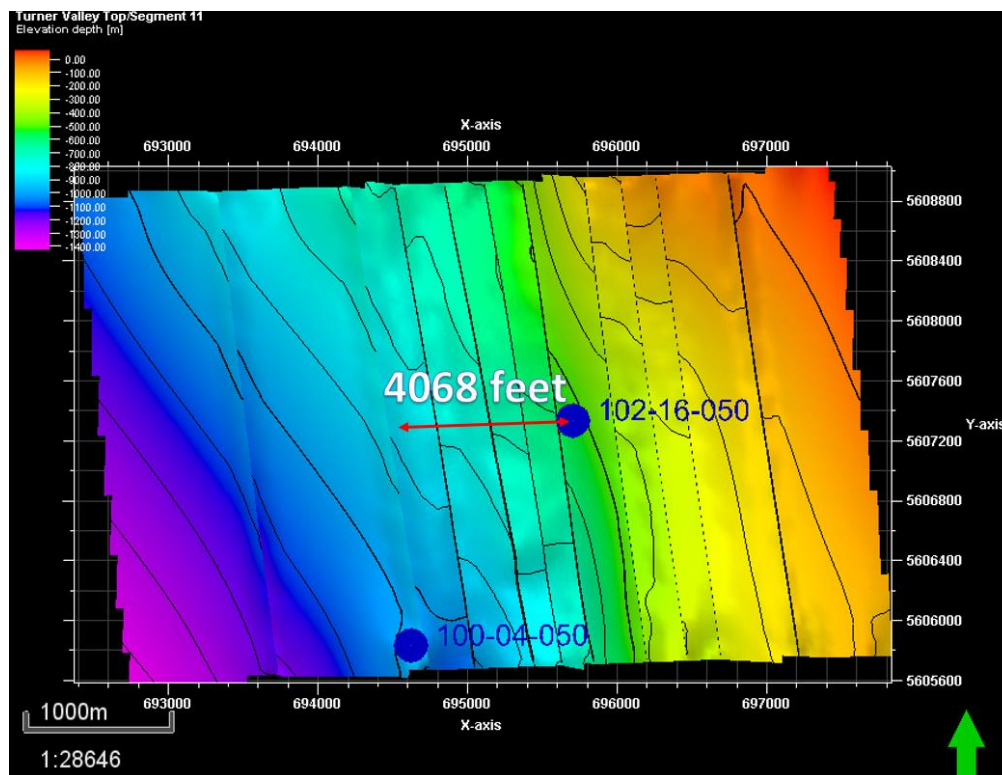
Figure 37: The two wells used in the comparison of formation thickness based on location.

The model's effective thickness was reduced by applying a zero percent porosity to a gradually increasing number of layers (from the bottom) towards the western end of the model. This method was successful in lowering the simulated production, but the model's production was still too high for both gas and oil. To reduce the simulated results of both phases even further, the upper layers of the reservoir were eliminated using the same method as before until the formation was thick enough to only contain the wells within the model. This resulted in total reservoir thickness of 417 feet at the eastern boundary and 167 feet at the western flank. The original model was 722 feet thick throughout the entire reservoir. Figure 38 shows the simulated results after the thickness of the formation had been modified. This method was once again

successful in lowering the surplus of production for both oil and gas but the simulated results still

showed excess production for both fluids.
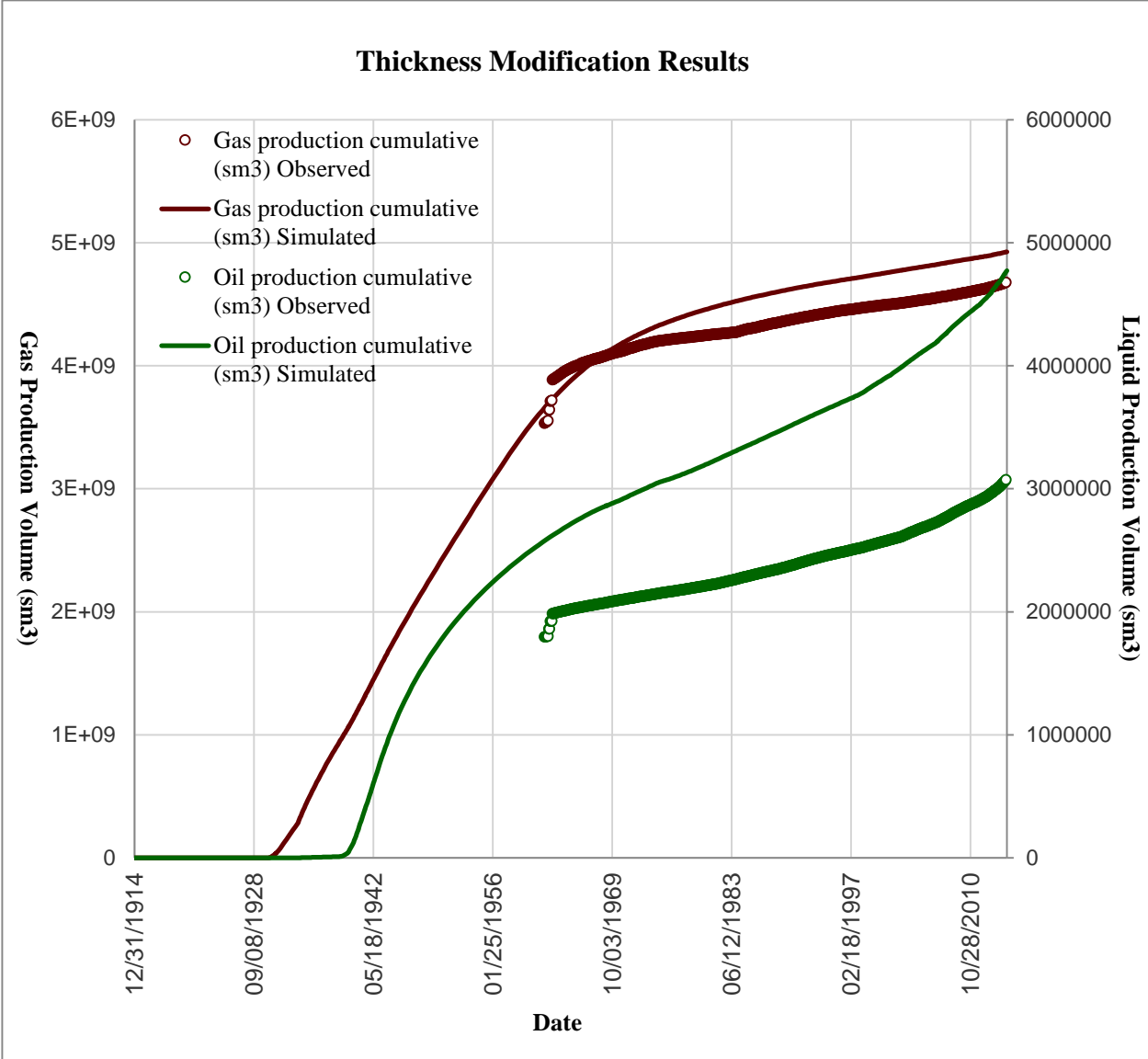
Figure 38: Simulated results after modifying the thickness of the formation.

Reducing the effective modeled reservoir thickness further could have potentially

excluded some of the producing wells from the model and thus to further reduce the volumes of

fluid production, the water oil contact was adjusted. The water–oil contact is located at

approximately 4,700 feet subsea in the northern portion of the field and at 4,500 feet subsea in the south (Paulson & Wahl, 1962). The simulations run after decreasing the water-oil contact depth resulted in a decrease of production from both the oil and gas phase.

The final value of 4,249 feet subsea applied to the water-oil contact resulted in an adequate history match shown in Figure 39. Once again, the thicker line represents the observed data while the thin line represents the simulated production. Although the simulated results do not exactly match the observed data in the early life of the reservoir, an exact match is accomplished in the second half of the field's life. The primary objective of history matching is to modify the models conditions to be representative of the reservoir's current hydrocarbon volumes. This was accomplished by matching the simulated results with the observed data in the last 20 years of the field's life.
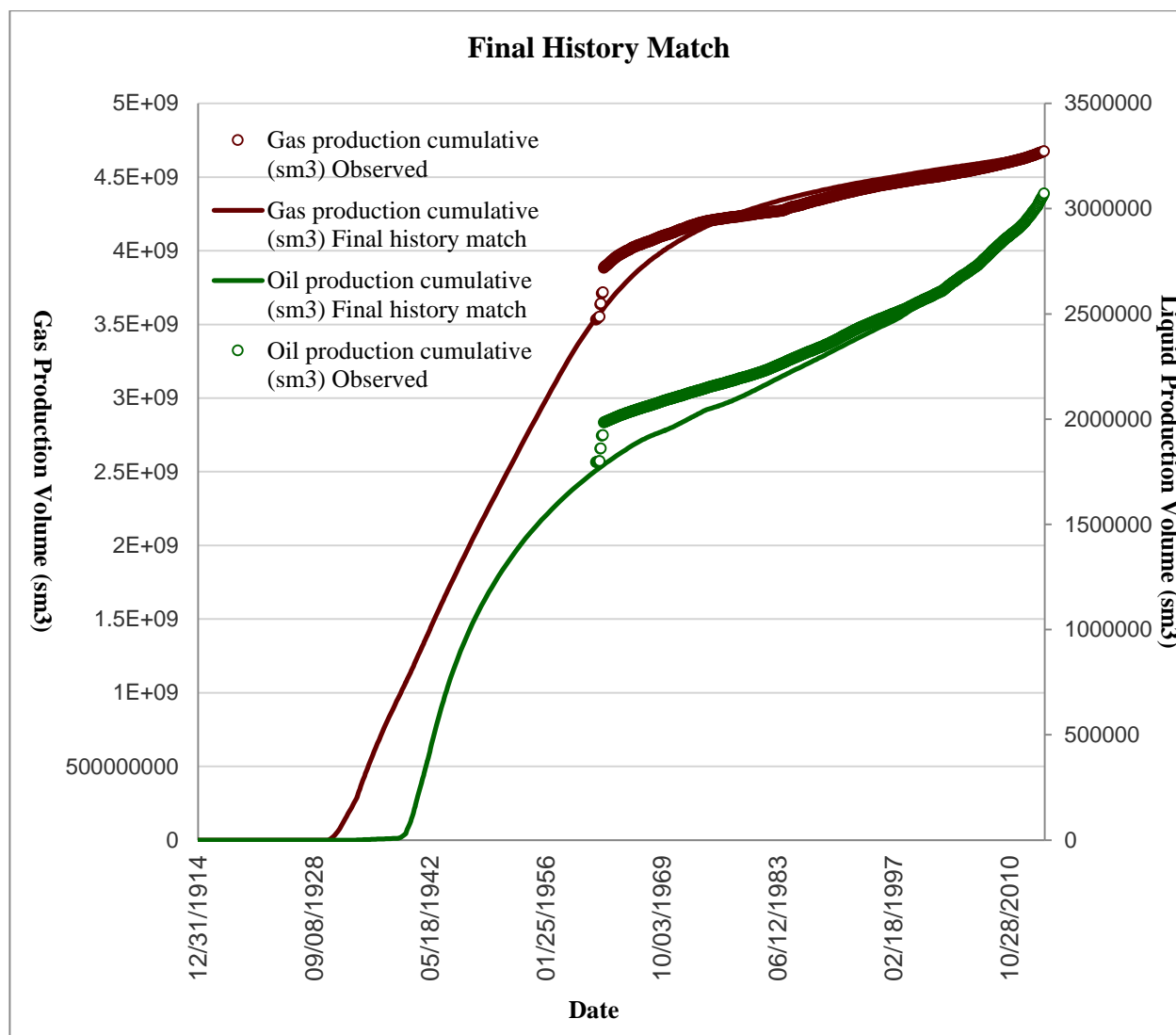
Figure 39: Simulated results for the final history match.

2.6. Solvent Model

Once an adequate history match had been attained, simulating the injection of nitrogen

commenced. To facilitate the injection of nitrogen, the solvent model was applied through the

Eclipse deck generated by Petrel. The solvent model is an extension of the black-oil model with

four components (solvent gas, gas, oil, and water) instead of three. The solvent model was

designed with the ability to model miscible interaction between the oil and solvent during

injection and describes three scenarios. The first scenario is with reference to areas where only solvent (in this case nitrogen) and oil exist, the oil and solvent are considered to be completely miscible and therefore the relative permeability for a two phase system (oil and water) is applied. The second scenario describes regions where only oil and gas exist, the two phases are considered immiscible and will interact in the same manner as in the original black-oil model. The solvent model also specifies a third scenario: areas where gas, oil, and solvent all co-exist, at which point an "intermediate behavior is assumed to occur." This "intermediate" behavior is described by the Todd-Longstaff model which introduces an empirical factor known as the mixing parameter ranging between zero and one. This mixing parameter describes the dispersion zone within each grid cell and the effects of dispersion between miscible phases, controlling the "degree of fluid mixing within each grid cell" (Schlumberger, 2014). In cases where the mixing parameter is set to one, the dispersion zone is considered to be larger than the grid cell and the constituents within the cell are fully mixed. In this case, both components which are miscible have the same density and viscosity. In cases where the mixing parameter is set to zero, the dispersion zone is too small to provide an affect and the components are considered to be immiscible; with each component having the viscosity and density of its pure phase (Schlumberger, 2014).

Since the nitrogen injection is planned to provide pressure maintenance by injection into the gas cap, the third scenario described by the Solvent model is the most relevant. The pressures at current reservoir conditions are too low, approximately 2,175 psi depending on the location in the reservoir, for miscibility between nitrogen and oil to be achieved. Tiwari and Kumar (2001) describes lab tests that were conducted on an oil of 42 ^{O}API from a mean formation depth of 9,711 feet to determine miscibility pressures between nitrogen and oil. The

results showed that a pressure of 6,000 psi downhole would need to be reached to achieve miscibility (Tiwari & Kumar, 2001). Judging from the similarities between Turner Valley and the reservoir described by Tiwari, and the discharge pressure of 4,000 psig provided by the nitrogen separation system, comparable pressures would need to be attained before miscibility between nitrogen and oil would be achieved. Therefore, the mixing parameter within the solvent model was set to zero to properly model the immiscible interaction between the nitrogen and oil. A sample of the Eclipse deck for the solvent model can be referenced to in Appendix B accompanied by a description of the necessary modifications.

2.7. Nitrogen Separation Unit

Nitrogen injection rates from the Tensleep reservoir and the studies performed by Tiwari and Kumar (2001) and Mungan (2000) were taken into consideration during the selection of the nitrogen supply system. Canadian Nitrogen Services Ltd. provided an estimate on a nitrogen membrane separation unit that would have the ability to provide an injection rate similar to the rate of injection which occurred in the Tensleep reservoir. Canadian Nitrogen suggested using an 800 HP (600 kW), 3 phase membrane separation unit which is capable of producing nitrogen at a rate of 2,160 SMCF/day and at pressures of up to 4,000 psi (Simard, 2015). The suggested unit has the ability to purify nitrogen up to 95% purity. The operation of the nitrogen separation unit can be referenced to in Appendix C (Canadian Nitrogen Service Ltd., 2015).

3. Results

Varying cases of nitrogen injection were run with the history matched simulator described above. They differed on the location of the injection wells to determine the resulting simulated production's sensitivity to injection well location. There are 10 existing wells producing above the gas-oil contact; the location of the nitrogen injectors depends on the pre-existing wells to avoid drilling expenses. The nitrogen separation unit requires an initial capital of 1.6 MM$ with a yearly maintenance cost of $30,000.

After several cases were run, with the location of the nitrogen injectors changing from the top of the gas cap to just above the gas-oil contact, similar results were attained and it was determined that the model is not sensitive to the location (within the gas cap) of nitrogen injection. After the sensitivity analysis was completed, three injection cases were run for 30 years using the Eclipse simulator. Table IV describes simulated injection cases.

Table IV: Injection Case Description

Case	Number of Injectors in the Gas Cap	Number of Producers in the Gas Cap	Position	Injection Rate (SMCF/Day)
1	1	0	Top of the gas cap	2,160
2	1	9	Top of the gas cap	2,160
3	6	0	Top of the gas cap	2,160

Economics were run at a 10% discount rate and at $40/bbl, $60/bbl, and $80/bbl based on incremental production; Table V shows the results. The following discussion will compare the three cases at $80/bbl of oil.

Table V: Economic breakdown based on 3 injection cases.

		Oil Price ($/BBL)		
		40.00	**60.00**	**80.00**
Case 1	**NPV @ 10%**	($2,557,000)	$294,000	$3,146,000
	ROR	-	14%	45%
Case 2	**NPV @ 10%**	$212,000	$3,049,000	$5,885,000
	ROR	12%	39%	64%
Case 3	**NPV @ 10%**	($30,708,000)	($26,598,000)	($22,489,000)
	ROR	-	-	-

4. Discussion

Case 2 proves to be the most promising alternative, with a net present value of 5.9 MM$ and a rate of return of 64%. Case 3 is definitely the worst of the three cases, resulting in a negative NPV value of 22.5 MM$. Figure 40 shows the simulated oil production profiles for all three cases starting at the year 2015 and ending in 2045. Case 1 is represented by the blue line, Case 2 is represented by the green line, Case 3 is represented by the red line, and the black line represents the base case (do nothing case). The content inside the blue circle represents the zoomed in area of the final oil production volumes for Case 1 and Case 2.
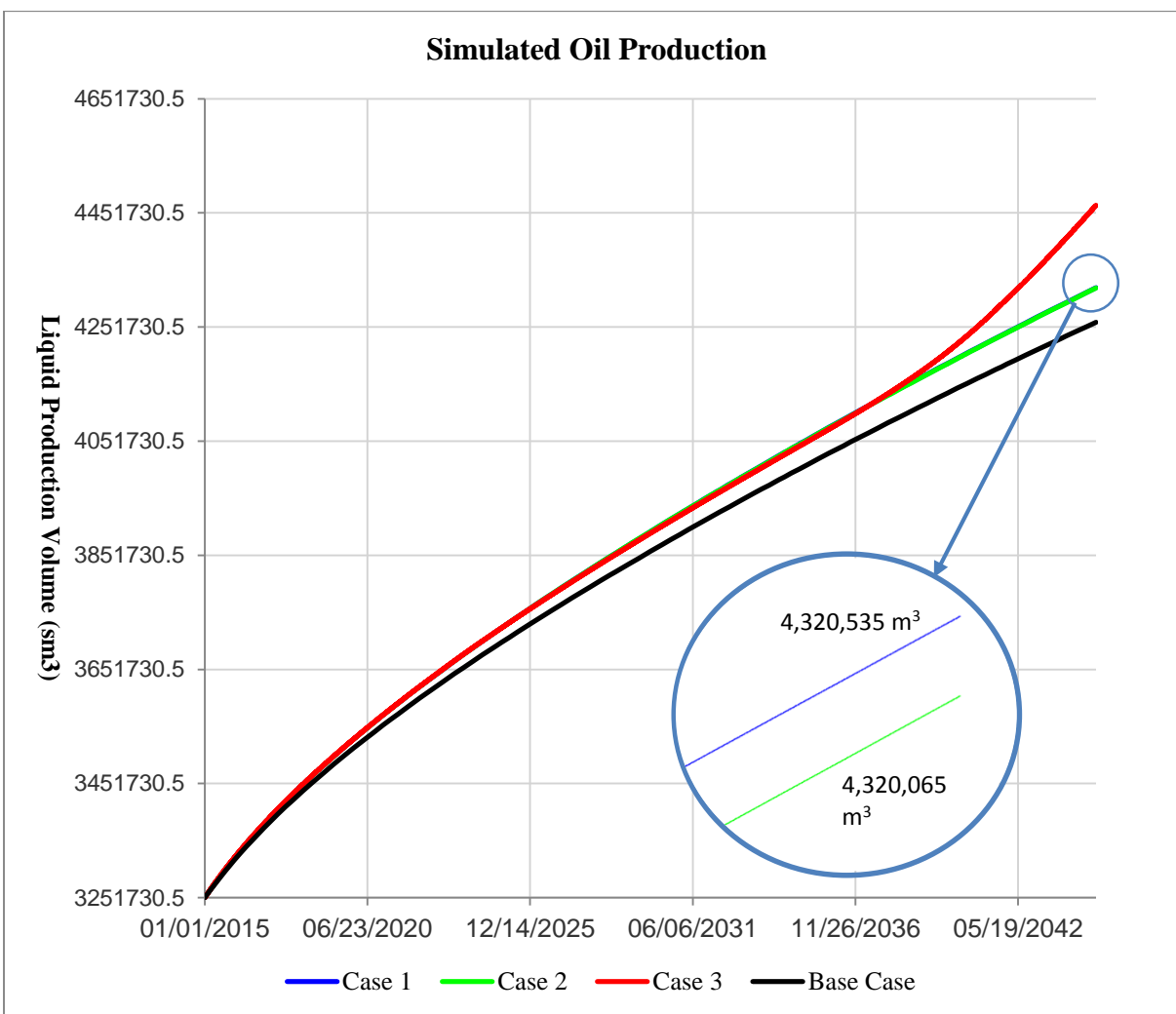
Figure 40: Oil production profiles for Case 1, Case 2, Case 3, and the base case.

Figure 40 shows that Case 1 has a slightly higher cumulative oil production when compared to Case 2, even though Case 2 results in a much higher NPV. This is a result of all the gas producing wells being shut at surface (excluding the injector) in Case 1, losing an incremental 2,212 MMSCF of gas production when compared to the base case. Because the gas producers are left open to production in Case 2, not only is that incremental production retrieved, but as a result of pressure maintenance supplied by the nitrogen injection, an incremental 14,595

MMSCF of gas is produced when compared to the base case. When comparing Case 2 to Case 1, an incremental 16,807 MMSCF of gas is produced.

There is no considerable deviation in the simulated oil production between Case 3 and Case 1 until year 2035 where the oil production rate starts increasing at an exponential rate. The reason for this is that until the year 2029, the pressure experienced in the gas cap is still lower than in the oil bearing portion of the reservoir and the only mechanism that is aiding in oil production is pressure maintenance. Figure 41 shows the pressure change experienced in Case 3 for years 2015, 2029, and 2045. At the beginning of the injection, the gas cap contains an average pressure of approximately 145 psig and the rest of the reservoir is pressurized at an average of 2,175 psig. Once the year 2029 is reached, pressure in the gas cap starts to increase above the pressure experienced in the rest of the reservoir and the oil becomes mobile.
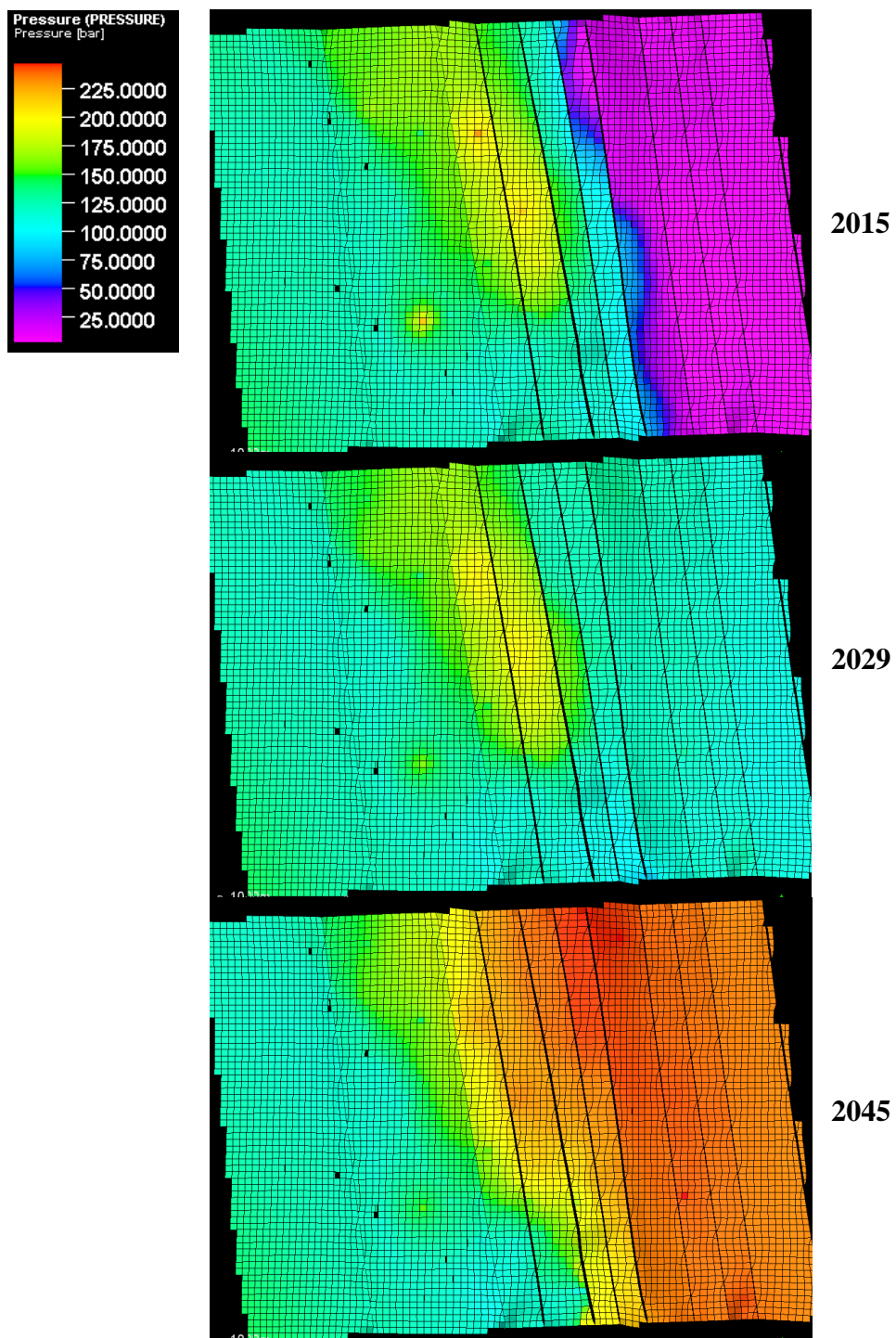
Figure 41: Case 3 reservoir pressure change.

Figure 42 shows the changes in oil saturation over the 30 year simulation. The spike in oil production is experienced around year 2035 as a result of the distance between the main horizontal oil producers and the initial gas-oil contact at the beginning of the simulation (2,912 feet). This is illustrated by the development of the high oil saturation front in year 2034, Figure 42. The incremental increase in cumulative oil production between the Case 3 and the base case is not enough to offset the initial capital of 17.6 MM$ for six nitrogen separation units and 76.6 MM$ for power consumption and maintenance over a 30 year span.
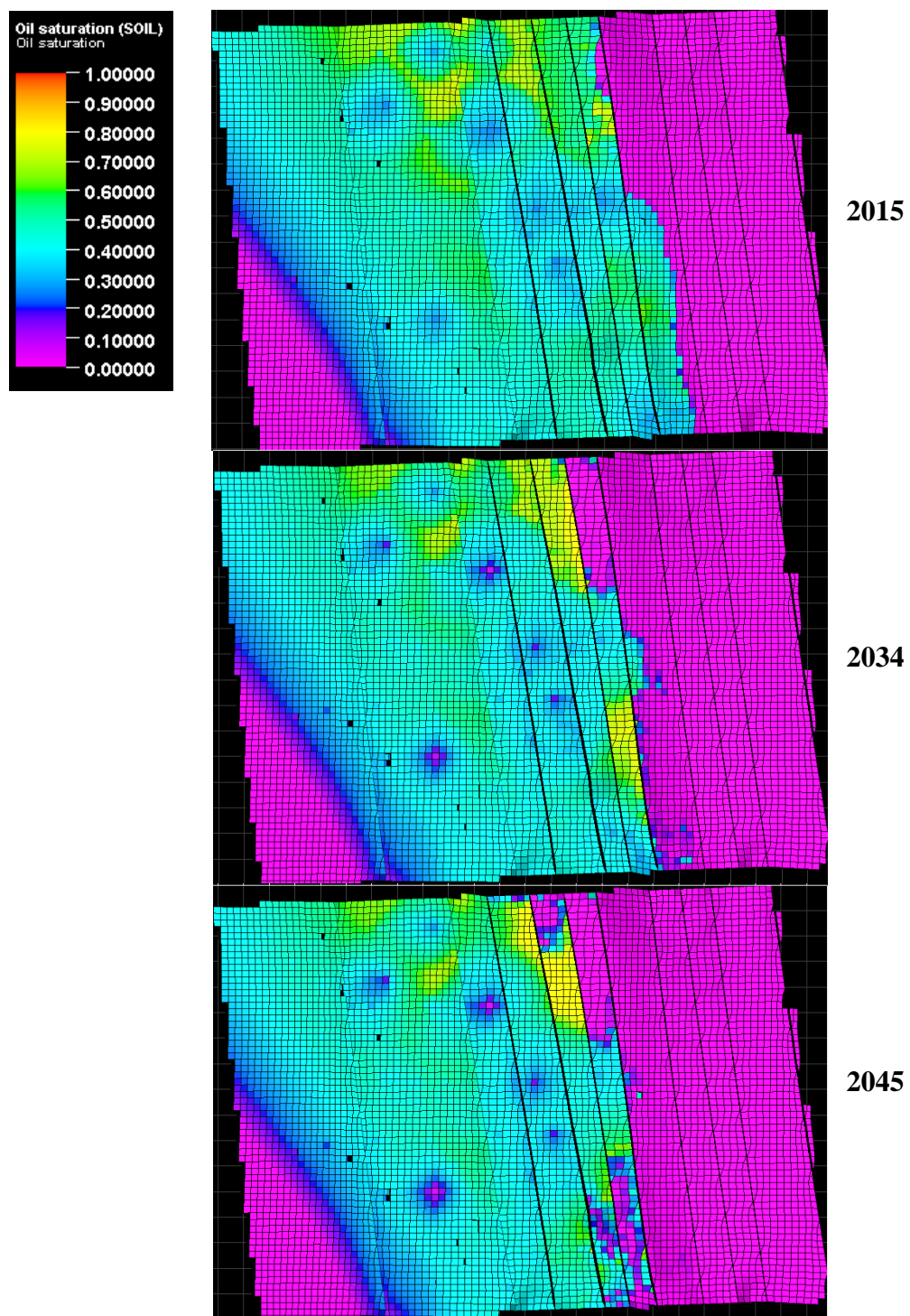
Figure 42: Case 3 oil saturation change.

5. Conclusion

Case 2 proves to be the most attractive alternative of the injection cases when compared to the base case. As can be seen in in Table V, even at an oil price of $40/bbl, the NPV for the project is still positive, having a value of almost $212,000. Due to the possibility of unforeseen difficulties and the risk of the investment, the price of oil should reach at least $60/bbl for nitrogen injection in Turner Valley (with the specified parameter in this report) to be viable. If the price of oil reaches $80/bbl, according to the simulated results, an investment in nitrogen injection in the Turner Valley oil field should definitely be considered.

6. Future Work

6.1. Improving the Structural Model

The highest degree of uncertainty within the created Turner Valley model is the structure which was developed from two parallel 2D seismic lines and the available formation top picks. Since only two lines were available, the placement of the faults forced a continuous fault line between the two seismic sections. To create a fault, an interpretation must be completed on the seismic section which acts as a plane in space and thus, faults could only be created by the connection of two planes in space. The obtained southern seismic section was of relatively high quality when compared to the northern section. Because of this, it was difficult to determine how the structure may have changed between the two parallel seismic lines and some faults were assumed to be continuous between the two planes. To increase the accuracy in the structural aspect of the model, pre-interpreted 3D seismic should be used to characterize formation surfaces and most importantly, the faulting framework. This would aid in the uncertainty of how the structure changes between the two parallel 2D seismic lines used to define the faulting framework of the model. To increase the accuracy of the structure map, formation top picks should be picked manually and compared to fault interpretations found in the logs.

6.2. Injecting Nitrogen into all Available Gas Cap Wells

In Case 3, only six wells were selected for nitrogen injection due to computing resource and time constraints. If more than six wells were assigned to injection, the maximum allowable number of problems would be exceeded due to time step and convergence issues. The simulator would make attempts to "chop" the time steps down to a solvable value resulting in a problem. If time was not a constraint, that maximum number of allowable problems could be increased and the time steps could manually be decreased to the smallest required solvable value to avoid

problem encounters. The exponential increase of oil production that arrives at the producers in year 2035 is not enough the offset the initial capital and power consumption for the six nitrogen separation units required for Case 3. If 11 wells are assigned to nitrogen injection, the gas cap would be pressurized at a considerably higher rate subsequently developing the high oil saturation front, mobilizing it at an earlier date. If the exponential increase in oil production is experienced sooner, it could potentially offset the costs and provide enough production for the project to be economically viable.

6.3.   Building a Simplified Model

Another solution for avoiding convergence issues would be to build a simplified Turner Valley model. Since the faults are not sealing, building a simplified theoretical model with similar rock and fluid properties could alleviate convergence issues when attempting to inject with 11 gas cap wells. This could potentially show how Turner Valley's oil production would be affected by injecting nitrogen into all available gas cap wells.

6.4.   Deterring and Applying Miscibility Pressures

Tiwari and Kumar (2001) describe a reservoir with a similar depth and oil gravity when compared to Turner Valley. Their laboratory research concluded that miscibility between the specified oil and nitrogen could be achieved at pressures above 6,000 psi. Due to such low gas cap pressures at current reservoir conditions, it was uncertain if miscibility pressure could be achieved within a reasonable time frame. Therefore the purpose of the project was to determine the effectiveness of an immiscible injection system and the miscibility function used was designed to facilitate only immiscible displacement. The solvent model in its current state is not equipped to simulated miscible behavior and thus laboratory tests need to be conducted on a

sample of Turner Valley oil to determine at which fractions of nitrogen and gas miscibility can

be achieved. Further testing for miscibility pressures between nitrogen and oil should be

conducted to verify if the oil in the Turner Valley field is comparable to the reservoir described

by Tiwari. Further evaluation of surface equipment also needs to be conducted, considering that

the current nitrogen separation units can only discharge at pressures of 4,000 psi. Economics

need to be run to determine if the incremental oil production obtained through a miscible system

would be worth the initial investment along with maintenance and power costs on units capable

of achieving miscibility pressures.

7. References

Alberta Energy Regulator. (2012). *Upstream Petroleum Industry.* Calgary: Alberta Energy

    Regulator.

Bennion, D., Thomas, F. B., Schulmeister, B., & Ma, T. (2002). A Correlation of Water and Gas-

    Oil Relative Permeability Properties for Various Western Canadian Sandstone and

    Carbonate Oil Producing Formations. *Petroelum Society's Canadian International*, 10.

Canadian Nitrogen Service Ltd. (2015). *Our Product:Canadian Nitrogen Service Ltd.* Retrieved

    from Canadian Nitrogen Services Web Site:

    http://www.canadiannitrogen.com/ourproduct.html

Craft, B., Hawkins, M., & Terry, R. E. (1990). *Applied Petroleum Reservoir Engineering Second*

    Edition. Upper Saddle River: Prentice Hall.

Galas, C., Clements, A., Jaafar, E., Jeje, O., Hoist, D., & Hoist, R. (2012). *Identification of*

    Enhanced Oil Recovery Potential in Alberta. Calgary: Sproule Associates Limited.

Green, D. W., & Willhite, G. P. (1998). *Enhanced Oil Recovery.* Henry L. Doherty Memorial

    Fund of AIME, Society of Petroleum Engineers.

Inc., P. C. (2015). *Land Sales: Petroleum Connection*. Retrieved from Petroleum Connection:

    http://petroleumconnection.landwork.ca/land.php

Lang, J. E. (1954). *Performance of Elk Basin Tensleep Reservoir with Nitrogen Injection.*

    Casper, WY: Stanolind Oil and Gas Co. .

Link, T. A., & Moore, P. D. (1934). Structure of Turner Valley Gas and Oil Field, Alberta.

    Bulletin of the American Association of Petroleum Geology VOL. 18, NO. 11

    (NOVEMBER), 1417-1453.

Mungan, N. (2000). Enhanced Oil Recovery with High Pressure Nitrogen Injection. *SPE/AAPG Western Regional Meeting* (pp. 1-4). Richardson, TX: Society of Petroleum Engineers.

New releases:PR Newswire. (2002, December 13). Retrieved from PR Newswire: http://www.prnewswire.com/news-releases/talisman-announces-pilot-project-for-enhanced-oil-recovery-77149362.html

Nitrogen generation:Wikipedia The Free Encyclopedia. (2015, October 17). Retrieved from Wikipedia The Free Encyclopedia: https://en.wikipedia.org/wiki/Nitrogen_generator#Membrane_technology

Paulson, M. P., & Wahl, J. (1962). Turner Valley Limestone Oilfield Past, Present, Future. *Journal of Canadian Petroleum Technology, Fall*, 95-103.

Rodriguez, F., Ortega, G., Sanchez, J. L., & Jimenez, O. (2001). Reservoir Management in the Cantarell Nitrogen Injection Project. *Offshore Technology Conference 13178* (pp. 1-7). Houston, Texas: PEMEX Exploracion y Produccion.

Schlumberger. (2014). Eclipse Reference Manual. Houston, Texas, United States of America.

Simard, J. (2015). Personal Communication.

Sinanan, B., & Budri, M. (2012). Nitrogen Injection Application for Oil Recovery in Trinidad. *SPETT 2012 Energy Conference and Exhibition SPE 156924* (pp. 1-11). Port of Spain, Trinidad: Society of Petroleum Engineers.

Taylor, V. (1939). *Development of the Turner Valley Gas and Oil Field.* New York: American Institute of Mining and Metallurgical Engineers, Inc. PETROLEUM TECHNOLOGY.

Tiwari, S., & Kumar, M. S. (2001). Nitrogen Injection for Simultaneous Exploration of Gas Cap. *Middle East Oil Show SPE 68169* (pp. 1-13). Richardson, Texas: Society of Petroleum Engineers.

Tododo, A. (2008). *Enchant Arcs CO2 Injection Pilot.* Calgary: Canadian Natural Resources Limited.

Wischnewski, B. (2015). *Thermodynamic Properties of Nitrogen: Peace Software*. Retrieved from Peace Software Web Site:

http://www.peacesoftware.de/einigewerte/stickstoff_e.html

8. APPENDIX A: Core Data

Well	Top	Bottom	Mid Point	Kmax	Kvert	Phi
100/16-20-018-02W5/0	2115.31	2115.92	2115.62			0.086
100/16-20-018-02W5/0	2115.92	2121.71	2118.82			
100/16-20-018-02W5/0	2121.71	2122.32	2122.02			0.091
100/16-20-018-02W5/0	2122.32	2124.76	2123.54			
100/16-20-018-02W5/0	2124.76	2125.06	2124.91			0.043
100/16-20-018-02W5/0	2125.06	2125.67	2125.37			0.111
100/16-20-018-02W5/0	2125.67	2126.89	2126.28			
100/16-20-018-02W5/0	2126.89	2127.50	2127.20			0.147
100/16-20-018-02W5/0	2127.50	2128.41	2127.96			
100/16-20-018-02W5/0	2128.41	2128.72	2128.57			0.109
100/16-20-018-02W5/0	2128.72	2129.33	2129.03			0.102
100/16-20-018-02W5/0	2129.33	2132.38	2130.86			
100/16-20-018-02W5/0	2132.38	2132.99	2132.69			0.085
100/16-20-018-02W5/0	2132.99	2133.90	2133.45			
100/16-20-018-02W5/0	2133.90	2134.51	2134.21			0.031
100/16-20-018-02W5/0	2134.51	2139.08	2136.80			
100/16-20-018-02W5/0	2139.08	2139.20	2139.14			0.112
103/08-32-018-02W5/0	1986.50	1987.20	1986.85	0.02		0.049
103/08-32-018-02W5/0	1987.20	1987.41	1987.31			
103/08-32-018-02W5/0	1987.41	1987.58	1987.50	0.08		0.024
103/08-32-018-02W5/0	1987.58	1987.92	1987.75	1.39	1.50	0.071
103/08-32-018-02W5/0	1987.92	1988.32	1988.12	0.47	1.06	0.007
103/08-32-018-02W5/0	1988.32	1988.59	1988.46	0.81		0.124
103/08-32-018-02W5/0	1988.59	1988.86	1988.73	0.05		0.058
103/08-32-018-02W5/0	1988.86	1989.75	1989.31	0.01		0.051
103/08-32-018-02W5/0	1989.75	1990.00	1989.88			
103/08-32-018-02W5/0	2009.00	2009.21	2009.11	0.26		0.050
103/08-32-018-02W5/0	2009.21	2009.42	2009.32			
103/08-32-018-02W5/0	2009.42	2009.71	2009.57	0.14	0.08	0.052
103/08-32-018-02W5/0	2009.71	2010.01	2009.86	0.13	0.13	0.046
103/08-32-018-02W5/0	2010.01	2010.33	2010.17			0.049
103/08-32-018-02W5/0	2010.33	2010.73	2010.53	0.16	0.11	0.052
103/08-32-018-02W5/0	2010.73	2011.03	2010.88			
103/08-32-018-02W5/0	2011.03	2011.23	2011.13	1.25	0.45	0.067
103/08-32-018-02W5/0	2011.23	2011.44	2011.34	0.47	0.27	0.059
103/08-32-018-02W5/0	2011.44	2011.61	2011.53	0.09	0.06	0.051
103/08-32-018-02W5/0	2011.61	2012.13	2011.87	0.08	0.08	0.028

103/08-32-018-02W5/0	2012.13	2012.47	2012.30	0.06	0.05	0.044
103/08-32-018-02W5/0	2012.47	2012.72	2012.60	13.40	0.54	0.054
103/08-32-018-02W5/0	2012.72	2012.94	2012.83	0.19	0.10	0.055
103/08-32-018-02W5/0	2012.94	2013.16	2013.05			
103/08-32-018-02W5/0	2013.16	2013.51	2013.34	0.05	0.11	0.050
103/08-32-018-02W5/0	2013.51	2013.73	2013.62	0.07	0.05	0.050
103/08-32-018-02W5/0	2013.73	2013.91	2013.82			
103/08-32-018-02W5/0	2013.91	2014.35	2014.13	0.07	0.05	0.048
103/08-32-018-02W5/0	2014.35	2014.53	2014.44	0.12	0.08	0.050
103/08-32-018-02W5/0	2014.53	2014.73	2014.63			
103/08-32-018-02W5/0	2014.73	2015.05	2014.89	2.57	0.46	0.061
103/08-32-018-02W5/0	2015.05	2015.11	2015.08	0.73		0.061
103/08-32-018-02W5/0	2015.11	2015.90	2015.51			
103/08-32-018-02W5/0	2015.90	2017.00	2016.45			
103/08-32-018-02W5/0	2017.00	2017.73	2017.37	5.32		0.109
103/08-32-018-02W5/0	2017.73	2018.20	2017.97	0.09		0.059
103/08-32-018-02W5/0	2018.20	2019.00	2018.60			
103/08-32-018-02W5/0	2020.60	2020.70	2020.65			
103/08-32-018-02W5/0	2046.00	2046.31	2046.16	0.01		0.017
103/08-32-018-02W5/0	2046.31	2046.63	2046.47			
103/08-32-018-02W5/0	2046.63	2047.00	2046.82	0.68		0.005
103/08-32-018-02W5/0	2047.00	2047.37	2047.19	0.01		0.012
103/08-32-018-02W5/0	2047.37	2047.56	2047.47			0.017
103/08-32-018-02W5/0	2047.56	2047.84	2047.70	0.03		0.013
103/08-32-018-02W5/0	2047.84	2048.04	2047.94			
103/08-32-018-02W5/0	2048.04	2048.30	2048.17	0.01		0.014
103/08-32-018-02W5/0	2048.30	2048.56	2048.43			
103/08-32-018-02W5/0	2048.56	2048.83	2048.70	0.02		0.012
103/08-32-018-02W5/0	2048.83	2049.36	2049.10	2.64	0.03	0.085
103/08-32-018-02W5/0	2049.36	2049.77	2049.57	0.03	0.01	0.019
103/08-32-018-02W5/0	2049.77	2049.98	2049.88			0.093
103/08-32-018-02W5/0	2049.98	2050.12	2050.05	0.18	0.06	0.032
103/08-32-018-02W5/0	2050.12	2050.34	2050.23			
103/08-32-018-02W5/0	2050.34	2050.41	2050.38	0.33		0.040
103/08-32-018-02W5/0	2050.41	2050.90	2050.66	0.11	0.30	0.026
103/08-32-018-02W5/0	2050.90	2051.11	2051.01			
103/08-32-018-02W5/0	2051.11	2051.49	2051.30	0.06		0.053
103/08-32-018-02W5/0	2051.49	2051.71	2051.60			
103/08-32-018-02W5/0	2051.71	2051.89	2051.80	4.33		0.076
103/08-32-018-02W5/0	2051.89	2052.08	2051.99			0.015

103/08-32-018-02W5/0	2052.08	2052.21	2052.15	0.57	0.26	0.063
103/08-32-018-02W5/0	2052.21	2052.47	2052.34	1.57	0.62	0.094
103/08-32-018-02W5/0	2052.47	2052.58	2052.53	2.74		0.099
103/08-32-018-02W5/0	2052.58	2052.66	2052.62	0.93		0.094
103/08-32-018-02W5/0	2052.66	2052.88	2052.77			
103/08-32-018-02W5/0	2052.88	2053.03	2052.96			0.078
103/08-32-018-02W5/0	2053.03	2053.36	2053.20	3.57	1.17	0.020
103/08-32-018-02W5/0	2053.36	2053.46	2053.41	0.69		0.098
103/08-32-018-02W5/0	2053.46	2053.66	2053.56			
103/08-32-018-02W5/0	2053.66	2053.82	2053.74	1.24		0.119
103/08-32-018-02W5/0	2053.82	2054.19	2054.01	19.00		0.091
103/08-32-018-02W5/0	2054.19	2054.56	2054.38			
103/08-32-018-02W5/0	2054.56	2054.99	2054.78			0.072
103/08-32-018-02W5/0	2054.99	2055.15	2055.07	9.16	3.59	0.107
103/08-32-018-02W5/0	2055.15	2055.30	2055.23	47.70	14.80	0.152
103/08-32-018-02W5/0	2055.30	2055.55	2055.43	31.40	12.60	0.117
103/08-32-018-02W5/0	2055.55	2055.74	2055.65			
103/08-32-018-02W5/0	2055.74	2055.87	2055.81	0.28		0.052
103/08-32-018-02W5/0	2055.87	2056.18	2056.03	15.00		0.112
103/08-32-018-02W5/0	2056.18	2056.47	2056.33	2.86		0.078
103/08-32-018-02W5/0	2056.47	2056.70	2056.59	3.68	2.90	0.086
103/08-32-018-02W5/0	2056.70	2056.95	2056.83			
103/08-32-018-02W5/0	2056.95	2058.00	2057.48			
100/10-32-018-02W5/0	2121.00	2122.65	2121.83			
100/10-32-018-02W5/0	2122.65	2122.80	2122.73	0.25	0.20	0.051
100/10-32-018-02W5/0	2122.80	2122.90	2122.85	0.10		0.080
100/10-32-018-02W5/0	2122.90	2123.45	2123.18			
100/10-32-018-02W5/0	2123.45	2123.65	2123.55	0.20	0.24	0.039
100/10-32-018-02W5/0	2123.65	2123.85	2123.75	0.04		0.055
100/10-32-018-02W5/0	2123.85	2124.20	2124.03			
100/10-32-018-02W5/0	2124.20	2125.10	2124.65			
100/10-32-018-02W5/0	2125.10	2126.95	2126.03			
100/10-32-018-02W5/0	2126.95	2127.05	2127.00	0.21		0.064
100/10-32-018-02W5/0	2127.05	2127.45	2127.25	0.82		0.045
100/10-32-018-02W5/0	2127.45	2127.85	2127.65			
100/10-32-018-02W5/0	2127.85	2127.99	2127.92			0.055
100/10-32-018-02W5/0	2127.99	2128.10	2128.05	1.60		0.064
100/10-32-018-02W5/0	2128.10	2130.05	2129.08			
100/10-32-018-02W5/0	2130.05	2130.15	2130.10	0.52		0.120
100/10-32-018-02W5/0	2130.15	2130.40	2130.28	6.10		0.051

100/10-32-018-02W5/0	2130.40	2130.95	2130.68			
100/10-32-018-02W5/0	2130.95	2131.20	2131.08	3.30	2.30	0.103
100/10-32-018-02W5/0	2131.20	2131.30	2131.25	3.00		0.139
100/10-32-018-02W5/0	2131.30	2131.75	2131.53			
100/10-32-018-02W5/0	2131.75	2131.85	2131.80	0.17		0.104
100/10-32-018-02W5/0	2131.85	2132.05	2131.95	0.20	0.15	0.049
100/10-32-018-02W5/0	2132.05	2132.30	2132.18			
100/10-32-018-02W5/0	2132.30	2132.52	2132.41	0.42		0.062
100/10-32-018-02W5/0	2132.52	2132.62	2132.57	0.70		0.072
100/10-32-018-02W5/0	2132.62	2132.98	2132.80	0.33	0.44	0.074
100/10-32-018-02W5/0	2132.98	2133.05	2133.02	0.80		0.102
100/10-32-018-02W5/0	2133.05	2133.52	2133.29			
100/10-32-018-02W5/0	2133.52	2133.70	2133.61	0.52		0.067
100/10-32-018-02W5/0	2133.70	2133.78	2133.74	0.15		0.079
100/10-32-018-02W5/0	2133.78	2134.20	2133.99			
100/10-32-018-02W5/0	2185.00	2185.20	2185.10			
100/10-32-018-02W5/0	2185.20	2185.29	2185.25	0.18	0.07	0.009
100/10-32-018-02W5/0	2185.29	2185.49	2185.39	0.06		0.029
100/10-32-018-02W5/0	2185.49	2187.45	2186.47			
100/10-32-018-02W5/0	2187.45	2187.80	2187.63			
100/10-32-018-02W5/0	2187.80	2188.25	2188.03			
100/10-32-018-02W5/0	2188.25	2188.37	2188.31	1.90	1.40	0.064
100/10-32-018-02W5/0	2188.37	2188.44	2188.41	13.00		0.120
100/10-32-018-02W5/0	2188.44	2188.92	2188.68			
100/10-32-018-02W5/0	2188.92	2189.10	2189.01	1.10	1.30	0.069
100/10-32-018-02W5/0	2189.10	2189.25	2189.18	1.70		0.064
100/10-32-018-02W5/0	2189.25	2189.95	2189.60			
100/10-32-018-02W5/0	2189.95	2190.25	2190.10	2.90	92.00	0.047
100/10-32-018-02W5/0	2190.25	2190.50	2190.38	0.70		0.102
100/10-32-018-02W5/0	2190.50	2191.47	2190.99			
100/10-32-018-02W5/0	2191.47	2191.62	2191.55	32.00	33.00	0.086
100/10-32-018-02W5/0	2191.62	2191.70	2191.66	20.00		0.114
100/10-32-018-02W5/0	2191.70	2192.80	2192.25			
100/10-32-018-02W5/0	2192.80	2192.85	2192.83	7.90		0.097
100/10-32-018-02W5/0	2192.85	2193.10	2192.98	12.00	13.00	0.100
100/10-32-018-02W5/0	2193.10	2193.45	2193.28			
100/10-32-018-02W5/0	2193.45	2193.52	2193.49	35.00		0.131
100/10-32-018-02W5/0	2193.52	2193.70	2193.61	20.00	12.00	0.107
100/10-32-018-02W5/0	2193.70	2194.25	2193.98			
100/10-32-018-02W5/0	2194.25	2194.32	2194.29	24.00		0.096

100/10-32-018-02W5/0	2194.32	2194.45	2194.39	2.20	2.70	0.072
100/10-32-018-02W5/0	2194.45	2194.90	2194.68			
100/10-32-018-02W5/0	2194.90	2194.96	2194.93	13.00		0.100
100/10-32-018-02W5/0	2194.96	2195.10	2195.03	11.00	7.40	0.094
100/10-32-018-02W5/0	2195.10	2195.55	2195.33			
100/10-32-018-02W5/0	2195.55	2195.65	2195.60	22.00		0.114
100/10-32-018-02W5/0	2195.65	2195.80	2195.73	5.20	2.70	0.094
100/10-32-018-02W5/0	2195.80	2195.95	2195.88			
100/10-32-018-02W5/0	2195.95	2196.40	2196.18			
100/15-06-019-02W5/0	2375.00	2376.30	2375.65			
100/15-06-019-02W5/0	2376.30	2376.50	2376.40			
100/15-06-019-02W5/0	2376.50	2376.65	2376.58			
100/15-06-019-02W5/0	2376.65	2376.75	2376.70			
100/15-06-019-02W5/0	2377.14	2378.96	2378.05			
100/15-06-019-02W5/0	2379.00	2381.00	2380.00			
100/15-06-019-02W5/0	2383.25	2385.60	2384.43			
100/15-06-019-02W5/0	2387.25	2388.65	2387.95			
100/15-06-019-02W5/0	2391.50	2393.40	2392.45			
100/15-06-019-02W5/0	2403.04	2411.88	2407.46			
100/15-06-019-02W5/0	2417.50	2417.69	2417.60	1.21	0.68	0.087
100/15-06-019-02W5/0	2417.69	2417.89	2417.79		2.82	0.132
100/15-06-019-02W5/0	2417.89	2418.02	2417.96		3.92	0.177
100/15-06-019-02W5/0	2418.02	2418.30	2418.16	2.47	1.66	0.141
100/15-06-019-02W5/0	2418.30	2419.75	2419.03			
100/15-06-019-02W5/0	2420.21	2420.46	2420.34	1.93	1.89	0.087
100/15-06-019-02W5/0	2420.46	2420.55	2420.51	0.93	0.93	0.068
100/15-06-019-02W5/0	2420.55	2420.84	2420.70	6.67	0.72	0.062
100/15-06-019-02W5/0	2420.84	2421.01	2420.93	0.81	0.75	0.072
100/15-06-019-02W5/0	2421.01	2421.16	2421.09	3.55	2.32	0.106
100/15-06-019-02W5/0	2421.16	2421.34	2421.25	0.60	0.48	0.059
100/15-06-019-02W5/0	2421.34	2421.46	2421.40	0.84	0.42	0.050
100/15-06-019-02W5/0	2421.46	2421.71	2421.59	0.10	0.10	0.043
100/15-06-019-02W5/0	2421.71	2422.26	2421.99			
100/15-06-019-02W5/0	2422.26	2422.41	2422.34	2.88	0.69	0.036
100/15-06-019-02W5/0	2422.41	2422.54	2422.48	0.18	0.17	0.043
100/15-06-019-02W5/0	2422.54	2422.72	2422.63			
100/15-06-019-02W5/0	2422.72	2422.94	2422.83	1.10	0.84	0.079
100/15-06-019-02W5/0	2422.94	2423.19	2423.07	1.12	0.89	0.056
100/15-06-019-02W5/0	2423.19	2423.49	2423.34	1.13	0.67	0.088
100/15-06-019-02W5/0	2423.49	2423.86	2423.68	23.40	0.93	0.138

100/15-06-019-02W5/0	2423.86	2424.02	2423.94	2.05	1.63	0.069
100/15-06-019-02W5/0	2424.02	2424.16	2424.09	71.00	0.53	0.086
100/15-06-019-02W5/0	2424.16	2424.35	2424.26	16.60	6.01	0.075
100/15-06-019-02W5/0	2424.35	2424.53	2424.44	0.80	0.62	0.090
100/15-06-019-02W5/0	2424.53	2424.75	2424.64	0.29	0.24	0.053
100/15-06-019-02W5/0	2424.75	2424.95	2424.85		0.15	0.062
100/15-06-019-02W5/0	2424.95	2425.22	2425.09	32.90	0.76	0.083
100/15-06-019-02W5/0	2425.22	2425.61	2425.42	8.22	0.79	0.088
100/15-06-019-02W5/0	2425.61	2425.83	2425.72			
100/15-06-019-02W5/0	2425.83	2426.11	2425.97	2.61	2.32	0.107
100/15-06-019-02W5/0	2426.11	2426.23	2426.17	0.99	0.99	0.098
100/15-06-019-02W5/0	2426.23	2426.46	2426.35	3.66	2.08	0.079
100/15-06-019-02W5/0	2426.46	2426.69	2426.58		27.30	0.100
100/15-06-019-02W5/0	2426.69	2426.99	2426.84		12.80	0.083
100/15-06-019-02W5/0	2426.99	2427.31	2427.15		9.35	0.079
100/15-06-019-02W5/0	2427.31	2427.62	2427.47	1.41	0.87	0.063
100/15-06-019-02W5/0	2427.62	2427.71	2427.67	4.85	2.53	0.064
100/15-06-019-02W5/0	2427.71	2428.11	2427.91	19.20	9.29	0.077
100/15-06-019-02W5/0	2428.11	2428.36	2428.24	1.41	0.87	0.063
100/15-06-019-02W5/0	2428.36	2428.75	2428.56	13.10	8.80	0.112
100/15-06-019-02W5/0	2430.37	2430.68	2430.53		27.50	0.087
100/15-06-019-02W5/0	2430.68	2430.87	2430.78	68.00	42.60	0.121
100/15-06-019-02W5/0	2430.87	2431.14	2431.01		11.20	0.081
100/15-06-019-02W5/0	2431.14	2434.25	2432.70			
100/15-06-019-02W5/0	2434.44	2443.28	2438.86			
100/08-30-019-02W5/0	1773.14	1773.27	1773.21	27.00	27.00	0.057
100/08-30-019-02W5/0	1773.27	1773.69	1773.48	1.10	0.42	0.128
100/08-30-019-02W5/0	1773.69	1774.15	1773.92	8.90	3.10	0.097
100/08-30-019-02W5/0	1774.15	1774.58	1774.37	0.23	0.49	0.068
100/08-30-019-02W5/0	1774.58	1775.98	1775.28			
100/08-30-019-02W5/0	1775.98	1776.22	1776.10			0.061
100/08-30-019-02W5/0	1776.22	1776.53	1776.38			0.058
100/08-30-019-02W5/0	1776.53	1776.74	1776.64		20.00	0.045
100/08-30-019-02W5/0	1776.74	1777.32	1777.03		20.00	0.045
100/08-30-019-02W5/0	1777.32	1777.47	1777.40	24.00	5.50	0.054
100/08-30-019-02W5/0	1777.47	1777.75	1777.61	6.20	6.70	0.061
100/08-30-019-02W5/0	1777.75	1777.93	1777.84	1.50	0.35	0.070
100/08-30-019-02W5/0	1777.93	1778.50	1778.22		1.40	0.095
100/08-30-019-02W5/0	1778.50	1778.51	1778.51	27.00	6.10	0.067
100/08-30-019-02W5/0	1778.87	1779.24	1779.06	15.00	9.70	0.091

100/08-30-019-02W5/0	1779.24	1779.54	1779.39	1.50	0.16	0.071
100/08-30-019-02W5/0	1779.54	1779.97	1779.76	9.10	0.47	0.076
100/08-30-019-02W5/0	1779.97	1780.21	1780.09	1.40	1.10	0.080
100/08-30-019-02W5/0	1780.21	1780.67	1780.44	1.80	1.40	0.084
100/08-30-019-02W5/0	1780.67	1781.04	1780.86	0.93	1.00	0.042
100/08-30-019-02W5/0	1781.04	1781.40	1781.22	0.41	0.01	0.063
100/08-30-019-02W5/0	1781.40	1781.80	1781.60	14.00	3.50	0.083
100/08-30-019-02W5/0	1781.80	1782.04	1781.92	36.00	16.00	0.132
100/08-30-019-02W5/0	1782.04	1782.50	1782.27	22.00	8.20	0.132
100/08-30-019-02W5/0	1782.50	1782.68	1782.59	10.00	6.70	0.114
100/08-30-019-02W5/0	1782.68	1782.84	1782.76			
100/08-30-019-02W5/0	1782.84	1785.20	1784.02			
100/08-30-019-02W5/0	1785.20	1785.21	1785.21	25.00	20.00	0.094
100/08-30-019-02W5/0	1785.49	1785.91	1785.70	16.00	14.00	0.038
100/08-30-019-02W5/0	1785.91	1786.31	1786.11	29.00	6.80	0.121
100/08-30-019-02W5/0	1786.31	1786.70	1786.51	17.00	20.00	0.118
100/08-30-019-02W5/0	1786.70	1786.74	1786.72	7.00	3.30	0.136
100/08-30-019-02W5/0	1787.10	1787.56	1787.33	2.60	0.82	0.074
100/08-30-019-02W5/0	1787.56	1787.90	1787.73	9.80	4.50	0.056
100/08-30-019-02W5/0	1787.90	1788.32	1788.11			0.136
100/08-30-019-02W5/0	1788.32	1788.84	1788.58	5.10	0.01	0.094
100/08-30-019-02W5/0	1788.84	1788.99	1788.92	39.00	35.00	0.108
100/08-30-019-02W5/0	1788.99	1789.30	1789.15	0.51	0.13	0.070
100/08-30-019-02W5/0	1789.30	1789.91	1789.61	0.72	0.01	0.055
100/08-30-019-02W5/0	1789.91	1790.24	1790.08	0.22	0.09	0.043
100/08-30-019-02W5/0	1790.24	1790.64	1790.44	0.51	0.01	0.063
100/08-30-019-02W5/0	1790.64	1790.94	1790.79	54.00	0.04	0.037
100/08-30-019-02W5/0	1790.94	1791.30	1791.12	4.50	4.40	0.101
100/08-30-019-02W5/0	1791.30	1791.31	1791.31			0.129
100/08-30-019-02W5/0	1791.61	1791.89	1791.75	12.00	5.50	0.118
100/08-30-019-02W5/0	1791.89	1792.04	1791.97			
100/08-30-019-02W5/0	1792.04	1792.25	1792.15	2.90	1.80	0.114
100/08-30-019-02W5/0	1792.25	1792.59	1792.42	78.00	6.40	0.098
100/08-30-019-02W5/0	1792.59	1792.96	1792.78	39.00	12.00	0.123
100/08-30-019-02W5/0	1792.96	1793.32	1793.14	15.00	1.40	0.063
100/08-30-019-02W5/0	1793.32	1793.41	1793.37			
100/08-30-019-02W5/0	1793.41	1793.75	1793.58	7.10	9.50	0.096
100/08-30-019-02W5/0	1793.80	1793.93	1793.87	3.40	0.86	0.090
100/08-30-019-02W5/0	1793.93	1794.30	1794.12	19.00	2.90	0.092
100/08-30-019-02W5/0	1794.30	1794.69	1794.50	5.20	2.70	0.124

100/08-30-019-02W5/0	1794.69	1795.15	1794.92	1.90	2.10	0.103
100/08-30-019-02W5/0	1795.15	1795.39	1795.27	44.00	14.00	0.135
100/08-30-019-02W5/0	1795.39	1795.64	1795.52	3.00	1.90	0.114
100/08-30-019-02W5/0	1795.64	1796.00	1795.82	0.81	0.01	0.100
100/08-30-019-02W5/0	1796.00	1796.49	1796.25	5.00	1.70	0.064
100/08-30-019-02W5/0	1796.49	1796.89	1796.69	18.00	0.83	0.075
100/08-30-019-02W5/0	1796.89	1797.37	1797.13	2.80	0.22	0.110
100/08-30-019-02W5/0	1797.37	1797.86	1797.62	0.65	0.11	0.076
100/08-30-019-02W5/0	1797.86	1797.92	1797.89			
100/08-30-019-02W5/0	1797.92	1798.78	1798.35			
100/08-30-019-02W5/0	1798.78	1801.06	1799.92			
100/08-30-019-02W5/0	1801.10	1801.70	1801.40			0.085
100/08-30-019-02W5/0	1801.70	1802.10	1801.90			0.028
100/08-30-019-02W5/0	1802.10	1802.28	1802.19			
100/08-30-019-02W5/0	1802.30	1802.65	1802.48			0.054
100/08-30-019-02W5/0	1802.65	1803.11	1802.88	3.00	2.80	0.054
100/08-30-019-02W5/0	1803.11	1803.38	1803.25	2.30	0.60	0.077
100/08-30-019-02W5/0	1803.38	1803.96	1803.67		12.00	0.075
100/08-30-019-02W5/0	1803.96	1804.57	1804.27	4.00	2.20	0.061
100/08-30-019-02W5/0	1804.57	1805.06	1804.82	17.00	5.30	0.063
100/08-30-019-02W5/0	1805.06	1805.94	1805.50			
100/08-30-019-02W5/0	1805.94	1842.82	1824.38			
100/08-30-019-02W5/0	1874.12	1874.46	1874.29	0.07	0.01	0.025
100/08-30-019-02W5/0	1874.46	1874.64	1874.55	0.27	0.01	0.032
100/08-30-019-02W5/0	1874.64	1875.16	1874.90	0.06	0.01	0.011
100/08-30-019-02W5/0	1875.16	1875.43	1875.30	0.02	0.01	0.013
100/08-30-019-02W5/0	1875.43	1875.80	1875.62	0.14	0.01	0.007
100/08-30-019-02W5/0	1875.80	1876.14	1875.97	0.21	0.01	0.011
100/08-30-019-02W5/0	1876.14	1876.62	1876.38	1.60	0.01	0.011
100/08-30-019-02W5/0	1876.62	1876.96	1876.79	0.22	0.01	0.017
100/08-30-019-02W5/0	1876.96	1888.85	1882.91			

9. Appendix B: Solvent Model Preparation

There are a number changes that need to be made to the summary, schedule, and property sections of the Eclipse deck for the solvent model to be valid. The changes made to the summary section include the addition of the SOLVENT keyword and the MISCIBLE keyword (describing the miscibility saturation function table dimensions), for the solvent model to be initiated. The WSOLVENT keyword needs to be applied to the schedule section which dictates the fraction of nitrogen that will be injected at each injection well.

Several more major additions were applied to the properties section of the Eclipse deck. The saturation functions generated by Petrel were removed and the SWFN and SGFN keywords were added which are the water and gas saturation function respectively. The values for water and gas relative permeability, along with the capillary pressures for both phases, were populated using the same water and gas relative permeability and capillary pressure values generated initially. The SOF2 keyword was another addition which specifies the relative permeability of miscible hydrocarbons in a solvent model. Since the mixing parameter was set to zero and the nitrogen and oil are considered to be immiscible, SOF2 identifies the relative permeability of only oil in a two phase system including oil-water and oil-gas. The SOF3 keyword was also a necessary addition which specifies the relative permeability of oil in both regions where only oil and water are present and where oil, connate water, and gas are present. Once again, the same values for oil relative permeability generated earlier were used for both SOF2 and SOF3 tables. While the new family of saturations function describes nothing more than the original saturation functions generate by Petrel, they were necessary modifications required for the solvent model to run (Schlumberger, 2014).

The primary changes in the description of rock and fluid interaction comes from the addition of the SSFN keyword which specifies the relative permeability of nitrogen. This is accomplished by specifying the fraction of the phase between nitrogen and gas (nitrogen saturation) and applying a solvent relative permeability multiplier to the gas relative permeability at that specified fraction (Schlumberger, 2014). This is essentially calculating a fraction of the gas relative permeability at a specific saturation in a nitrogen-gas system and assigning that fraction as a nitrogen relative permeability. Since the nitrogen has a similar molecular weight when compared to methane gas (14 g/mol compared to 16 g/mol) it was assumed that the relative permeability to nitrogen is very similar to that of gas and relative permeability multipliers of one was applied.

The MISC keyword is another essential addition describing the miscibility function of the model which controls the transition between miscible and immiscible displacement (Schlumberger, 2014). This is done by specifying the solvent fraction (between nitrogen and gas) and assigning a miscibility value, ranging from zero to one. A value of zero relates to immiscible relative permeability and a value of one corresponds to miscible relative permeability. Since an immiscible mechanism is desired the miscibility values have been set to zero at all solvent fractions except for at 100% solvent composition. Since the miscibility function interpolates monotonically increasing values linearly, the miscibility value had to be set to zero at 99% composition prior to increasing the miscibility to one at a composition of 100% solvent.

The final change that was made to the Petrel generated ECLIPSE deck was the addition of the PVDS keyword that specifies the PVT properties of the solvent being injected (Schlumberger, 2014). Peace Software is a publically available tool that determines the thermodynamic properties of various pure gases. The software was used to obtain the viscosity

and the compressibility factor of nitrogen at reservoir temperature (140 ^{O}F) and the same

pressure range (14.7 psia to 8,000 psia) as the PVT properties for oil and gas (Wischnewski,

2015). The compressibility factors and Equation 9 were used to calculate the nitrogen formation

volume factor.

SOLVENT MODEL SAMPLE

<u>RUNSPEC</u>

TITLE   -- Generated : Petrel
NEWFIRST100_RESTART_23

WELLDIMS   -- Generated : Petrel
 96 125 2 96 /

START   -- Generated : Petrel
 31 DEC 1914 /

DISGAS   -- Generated : Petrel

WATER   -- Generated : Petrel

OIL   -- Generated : Petrel

GAS   -- Generated : Petrel

SOLVENT

MISCIBLE
 1 20 'NONE' /

PETOPTS   -- Generated : Petrel
INITNNC EDITSUPP /

MONITOR   -- Generated : Petrel

MULTIN   -- Generated : Petrel

METRIC   -- Generated : Petrel

DIMENS   -- Generated : Petrel
 110 69 60 /

```
TABDIMS                     -- Generated : Petrel
  1* 1* 32 81 1* 25 6* 1 /

GRID

INCLUDE                     -- Generated : Petrel
'NEWFIRST100_RESTART_23_GRID.INC' /

NOECHO                      -- Generated : Petrel

PETGRID                     -- Generated : Petrel
'NEWFIRST100_RESTART_23.GSG' /

ECHO                        -- Generated : Petrel

EDIT

PROPS

INCLUDE                     -- Generated : Petrel
'NEWFIRST100_RESTART_23_PROPS.INC' /

REGIONS

NOECHO                      -- Generated : Petrel

ECHO                        -- Generated : Petrel

SOLUTION

INCLUDE                     -- Generated : Petrel
'NEWFIRST100_RESTART_23_SOL.INC' /

SUMMARY

INCLUDE                     -- Generated : Petrel
'NEWFIRST100_RESTART_23_SUM.INC' /

SCHEDULE

INCLUDE                     -- Generated : Petrel
PROPERTIES

ROCKOPTS                    -- Generated : Petrel
```

1* 1* ROCKNUM /

ROCK   -- Generated : Petrel
   166.4877   0.00020058 /

PVTW   -- Generated : Petrel
   166.49   1.0081 4.0294E-005   0.45854   0 /

PVTO   -- Generated : Petrel
   0.33657   1.0135   1.04114635   1.2934 /
   3.9934   7.9083   1.04998578   1.1637 /
   8.4948   14.803   1.06107435   1.0443 /
   13.462   21.698   1.07355210   0.94521 /
   18.766   28.593   1.08713598   0.86362 /
   24.341   35.487   1.10167299   0.79592 /
   30.142   42.382   1.11706346   0.73907 /
   36.14   49.277   1.13323535   0.69075 /
   42.313   56.172   1.15013311   0.6492 /
   48.642   63.066   1.16771194   0.61309 /
   55.114   69.961   1.18593459   0.58142 /
   61.717   76.856   1.20476933   0.55339 /
   68.443   83.751   1.22418865   0.52841 /
   75.283   90.645   1.24416836   0.506 /
   82.23   97.54   1.26468697   0.48576 /
   89.277   104.43   1.28572516   0.46739 /
   96.421   111.33   1.30726545   0.45063 /
   103.66   118.22   1.32929195   0.43527 /
   110.98   125.12   1.35179006   0.42113 /
   118.38   132.01   1.37474636   0.40808 /
   125.86   138.91   1.39814844   0.39598 /
   133.42   145.8   1.42198477   0.38473 /
   141.05   152.7   1.44624459   0.37424 /
   148.76   159.59   1.47091786   0.36444 /
   156.53   166.49   1.49599516   0.35524
               173.38   1.49294518   0.35851
               180.28   1.49013402   0.36192
               187.17   1.48753469   0.36548
               194.07   1.48512412   0.36918
               200.96   1.48288246   0.37301
               207.86   1.48079258   0.37697
               214.75   1.47883956   0.38105
               221.65   1.47701039   0.38526
               228.54   1.47529364   0.38959
               235.44   1.47367927   0.39404
               242.33   1.47215838   0.3986

```
249.22   1.47072309    0.40327
256.12   1.46936636    0.40806
263.01   1.46808191    0.41294
269.91   1.46686413    0.41793
 276.8   1.46570794    0.42302
 283.7   1.46460881    0.42821
290.59   1.46356259     0.4335
297.49   1.46256557    0.43887
```

SCHEDULE

WCONPROD   -- Generated : Petrel
 3-03-070 1* BHP 5* 114.5000 /
 /

DATES   -- Generated : Petrel
 1 DEC 2014 /
 /

SKIP   -- Generated : Petrel
--Hint: Select wells on the input tree, drop in with the blue arrow, then add rules with the rule
pop-up

ENDSKIP   -- Generated : Petrel

GCONPROD   -- Generated : Petrel
 'GROUP 1' NONE /
 /

DATES   -- Generated : Petrel
 1 JAN 2015 /
 /

WELSPECS   -- Generated : Petrel
--'0-07-090' is the simulation well name used to describe flow from '100-07-090'
--
 0-07-090 'GROUP 1' 91 23 1* GAS /
 /

GRUPTREE   -- Generated : Petrel
 'GROUP 1' FIELD /
 /

WCONINJE   -- Generated : Petrel
 0-07-090 GAS 1* RATE 61164.39 /

```
 /

WSOLVENT
 0-07-090 1.0 /
 /
```

10. Appendix C: Nitrogen separation unit operation

The nitrogen membrane unit is mounted on a trailer and divided into four main components: the initial compressor unit, the membrane pretreatment system, the air separation membrane system, and the final pressure boosting system (Canadian Nitrogen Service Ltd., 2015). Ambient air enters the initial compressor unit where it travels through the intake filter and is supplied to the oil separator which builds the pressure between 40-60 psig. The control system supplies the pressurized air to the compressor, increasing the pressure further to 350 psig. The compressor then supplies the air to the membrane pretreatment system, passing through the second oil separator which removes any oil droplets present in the air. The air then travels to the air aftercooler which causes water vapor and any leftover oil vapor to condense. The aftercooler supplies the air to a system of separators and filters that remove any condensate and large particulates. The air then travels through a coalescing filter which filters the air further and removes aerosols and fine particulates. The air is then re-heated before entering the carbon tower which maintains the temperature above the dew point temperature of the air. Any vapors that maybe still entrained in the air are removed within the carbon tower. The air is then supplied to the membrane air separation unit for nitrogen separation. Figure 43 shows the components of a membrane nitrogen separation unit.
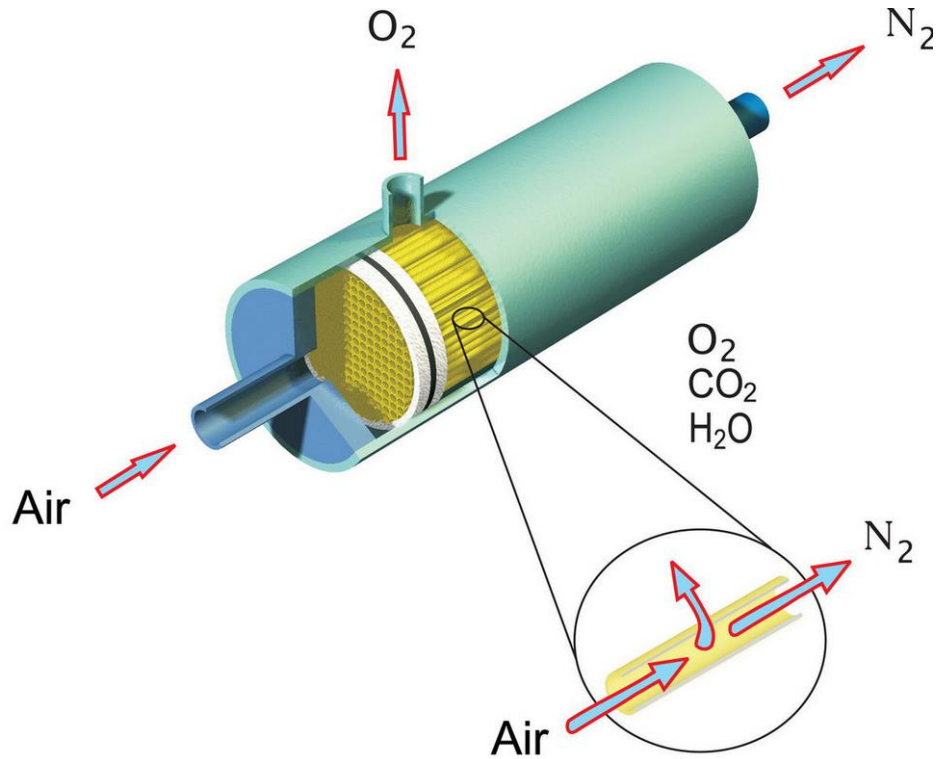
Figure 43: Membrane nitrogen separation unit (Nitrogen generation: Wikipedia The Free Encyclopedia, 2015)
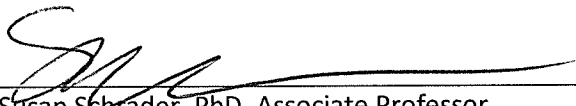
The membrane cartridge is structurally a cluster of hollow-fiber tubes composed of reeled polymer fibers. Pressurized air flows through the cluster of hollow membrane fibers, and due to the difference in pressures between the interior and the exterior of the tubes, gases such as oxygen, carbon dioxide, and water vapor are removed. Different gases permeate through the membrane at varying velocities and therefore only nitrogen is able to pass through the separation unit. Membrane separation units are not sensitive to moisture, they are inert to oil and grease, and they are very resistant to vibration and shock. Membrane separation units are also highly

dependable considering the fact that they contain no moving parts and they can operate over a large temperature range (-40 ^{O}F to 140 ^{O}F). Membrane units have a life span of up to 20 years of continuous operation.
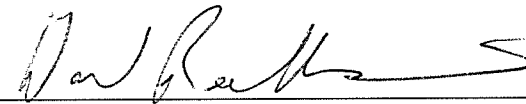
After the air has traveled through the membrane separation unit, the purified nitrogen is collected into a manifold at which point a product valve vents and regulates the flow until the purity of the nitrogen reaches requirements. The nitrogen then travels to the final compression system where it is gathered by a nitrogen receiver vessel. The nitrogen supplied by the receiver travels through a series of pressure boosters and heat exchangers, increasing the pressure of the nitrogen up to 4,000 psig.
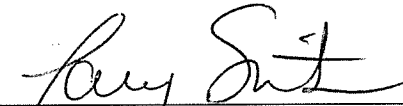
SIGNATURE PAGE

This is to certify that the thesis prepared by Igor Koracin entitled "Investigating the Feasibility of Nitrogen Injection in the Turner Valley Oil Field" has been examined and approved for acceptance by the Department of Petroleum Engineering, Montana Tech of The University of Montana, on this 4th day of December, 2015.

Susan Schrader, PhD, Associate Professor
Department of Petroleum Engineering
Chair, Examination Committee

David Reichhardt, MS, Assistant Professor
Department of Petroleum Engineering
Member, Examination Committee

Larry Smith, PhD, Associate Professor
Department of Geological Engineering
Member, Examination Committee